ANFIS Based Fractional-Order PID Speed and PI with Anti-Windup Current Control of Permanent Magnet Synchronous Motor for Electric Vehicle: The Case of ECADO-4EV

Tsion Abebe Muche

A Thesis Submitted to

The Department of Electrical Power and Control Engineering, School of Electrical Engineering and Computing

Presented in Partial Fulfillment of the Requirement for the Master of Science Degree in Electrical Power and Control Engineering (Specialization in Control Engineering)

Office of Graduate Studies

Adama Science and Technology University

September, 2021

Adama, Ethiopia

ANFIS Based Fractional-Order PID Speed and PI with Anti-Windup Current Control of Permanent Magnet Synchronous Motor for Electric Vehicle: The Case of ECADO-4EV

Tsion Abebe Muche

Advisor: Prof. Gang Gyoo Jin

A Thesis Submitted to
The Department of Electrical Power and Control Engineering
School of Electrical Engineering and Computing

Presented in Partial Fulfillment of the Requirement for the Master of Science Degree in Electrical Power and Control Engineering (Specialization in Control Engineering)

Office of Graduate Studies
Adama Science and Technology University

September, 2021
Adama, Ethiopia

DECLARATION AND RECOMMENDATION

Declaration

I hereby declare that this Master Thesis entitled "ANFIS Based Fractional-Order PID Speed and PI with Anti-Windup Current Control of Permanent Magnet Synchronous Motor for Electric Vehicle: The Case of ECADO-4EV" is my original work. That is, it has not been submitted for the award of any academic degree, diploma, or certificate in any other university. All sources of materials that are used for this thesis have been duly acknowledged through citation.

Tsion Abebe Muche	____________	September 10, 2021
Name of the student	Signature	Date

Recommendation

I, the advisor of this thesis, hereby certify that I have read the revised version of the thesis entitled "ANFIS Based Fractional-Order PID Speed and PI with Anti-Windup Current Control of Permanent Magnet Synchronous Motor for Electric Vehicle: The Case of ECADO-4EV" prepared under my guidance by Tsion Abebe Muche submitted in partial fulfillment of the requirements for the degree of Master of Science in Control Engineering. Therefore, I recommend the submission of the revised version of the thesis to the department following the applicable procedures.

Prof. Gang Gyoo Jin		September 10, 2021
Advisor	Signature	Date

APPROVAL SHEET

I, the advisor of the thesis entitled "ANFIS Based Fractional-Order PID Speed and PI with Anti-Windup Current Control of Permanent Magnet Synchronous Motor for Electric Vehicle: The Case of ECADO-4EV" and developed Tsion Abebe Muche, hereby certify that the recommendation and suggestions made by the board of examiners are appropriately incorporated into the final version of the thesis.

Prof. Gang Gyoo Jin	____________	September 9, 2021
Advisor	Signature	Date

We, the undersigned, members of the Board of Examiners of the thesis by Tsion Abebe Muche have read and evaluated the thesis entitled "ANFIS Based Fractional-Order PID Speed and PI with Anti-Windup Current Control of Permanent Magnet Synchronous Motor for Electric Vehicle: The Case of ECADO-4EV" and examined the candidate during the open defense. This is, therefore, to certify that the thesis is accepted for partial fulfillment of the requirement of the degree of Master of Science in Control Engineering.

____________	____________	____________
Chairperson	Signature	Date
____________	____________	____________
Internal Examiner	Signature	Date
Dr. Beteley Teka	____________	September 08, 2021
External Examiner	Signature	Date

Finally, approval and acceptance of the thesis are contingent upon submission of its final copy to the Office of Postgraduate Studies (OPGS) through the Department Graduate Council (DGC) and School Graduate Committee (SGC).

____________	____________	____________
Department Head	Signature	Date
____________	____________	____________
School Dean	Signature	Date
____________	____________	____________
Office of Postgraduate Studies, Dean	Signature	Date

ACKNOWLEDGMENTS

First of all, I am grateful to God who always loves me and holds my life by his shoulders. I am also thankful for the knowledge from his cosmic wisdom.

I would like to extend my deepest and most sincere gratitude to my supervisor Prof. **Gang Gyoo Jin** who gave me so much knowledge and support without hesitation and helped me in preparing this document.

I extend my huge gratitude to **Dr. Tefera Terefe Yetayew** for his support and advice about controller design. I would like to thank **Dr. Tafese Asrat** for his helpful advice, for giving me reference papers regarding the Electric Vehicle and document review.

I would like to extend my deepest and most sincere gratitude to PG coordinator **Dr. Milkias Berhanu** and EPCE department head **Mr. Mesfin Megra** for their supports and organize the schedule for Thesis presentation.

Last but not least I am deeply thankful to **Miss Tsion Tigistu** and **Miss Rahel Shirge** for the support as sisterly, friendly and I also wish God to give you peace and prosperity in your life. Finally, I am thankful to my families I don't have the words to express my gratitude. I just wish to live in peace.

TABLE OF CONTENTS

LIST OF TABLES

LIST OF FIGURES

LIST OF ACRONYMS

ANFIS	Adaptive Neuro-Fuzzy Inference System
ASTU	Adama Science and Technology University
BLDCM	Brushless Direct Current Motor
CTVE	Center of Transportation and Vehicle Engineering
DTC	Direct Torque Control
DSP	Digital Signal Processor
ECADO-4EV	Ethiopian Can-Do Four-Wheel Electric Vehicle
EMF	Electromotive Force
EV	Electric Vehicle
FMINCON	Interior-Point Algorithm
FOC	Field Oriented Control
GA	Genetic Algorithm
GA tuned FOPID	Genetic Algorithm tuned fractional-order PID
GA tuned PI	Genetic Algorithm tuned PI
GA tuned PI-AW	Genetic Algorithm tuned PI with Anti-Windup scheme
GA tuned PID	Genetic Algorithm tuned PID
PID	Proportional Integral Derivative
PI	Proportional Integral
IAE	Integral Absolute Error
ISE	Integral Square Error
ITAE	Integral Time Absolute Error
ITSE	Integral Time Square Error
LMI	Linear Matrix Inequality
IGBT	Insulated Gate Bipolar Transistor
IM	Induction Motor
PMSM	Permanent Magnet Synchronous Motor
PSO	Particle Swarm Optimization
SOC	State of Charge
SRM	Switched Reluctance Motor
SVPWM	Space Vector Pulse Width Modulation
VSI	Voltage Source Inverter

LIST OF SYMBOLS

A	Frontal area of the car
B	Friction coefficient
Cr	The coefficient of rolling resistance
G	Gravitational acceleration
I_d	Direct-axis current
I_q	Quadrature current
J	The rotor moment of inertia
K_b	Back EMF constant
K_i	Value of the line-to-line inverter gain
K_f	Current filter feedback gain
K_t	Electromagnetic torque constant
La	Armature inductance
M	Gross mass of the vehicle
$P_{total\ driving\ power}$	Total driving power of the vehicle
P	The number of poles
P_m	Input power of the motor controller
S	Endurance mileage
Ra	Stator resistance
T_e	Electromagnetic torque
T_f	Current filter time delay
T_l	Load torque
T_i	Delay time of the inverter switches
V_{cm}	The maximum control voltage
V_c	Carrier voltage
V_{dc}	The DC link voltage
W_{road}	Energy needed for mileage S
Θ_r	Rotor position
ω_m	Motor speed

ABSTRACT

Electric vehicles (EVs) are an alternative solution for the reduction of air pollution. Apart from the reduction of environmental pollution roles EV has problems with energy efficiency and utilization issues. PMSM is selected for electric vehicle propulsion because of highly efficient than other electric drives even though it's high cost. Since any electric vehicle needs a precise motor speed and current controller which have better dynamic performances. In this research work, both speed and current control of PMSM are implemented. Vehicles are subject to severe disturbances and load variation while driving due to passenger boarding, road conditions, and resistive force which leads to the steady-state error on the actual speed. To mitigate these, ANFIS based FOPID speed controller is implemented. Naturally, electric motors have a high starting current overshoot. PI with Anti-Windup current controller cascaded in speed controller is implemented. To show the performance of the controller, vehicle dynamics (the case of ***ECADO-4EV****), PMSM, and inverter models are done mathematically. The proposed system model is implemented using MATLAB Software. Different controllers are implemented for speed and current controllers of the PMSM motor. Based on the simulation, both ANFIS based FOPID and GA tuned FOPID speed controller has the steady-state error of 0% at no-load condition while GA tuned PID speed controller has a 0.016% steady-state error. Hence every time the vehicle has different loads. In this case, ANFIS based FOPID has better performance during load changes. It has 0% steady-state error whereas GA tuned FOPID and GA tuned PID has 0.005% and 0.1% steady-state error respectively. In addition, GA tuned PI and GA tuned PI with Anti-Windup current controllers are implemented. GA tuned PI-AW current controller has 0.006% overshoot, 0% steady-state error, whereas GA tuned PI has 0.44% overshoot, 0.18% steady-state error. So, the GA tuned PI with Anti-Windup current controller of the PMSM has better performance.*

Key Words: ANFIS; ECADO-4EV; EV; GA tuned FOPID; GA tuned PI; GA tuned PI with Anti-Windup; GA tuned PID and MATLAB Software.

CHAPTER ONE

INTRODUCTION

1.1 Background

The need of human nature to search for new, better, and safe technology from the existing one has been part of routine life since time unknown. The rivalry between car-producing companies and individuals to develop electric vehicle technology over the combustion engine is one of the significant aspects of it. Although the introduction of electric vehicles in time order comes earlier than that of the combustion engine, the drawback it showed like that of the longer duration to charge the battery and the battery lifetime per charge hinder its acceptance and existence in the market. By the time the combustion engine cars seemed more advanced and advantageous because it takes a short time to refuel and can cover long distances per fuel.

With the development of various innovations and the rising concern about environmental pollution, the combustion engine has become a target for global enemies that challenge its contribution to carbon emissions into the atmosphere. This fact leads to the return of the electric vehicle to the market with a significant achievement that overcame its earlier limitations in terms of battery life and range per charge, and, most significantly, it is non – toxic [1][2][3].

An electric vehicle (EV) is a vehicle that is powered by electric energy that is stored in batteries and driven by an electric motor. The popularity of electric vehicles has grown as a result of their quiet operation and low emissions. For decades, internal combustion engines have ruled the streets. It is the source of energy for the vast majority of automobiles on the planet. Nonetheless, technology continues to advance, and with it comes new ground-breaking ideas that have the potential to be revolutionary.

Although electric cars have been around for more than a decade, it is only now, thanks to advancements in specialized technologies, that they are becoming more popular. Burning is an exothermic chemical reaction that requires fuel and oxidants, and it is referred to as combustion. The internal combustion engine is based on this idea, with fuel, air, and a few dozen pieces working together to manage the process. The heat generated by combustion is used to drive a car forward from a standstill. The electric engine, unlike the internal combustion engine, has no moving parts. There are simply a few fundamental components. The cost of maintenance is significantly reduced as a result of this component. Magnetism lies at the heart of the electric engine concept. The battery provides power to the engine, which creates a magnetic force that propels the automobile forward. The electric motor, controller, and battery are the three main components of an electric vehicle. Electric automobiles are much faster than cars with internal combustion engines. This is due to the fact that an electric automobile can develop a lot of torque right away, whereas a combustion engine can only achieve such torque after gaining speed. Electric automobiles are lighter since they do not include kilos of metal.[4].

A tractive motor is the main component used to design the overall system of the vehicle. The speed of EVs is varying time to time due to passengers boarding, road type, and resistive force. So, it needs a tractive motor that has variable speed for driving system. The major requirement of tractive motors that are used to drive EVs are mentioned below [5].

- Very wide speed range including constant-power regions and constant- torque,
- Fast torque response,
- High efficiency over a wide speed and torque ranges,
- Regenerative braking capacity,
- High reliability and robustness for various vehicle operating conditions,
- High fault-tolerance,
- Power converter technology,
- less periodic cost,
- high-power density and High instant power,
- High torque at low speeds for starting and climbing, and high power at high speed for cruising.

To design the overall EVs system, it needs different components such as an electric motor, controller, inverter, convertors battery, and charging module. The tractive motor used for driving EVs should satisfy the major requirement mentioned above. To give sufficient power to drive the vehicle, to overcome the resistive force acting on the vehicle, and the force due to load change during passenger boarding. So, the tractive motor that chosen is used for the propulsion system should be effective and efficient. PMSM, IMs, and DC motors have been widely used to drive EVs [6].

PM motors have permanent magnets in the rotor part. Due to this, there is no additional copper loss in the rotor leads to higher efficiency than IMs. It has less overall weight due to the absence of rotor winding than DC and IMs motors, high torque to inertia ratio, less maintenance cost due to no rotor winding, and high-power density. It has better performance in the field weakening region. Due to the above-mentioned advantages, PMSM has been widely used for variable speed drive applications like in an electric vehicle and industry [7][8].

Based on stator winding and current waveform, PM motors can be classified as brushless DC (BLDC) motors and permanent magnet synchronous motors (PMSM). PMSM has distributed winding (more than one slot) makes to produce sinusoidal back EMF and current waveform. BLDC has concentrated winding in the stator part of the motor. It has square back EMF and current waveform. It leads to produce current harmonic, torque ripple, and noise.

The control mechanism of PMSM can be divided into two: Scalar and Vector control methods. The Scalar control method is simple and implements easily. In Scalar control method there is no feedback control signal. It is an open-loop system that leads to present system instability whereas the Vector control method has a feedback control signal that leads to the system has better performance. There are two types of vector control methods such as DTC and FOC control. In DTC, it needs only one parameter, the stator resistance. It's simple to implement. There is no current control in the DTC vector control technique [9].

The FOC includes controlling the stator currents represented via way of means of a vector. This manage is primarily based totally on projections that rework a three-phase time and speed-structured version right into a -coordinate (d and q coordinates) time-invariant model. These projections cause a shape much like that of a DC system manage. FOC machines want constants as enter references: the torque component (aligned with the q co-ordinate) and the flux component (aligned with d co-ordinate). As FOC is honestly primarily based totally on projections, the manage shape handles on the spot electric quantities. This makes the manage correct in each running operation (steady-state and transient) and impartial of the constrained bandwidth mathematical version. In FOC impartial manage of torque and flux, much like DC motor [10].

This research work is done based on the FOC techniques of speed control of PMSM. It is a non-linear, multivariable, time-varying system. It is subjected to unknown disturbance and variable parameter variation. In this research work, GA tuned fractional order PID (FOPID) speed controller of PMSM is implemented and also ANFIS controller has designed during disturbance applied. To reduce the starting current of the motor, GA tuned PI with Anti-Windup technique current cascaded in speed control of PMSM for ECADO-4EV electric vehicle is proposed. For comparison, GA tuned PI current cascaded in GA tuned PID speed controller of PMSM is also discussed. The proposed control and drive systems will be implemented and simulated by using MATLAB software tool.

1.2 Statement of the Problem

The vehicle that needs gasoline and petrol is one of the sources of air pollution in the environment and not suitable for human beings and also combustion engine vehicle is not suitable to the environment. To improve these problems, gasoline-based vehicles have to be replaced by electric vehicles (EV). The major issues of EVs are Energy utilization and minimal power requirements for propulsion. The electric motor is one of the design components of EVs. There are different types of electric motors used to drive electric vehicles.

For this work, PMSM is selected to drive the electric vehicle because of having less torque ripple due to having distributed winding in the stator part of the motor leads to less noise, lighter weight due to no rotor winding, no rotor winding no additional copper loss in the rotor part, better efficiency, and less periodic maintenance makes to increase the life span of the vehicle.

The rotor part of the PMSM is made up of permanent magnet (PM) materials, the PMs materials may be accidentally demagnetized due to high ψ_{ar} and high operating temperature during operation because of PMs properties are temperature dependant [6]. To overcome this, the motor should be designed properly and select an appropriate magnetic material with a suitable operating temperature. The PMSM has a highly nonlinear characteristic because the rotor is made of a permanent magnet (PM). This makes the developed torque nonlinear. It has a nonlinear relationship between the winding current and rotor speed. As a result, the linear PID controller may have difficulty in speed control. Since any electric motor may have a high current at starting, this may lead to heating of the motor stator windings. In the case of electric vehicles, the motor's speed and current dynamic performance characteristics are critical.

To mitigate the problems mentioned above, GA tuned fractional-order PID (FOPID) speed controller of PMSM is discussed whereas ANFIS controller has also design during disturbance applied. To reduce the starting current of the motor, GA tuned PI with Anti-Windup technique current cascaded control of PMSM for ECADO-4EV electric vehicle is proposed. For comparison, GA tuned PI current cascaded in GA tuned PID speed controller of PMSM is also discussed. The proposed controller and drive systems will be implemented and simulated by using MATLAB software tool.

1.3 Objective the Study

1.3.1 General Objective

To design ANFIS Based Fractional-Order PID Speed and PI with Anti-Windup Current Control of Permanent Magnet Synchronous Motor for Electric Vehicle: The Case of ECADO-4EV

1.3.2 Specific Objectives

The specific objectives of this research are:

- To analyze the vehicle dynamic and select the appropriate rated motor for the driving system.
- To model the entire system using MATLAB/Simulink software
- To compare and evaluate different speed controllers according to error evaluation, a system performance criterion and select the suitable speed controller.
- To compare and evaluate different current controllers according to error evaluation, a system performance criterion and choose the efficient current controller.
- To select suitable, optimal and efficient speed and current controller of PMSM based on system performance evaluation.
- To draw conclusions and recommendations.

1.4 Motivation of the Study

To replace IC-based cars with EVs is the current research idea in the world and our country due to the air pollution and wastage of energy. The battery technology is getting better from time to time, which gives hope for EVs' easy use and prospect. Some firms, such as Marathon Motors Engineering plc, Tom Tadas, and Solari's, are now planning to produce electric vehicles in our country, and there is also a transportation and automotive engineering center at Adama Science and Technology University (ASTU) since 2017. The members of this institute have proposed the EVs known as “ECADO-4EV”. which is named by prof. Yong. Joo Kim. He was the director of CTVE at that time, according to him ECADO-4EV means “Ethiopian can do four-wheels Electric Vehicle”.

The vehicle's drivetrain should be correctly designed and modeled. The PMSM was chosen to propel the vehicle because of its higher efficiency, smaller weight, lower noise, and lower maintenance requirements, resulting in a longer lifespan. The rotor component of the PMSM has no winding, which helps to minimize the overall weight of the vehicle.

1.5 Limitations of the Study

This research only focused on designing and analyzing the system modeling on MATLAB software in Simulink and code. To implement the system modeling practically, it needs different components. The components are the PMSM, three-phase inverter, DC power supply, and digital signal processing (DSP) kit. Unfortunately, these components do not easily accessible in our country. Due to these problems, the prototype implementation of the system could not be conducted.

1.6 Significance of the Study

The primary significance of this research work in Ethiopia is to transfer technology. for ASTU Center of Transportation and Vehicle Engineering (CTVE) and E-Bajaj center of excellences are very important because the members are trying to design and develop their EVs for the Ethiopian market.

1.7 Thesis Organization

This thesis work is organized into six chapters as follows

Chapter one: The introduction of the research work, statement of the problem, the aims of the research including the general objective and specific objective of the research, limitation, motivation, and significance of the study are discussed.

Chapter two: In this chapter, advantages of PMSM than others is discussed, related work about speed control of PMSM is also discussed

Chapter three: This chapter is included, the methodology that followed in this research work, the design part of the proposed system. design and analysis of electric vehicle dynamics based on the overall resistive force exerted on the vehicle. The Drive system, battery specification, gear ratio, inverter topology, and switching techniques are also discussed.

Chapter four: This chapter is discussed about design of cascaded speed, current controller, and its implementation for PMSM. GAs optimization tool is also discussed.

Chapter five: This chapter included the simulation result of the park and Clark's transformation. Design and comparison of speed and current controller of the PMSM using graphically and in table form.

Chapter six: It is the final chapter. It discussed the conclusion of the overall thesis work and recommends additional possible research directions to the future based on the discussion of the previous chapters.

CHAPTER TWO

LITERATURE REVIEW AND RELATED WORKS

2.1 Chapter Overview

In this chapter, an overview of vehicles is present. different types of electric motors that are used for driving EVs are discussed. The advantages of PMSM over others motors are discussed, and closely related works regarding the speed and current control of PMSM with their drawback also discussed.

2.2 Electric Vehicles

There are different types of vehicles that have been proposed such as ICEVs EVs, pure EVs, and hybrid EVs. Among them, EVs are the current attractive technology that has zero emissions of CO_2 and has no harmful gases generates to the environment. EVs can collect kinetic energy from braking and use it to recharge the battery, but ICEVs waste this kinetic energy as heat in the brake discs. The energy efficiency of electric vehicles can be increased by up to 10% using this regenerative braking technique. ICEVs are responsible for more than half of all dangerous air pollutants and smog-forming chemicals in many cities. The usage of electric vehicles (EVs) is the most viable option for reducing air pollution from road transportation [6][5].

As battery costs fall and power density rises, the percentage of electric vehicles on the road is continuously increasing. The motor for vehicle driving should have a strong beginning torque and deliver a lot of power at high speeds. In comparison to electric motors, internal combustion engines (ICEs) have a restricted operating range. ICEs, for example, cannot produce torque at zero speed and lose efficiency rapidly as speed increases. Gear shift and slip mechanisms are used to overcome these limitations. Electric motors, on the other hand, have a high beginning torque and can operate at a wide speed range. In most cases, electric motors are employed without a gear shifting system [7][11].

2.3 Electric Motor Varieties

High power density, short-time overload capability, a wide constant power speed range (CPSR), high efficiency, and robustness are all requirements for EV motors. High power density and efficiency are the most significant properties that a propulsion device should have, according to the specifications. Based on driving cycles, the overall efficiency must be assessed. As a result, an EV motor must be optimized in a highly used location. However, increasing efficiency while reducing material costs and size is not straightforward [12][6].

The dc motor, induction motor, permanent magnet synchronous motor, and switching reluctance motor are some of the major types of electric motors used or under consideration for electric vehicles. Among them, The PMSM is frequently machine that choice due to its high efficiency because of no rotor winding, no additional copper loss, absence of commutator leads to no frequent maintenance during operation, and high power density [13][14]. Figure 2.1 shows, classification of electric motors based on the power source and their behaviors.

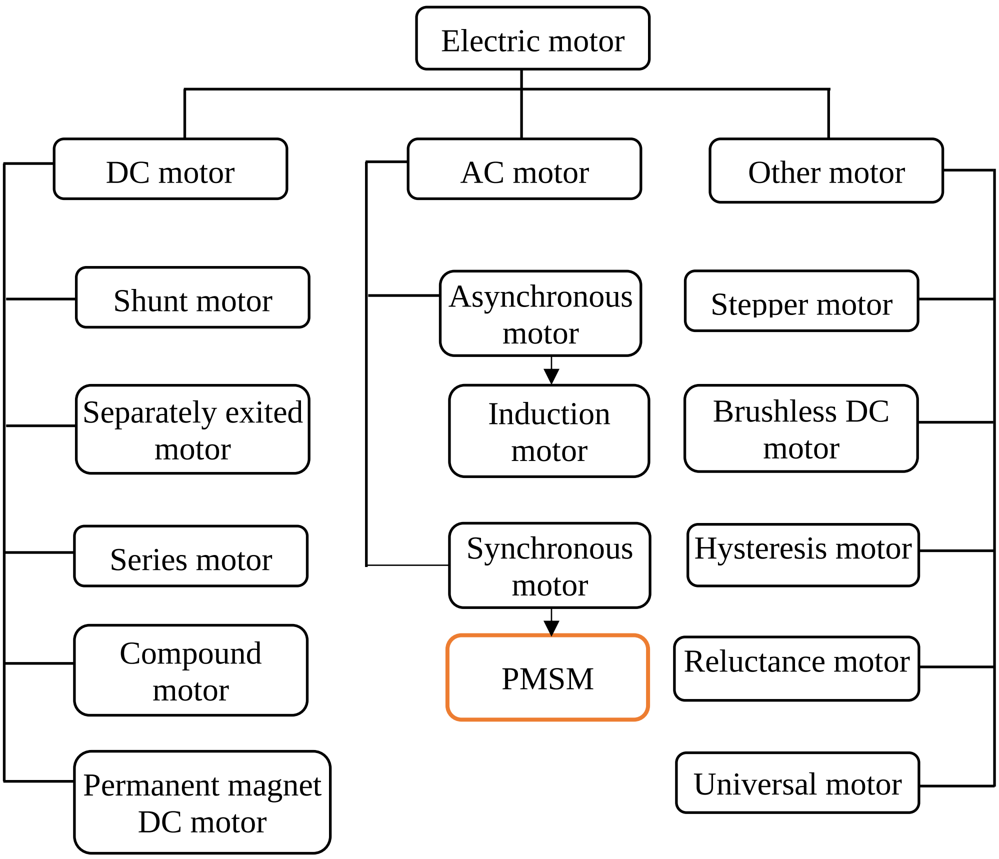

Figure 2.1 Classification of drives based on source and their behavior [13][14]

2.3.1 Comparison of Electric Motors based on Their Performance

Electric vehicles are propelled by a variety of electric motors. However, due to flaws in some of their characteristics, not all types of motors are equally used. Because of the advantages and disadvantages of electric motors, not all electric motors are employed equally for electric propulsion. The comparison explains how it may be generally accepted in comparison to other types for usage in electric vehicles as well as most other applications. In addition, the comparison demonstrates how the PMSM as the potential to replace all other types due to its wide range of benefits and ability to be used in practically all applications that demand a motor with only a simple drive system. Table 2.1 shows, comparison of electric motors based on their performance.

Table 2.1 Advantage and disadvantage of Electric Motors used for EVs [15][16][17]

Electric Motor	Advantage	Disadvantage
DC Motor	Maximum torque at low speed Good controllability Linear torque current curve Low torque ripple	Bulky structure Low reliability Requires maintenance Low overloading capability Low heat dissipation
IM	Excellent dynamics with proper control High-speed operation possible Less price and simple construction Durable Several suppliers available	Complicated control Always lagging power factor Low efficiency with lighter loads
SRM	Have simple and rigid construction High fault tolerance Excellent torque-speed Wide constant power region High starting torque High torque-inertia ratio	High noise High torque ripple Need special converter topology Have an electromagnetic interference Complex control mechanism

BLDC	High power density and torque-to-inertia ratio Good heat dissipation good overloading capability	Expensive Torque ripple The danger of demagnetization of the magnets Poor field weakening
PMSM	Smooth torque possible High efficiency High torque/volume High pull-out torque is possible Good heat dissipation Good overloading capability Good field weakening	Expensive The danger of demagnetization of the magnets

2.3.2 Permanent Magnate Motors

Based on stator winding structure, permanent magnet motors can be classified as BLDCM and PMSM. PMSM has sinusoidally distributed winding whereas BLDC motor has concentrated winding in the stator part of the motor. Based on the above definition, PMSM does not have torque ripple leads to better in field weakening operation (the motor-operated above base speed) and high-speed range application than BLDC motor. Nowadays both motors have been used for electric vehicle propulsion systems. However, BLDC motor has trapezoidal Back EMF leads to high torque ripple corresponding to increase speed of the motor. Table 2.2 and 2.3 shows, the comparison of PMSM with other motors[17][18].

Table 2.2 Advantage of PSMM over others [17][18]

Advantages of PMSM over DC motor	Advantage of PMSM over induction motor
Less audible noise	Higher efficiency
Longer life	Higher power factor
Less frequent maintenance	Higher power density
Sparkless (no fire hazard)	Light-wight
Higher speed	No rotor loss due to no rotor winding
Better heat transfer	Higher flux densities
Higher power density and smaller size	No-slip power loss

Table 2.3 Comparison of the PMSM with BLDC motor [18]

PMSM	BLDC motor
It uses AC power source	It uses DC power source
It has sinusoidal back EMF	It has trapezoidal back EMF
No torque ripple present	Higher torque ripple due to trapezoidal back-EMF
It is used for higher power applications (Electric vehicle (EV), industrial drives, and others)	It is used for small power/ low-cost drives <5kW (home appliance, blowers, and others)
It has less noise operations	Due to torque ripple present, it has relatively more noise operation
Higher efficiency, higher torque	Less efficient, lower torque
No rotor loss due to no rotor winding	No rotor loss due to no rotor winding
High cost but high performance	High cost but high performance
High starting cost but no frequent working maintenance	High starting cost but no frequent working maintenance
There is no rotor winding, there is no rotor copper (I^2R) loss	There is no rotor winding, there is no rotor copper (I^2R) loss

2.4 Control Mechanism of PMSM

Scalar and Vector control methods can be found in PMSM's control mechanism. The scalar control mechanism is easy to understand. However, it is ineffective for system performance, whereas PMSM's Vector control approach performs better. Currently, the vector control approach is used. It's crucial to manage the flux and torque of the PMSM independently. Scalar control is working based on steady-state response. The controlled variables' amplitude and frequency are taken into account. The amplitude and position of a controlled space vector are taken into account in vector control. These correlations hold even during transients, which is critical for PMSM to maintain exact torque and speed control Some of the control techniques are shown in Figure 2.2 [9][10].

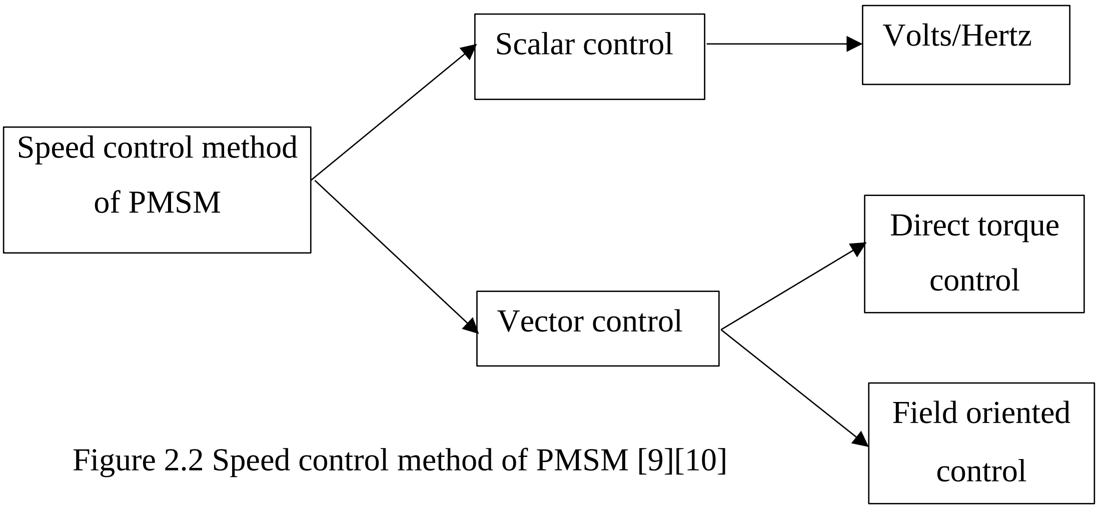

Figure 2.2 Speed control method of PMSM [9][10]

2.4.1 Scalar Control

The scalar control technique is primarily based on relationships valid in steady-state. Only magnitude and frequency of voltage and current are controlled. Scalar control is used where in several motors are driven in parallel through the same inverter [19][10]. The most important concept of this method is a variation of the supply voltage frequency abstractedly from the shaft response (position, angular speed).

The magnitude of the supply voltage is changed consistent with the frequency in a constant ratio. Then the motor is in the condition, where in the magnetic flux represents the nominal value and the motor is neither overexcited nor under excited. The method uses an open-loop control technique without any feedback on motor parameters or their position. This makes the scalar control method easy to implement and with low demands on the computation power of the control hardware. On the other side, the big disadvantages are the speed dependence on the external load torque, mainly for PMSM, and decreased dynamic performance [20].

2.4.2 Vector Control

The problem with the scalar control method is that in which the motor flux and torque are coupled. This inherent coupling affects the response and makes the system prone to instability if it is not considered. In vector control, not only the magnitudes of the stator and rotor fluxes are considered but also their mutual angle. Generally, the vector control of PMSM allows separate control of both the flux and torque. Hence, achieving a similar control structure to that of a separately excited DC machine [21].

2.4.2.1 Direct Torque Control

The principle of Direct Torque Control (DTC) is to directly select voltage based on the difference between the reference and actual value of torque and flux linkage. Torque and flux errors are compared in hysteresis comparators.

The advantages of DTC are low complexity and that it only needs to apply one motor parameter, the stator resistance. The system possesses proper dynamic performance however indicates pretty poor performance in steady-state for the reason that crude voltage selection criteria give rise to high ripple levels in stator current, flux linkage, and torque. Its simplicity makes it possible to execute every computational cycle in a short time and use a high sampling frequency [9].

2.4.2.2 Field Oriented Control (FOC)

To achieve higher dynamic performance, a greater complicated control scheme desires to be applied to control the PMSM with the mathematical processing power supplied through the DSP advanced control techniques can be implemented, which uses mathematical transformations to decouple the torque generation and the magnetization functions in the PMSM. Such decoupled torque and magnetization control is commonly known as rotor flux-oriented control (FOC). The vector manipulates of currents and voltages will become on top of things of the spatial orientation of the electromagnetic fields withinside the system and has caused the call subject orientation control. FOC generally refers to controllers which keep an electric powered attitude among rotor and stator field components [22].

The FOC consists of dominant the mechanical device currents delineate by a vector. This management is predicated on projections that remodel a three-phase time and speed-dependent model into a two-coordinate (d and letter coordinates) time-invariant model. These projections result in a structure like that of a DC machine management. FOC machines would like 2 constants as input references: the torque element (aligned with the letter q co-ordinate) and the flux element (aligned with d co-ordinate). As FOC is solely supported based on projections, the control structure handles instant electrical quantities. This makes the control precise in each operating operation (steady-state and transient) and freelance of the restricted information measure mathematical model.

Thus, the advantages of FOC:

- Transformation of a complex and coupled AC model into a simple linear model
- Independent control of torque and flux, similar to a DC motor

- Fast dynamic response and good transient and steady-state performance
- High torque and low current at startup
- High Efficiency
- Wide speed range through field weakening

Because of the above advantages and others, this research work is done based on the FOC techniques of speed control of PMSM.

2.5 Related Works on Speed Control of PMSM Motor

At different times, many researchers conducted different types of research for EVs. They also studied how to design speed controllers of PMSM for different applications and EVs. The authors in [17] are proposed a “review of speed controller of the PMSM by using A hybrid differential artificial bee colony algorithm-based tuning of fractional order (HDABCA) controller”. An artificial bee colony algorithm optimizes the fractional-order PI (FOPI) controller parameters and compares the simulation result of FO-PI optimized. By using differential evolution (DE), Artificial Bee Colony (ABC), and hybrid differential Artificial bee colony algorithm (HDABCA) based on the objective function (IAE, ISE, ITAE, and ITSE) and rising time, settling time, Peak overshoot, and steady-state error of the system comparison. However, the authors at the design time, did not consider the parameter variation such as speed variation and how they can improve it. Moreover, they did not discuss the system's internal current loop controller to limit the starting current overshoot.

The authors in [18] also proposed a “Review of speed control of PMSM by using intelligent, direct torque control (DTC) technique for Permanent Magnet Synchronous Motor (PMSM) drive based on Adaptive Neuro-Fuzzy Inference Systems (ANFIS)”. This paper also improves the rising time, settling time, peak overshoot, and steady-state error. Moreover, also it considered when the system variation occurs and how to overcome it. However, they did not discuss the internal current control loop of the motor, and also, they didn’t discuss the system performance during a disturbance applies.

The authors in [23] presented “speed control of PMSM using Fuzzy with PID controller”. They present a comparison of PID controller and fuzzy-PID controller. The PID speed controller of the PMSM has 2.5% overshoot and 0.2 settling time, whereas Fuzzy with PID controller has 2.4% overshoot and 0.05 settling time. But they didn’t discuss the steady-state error of the system. They didn't discuss how it can improve for the problem, like when the sudden load change, disturbance, and starting current overshoot are occurring.

The authors in [24] proposed a research work entitled "Adaptive Nero-Fuzzy Inference System Based Field Oriented Control of PMSM and Speed Estimation". They discussed and compared the adaptive neuro-fuzzy inference System with model reference adaptive control systems based on field-oriented control techniques. The system is simulated at a constant speed and variable speed. They try to analyze the system performance using the Performance parameters criterion as shown in Table 2.4. The simulation shows, still the system has a sluggish process. They didn't discuss the system performance during a disturbance or load variation which means they only focused on no-load conditions and also, they didn't mention the current regulator mechanism. The drives that used for industrial and EVs application needs current regulator (controller).

Table 2.4 System performance analysis of PMSM using different controllers [24]

Speed type	Controller type	Performance criterion			
		t_r (ms)	t_s (sec)	M_p (%)	e_{ss} (%)
Constant speed	MRAS	0.0001	0.01	10	0.3
	MRAS	0.0001	0.009	9	5
Variable speed	ANFIS	0.0001	0.01	2	8
	ANFIS	0.0001	0.02	2	5

where t_r, t_s, M_p and e_{ss} are rise time, settling time, maximum overshoot, and steady-state error respectively. The result shows ANFIS controller has better system performance than MRAS controller.

The authors in [25] presented a research work entitled "Fuzzy-PI control for speed control of PMSM". They discussed and compared Fuzzy-PI with PI speed control of PMSM based on indirect field-oriented control technique. The result shows Fuzzy-PI has better performance than PI controller. They didn't discuss the system performance during a disturbance or load variation which means they only focused on no-load conditions and also, they didn't mention the current regulator mechanism.

The authors in [26] proposed a research work entitled "Speed Control Based on Adaptive Neuro-Fuzzy Inference System for Permanent Magnet Synchronous Motor". They discuss

(PID) controller based on Adaptive Neuro-Fuzzy inference system (ANFIS) speed control of PMSM. They discussed and compared Artificial intelligence (ANFIS) with PID speed control of PMSM. The system is simulated at no-load and load conditions. They try to analyze the system performance using the Performance parameters criterion. The result shows ANFIS based PID controller has better system performance than others which has 0.2508sec settling time, 0.0761sec rise time, 0% maximum overshoot, and 0% steady-state error at no-load and 0.4581sec settling time, 0.0781sec rise time, 6.6844% maximum overshoot and 0.4892% steady-state error during load applied whereas IMC-PID controller has 0.3983sec settling time, 0.2191sec rise time, 0% maximum overshoot and 0% steady-state error at no-load and 0.5198sec settling time, 0.3064sec rise time, 20.3046% maximum overshoot and 07897% steady-state error during load applied. In this research work also, there is no current regulator discussion.

Based on the reviewed literature in this section, the authors didn't discuss the internal current of the drive and how to improve it. Hence, naturally electric motor has a high starting current that leads to heat the motor winding and burning of the internal circuit. So, the current controller is cascaded with a speed controller is needed to regulate the starting current of the motor. This research work focused on the design and analysis of speed controller cascaded in current control. Disturbance rejection test, set-point tracking test, and Effect of disturbance on the speed of the motor were also presented.

CHAPTER THREE

MATERIALS AND METHODS

3.1 Chapter Overview

This chapter discusses the methodology that has been followed in this research work, Specification Data of the electric vehicle (the case of ECADO-4EV) and tractive motor are presented. design and analysis of vehicle dynamics based on the parameter specification of the selected electric vehicle are discussed. The design and modeling of the tractive motor are presented. Inverter topology and switching technique (SVPWM) that is used to ‘on’ and ‘off’ the three-phase inverter is also discussed in this chapter.

3.2 Materials Used

This thesis work uses different software such as MATLAB/2019b, Microsoft office 2019, MathType 6.0 equation, Mendeley, and Diagrams.net. MATLAB is the computing software that consists of technical toolboxes and Simulink. When the system is not implemented on hardware due to scarcity of some material, system simulation needs to understand how the system works. Microsoft office is one of the application software used for formatting the thesis documentation. Since writing equations and formulas on Microsoft office word are time-consuming tasks, MathType 6.0 is used. It is used to add a new equation editor on Microsoft and PowerPoint. Mendeley is software. It is installed on the computer, which automatically inserts citations of the reference paper and Bibliography. Diagram net is also an online diagram and flowchart maker. It is used to draw the diagram that is not easy to draw on Microsoft office word.

3.3 Methods

Figure 3.1 shows, the progress that follows when to finish this research work. Closely reference papers are reviewed. Related information is collected from Marathon Motors Engineering. It is found in Addis Abeba, Ethiopia. Parameter specifications of an electric vehicle are collected from ECADO_4EV documentation. It was proposed in ASTU center of transportation and vehicle engineering (CTVE). It was proposed since 2017. The parameter specification of an electric motor is collected from websites [L1] and literature. Specification of mechanical transmission and battery sizing are collected.

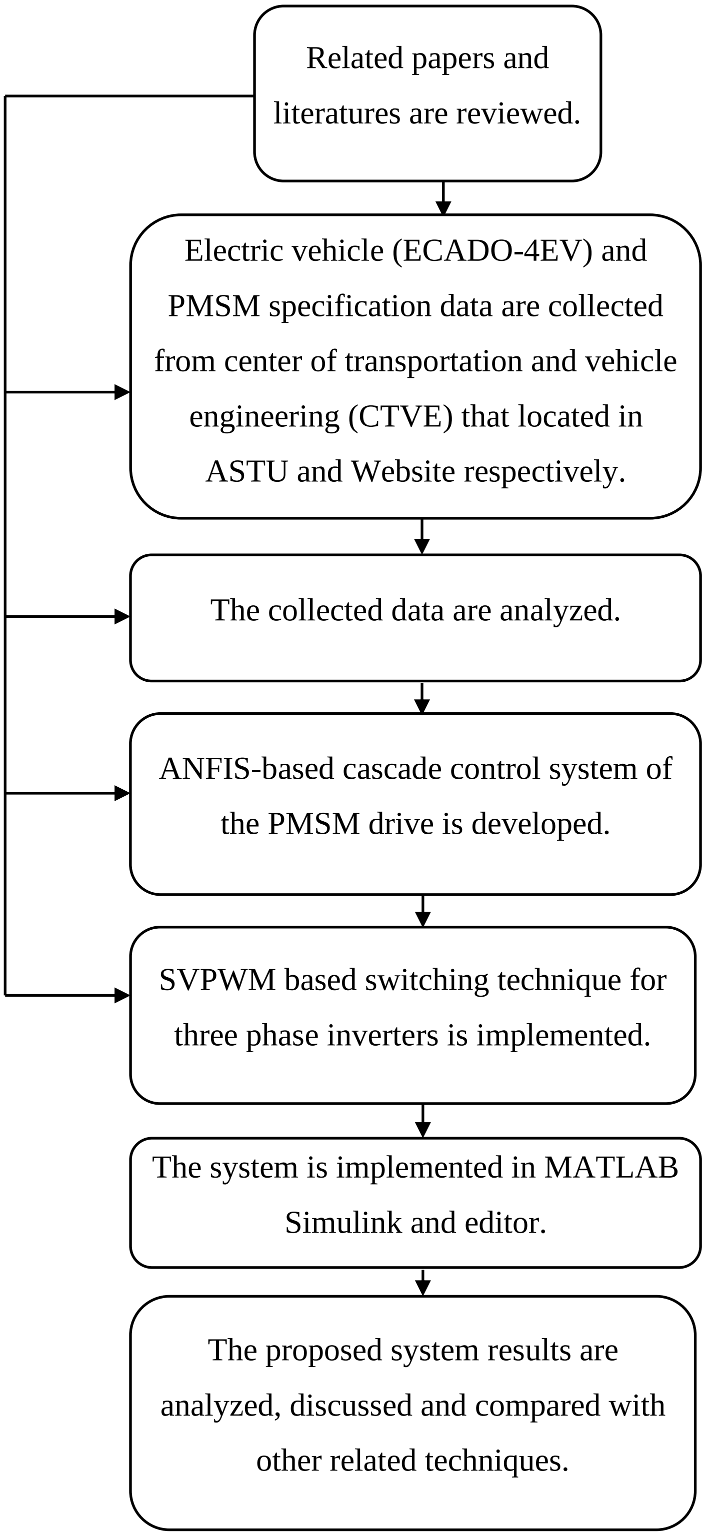

Figure 3.1 Steps of the research work

3.4 The Overall Block Diagram of the Proposed System

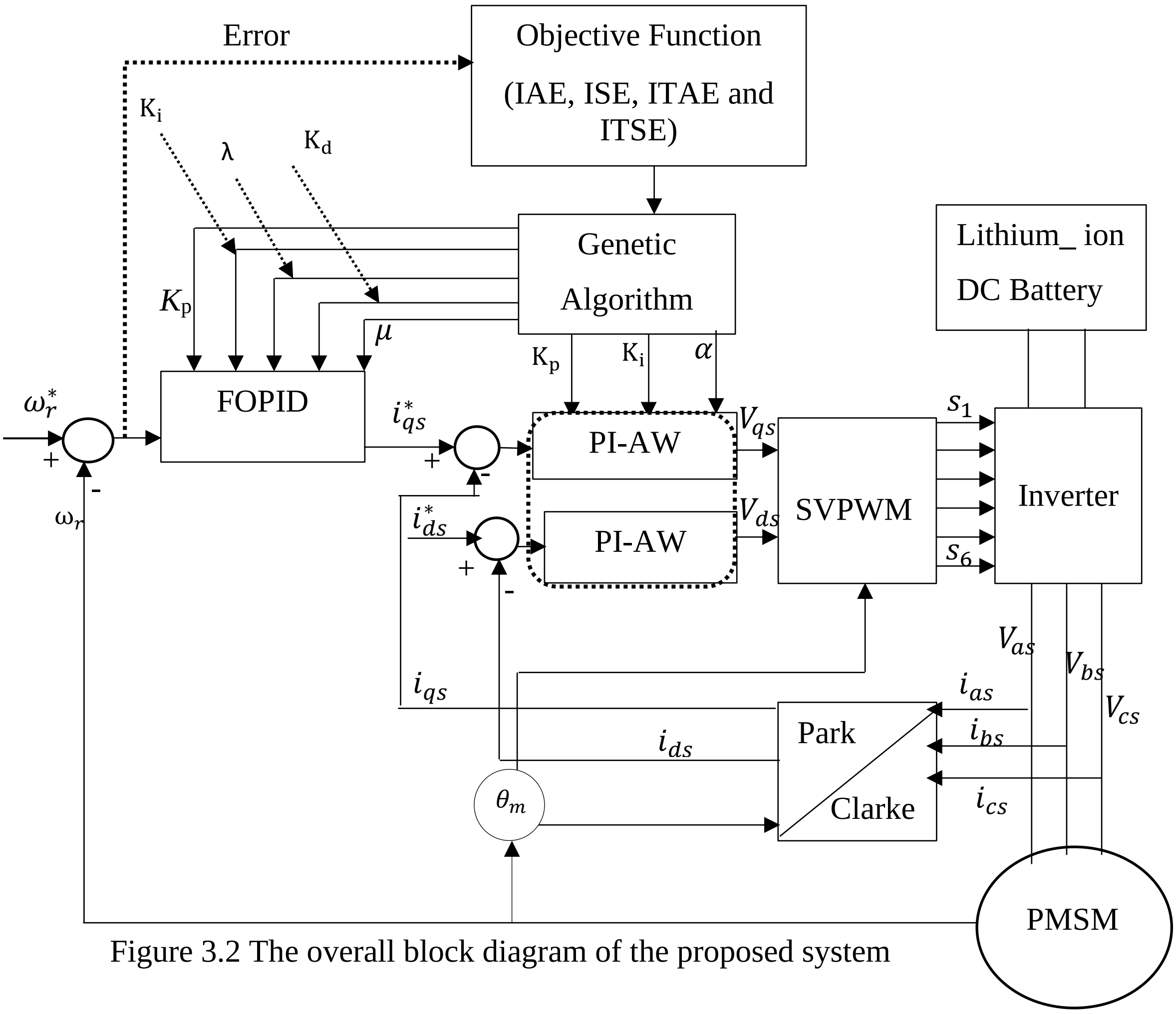

Figure 3.2 The overall block diagram of the proposed system

Figure 3.2 shows, the overall block diagram of the proposed system. The value of the error is the difference between the desired (ω_r^*) and actual (ω_r) speed. The error is the input of the speed controller. The speed controller (FOPID) is used to minimize the magnitude of the error value based on the objective function (ISE, IAE, ITSE, and ITAE). It has five parameters which are tuned using GAs optimization technique. Here, FOPID controller is present for speed control of the PMSM which is used as a primary controller, and ANFIS controller is used for error training during speed error variation which is discussed at the end of this chapter whereas PI-AW current controller is used as a secondary controller. The speed controller output is used as the reference or input to the current controller. Naturally, the electric motor has a high starting current. This leads to overheating of the internal circuit, and burn it. To mitigate this, an internal current regulator should be used. In this research work, GA tuned PI with an Anti-Windup scheme current controller of PMSM is used. The current controller output is voltage in dq reference frame. SVPWM is used for 'on' and 'off the inverter. The tractive motor is getting power from the rechargeable lithium-ion battery. The electric energy stored in the battery is a DC source. But AC motors are used AC source. The inverter is used to convert the DC source to an AC source. To reduce the complexity of the equation and implement it easily, the three-phase components should be transformed into two-phase components. Clark transformation is used to convert the three-phase system to two phases (αβ) rotating frame whereas Park transformation is used to convert two-phase (αβ) rotating frame to dq reference frame. θ_m is directly measured from the motor shaft that means the system is works based on a direct field-oriented control technique.

3.5 Electric Vehicle Dynamic Analysis

"An entire electric vehicle mainly included the DC battery, power converter, electric motor, controller, and mechanical transmission. DC battery is used as an energy source. It is recharge from mains electric city via a plug and battery charging unit that can be either carried on board or fitted at the charging point. The controller is to maintain the power provided to the electric motor and hence the vehicle speed in forward and reverse direction. The electric motor is used for drive the EVs, and the mechanical transmission system is used to increase or decrease the speed and torque of the tire of the electric wheels [27] ".

In this research work, the energy source is the lithium-ion battery, the electric motor is PMSM due to the advantages of light-weight, better efficiency and also used for high power application such as for Electric Vehicles and industrial drives than others motor, the mechanical transmission is used as a bridge between the wheel of the vehicle and the Motor shaft. It is increased or reduced the vehicle's speed based on the speed of the wheel and electric motor.

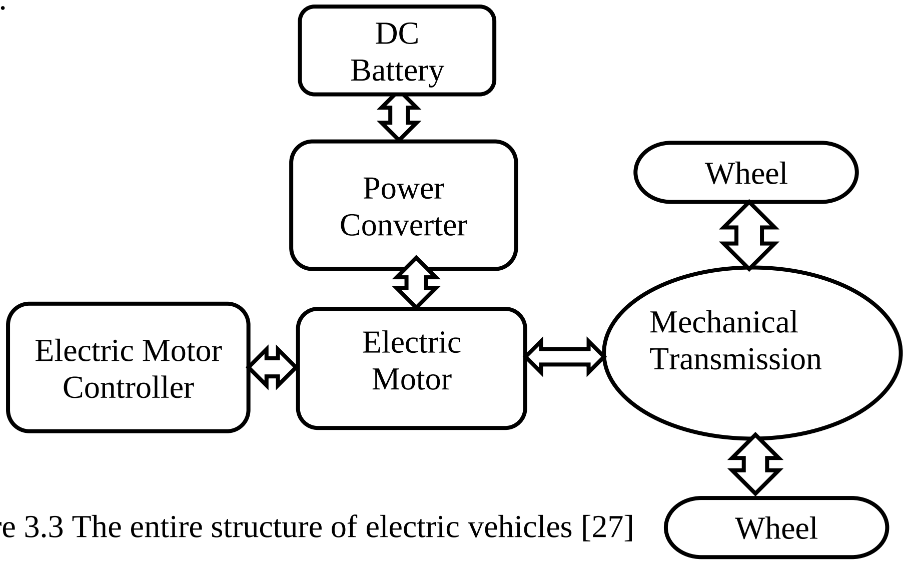

Figure 3.3 The entire structure of electric vehicles [27]

3.5.1 Vehicle Dynamic and Power Required to ECADO_4EV

In this section, the analysis of vehicle dynamics is calculated. To select the appropriate electric motor that is used to drive the vehicle, first find the desired performance of the electric vehicle and parameter specification the vehicle. Then calculate all force exerted on the vehicle when it is in motion. To design the overall system of the electric vehicle, the selection of traction motor and battery is a very important step that requires special attention [28].

The net force from the wheel is the summation of motor torque, the gear ratio, and motor efficiency. The net force or tractive force should overcome the total force exerted on the vehicle when it is in motion. So, it depends on the motor power, gear ratio, and radius of the wheel. The motor parameter specification such as the minimal power of the motor and the speed of the motor is selected based on the total power of the vehicle that is used when it is in motion. The total power or driving power is calculated from the total force exerted on the vehicle when it is in motion and the vehicle's speed. So, to find the total power that is for the propulsion system, the total resistive force exerted on the vehicle must be analyzed and calculated [29]. The total force or the road load consists of:

$$F_w = F_{ro} + F_{cl} + F_{ar} + F_o \tag{3.1}$$

where F_w is the total force or road load, F_{ro} is the rolling resistance force, F_{cl} is the hill-climbing (consider as resistive) force whereas Downgrade (consider as applied) force, F_{ar} is aerodynamic drag force and F_o is the summation of other forces exerted on the vehicle. It is taken by assumption.

3.5.1.1 Rolling Resistance Force

The rolling resistance force is the force that resists the motion of the vehicle which opposes the rolling of the wheel. This force is presented due to the friction of the vehicle’s tire with the contact surface of the road. The tractive force produces by the motor should overcome the force that opposes the vehicle when it is in motion. To minimize this force, the tire should be smooth if it is possible [28][29]. It is depending on the mass of the vehicle, the type of the road, and the gradient (also called slope, incline, pitch, or rise) angle of the vehicle to horizontal.

$$F_{rolling} = F_{normal\_force} \times C_r \times \cos(\alpha) \tag{3.2}$$

$$F_{rolling} = 1500kg \times 9.81\frac{m}{s^2} \times 0.01 \times \cos(26^0) = 132.12272N \tag{3.3}$$

$$\mathrm{P}_{rolling} = F_{rolling} \times speed(\frac{m}{\sec}) = 132.12272N \times \frac{100m}{3600\sec} = 3.673kW \tag{3.4}$$

where M is the mass of the electric vehicle (ECADO_4EV) platform in kg, α is the gradient angle in rad, g is the acceleration due to gravity in m/s^2, and C_r is the tire rolling resistance coefficient. It depends on the type of the road, the type of tire, and the tire pressure of the vehicle. Figure 3.4 shows, the total resistive force exerted on the vehicle when it's in motion.

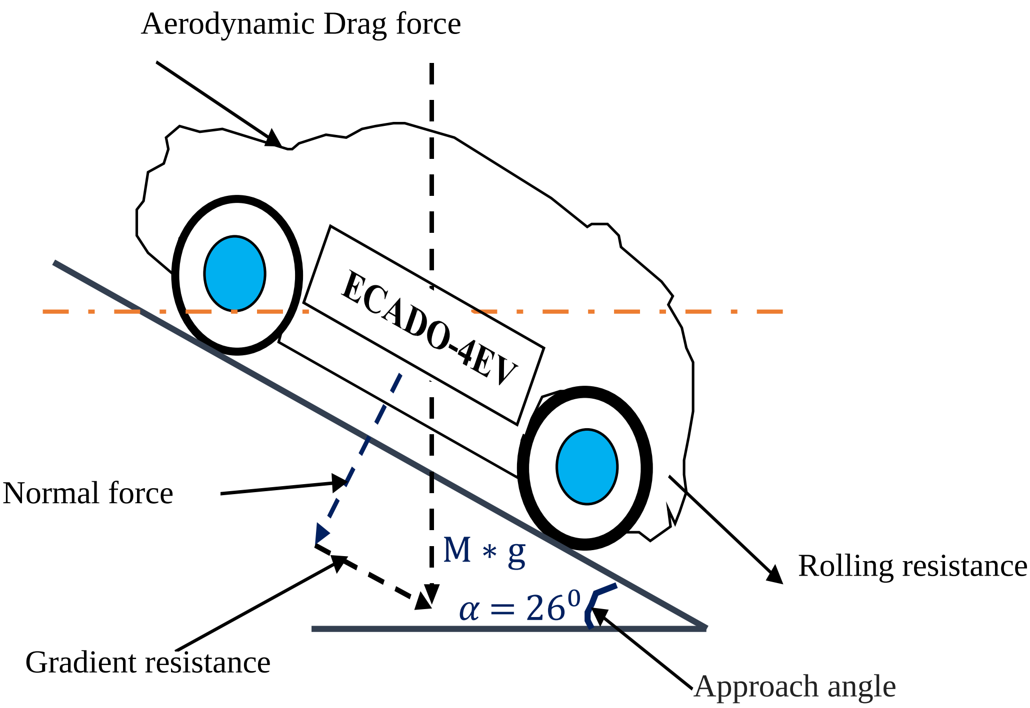

Figure 3.4 The resistive forces exerted when the vehicle is in motion

Table 3.1 Friction coefficients for different types of surface [30].

Contact surface	Coefficient of friction
Concrete surface (good/fair/poor)	0.010/0.015/0.02
Asphalt (good/fair/poor)	0.012/0.017/0.022
Snow/dirt	0.025/0.037
Mud (firm/medium/smooth)	0.037/0.09/0.15
Grass (firm/soft)	0.055/0.037
Sand (firm/soft/dune)	0.060/0.15/0.3

3.5.1.2 Downgrade and Hill-Climbing Resistance Force

The Hill _Climbing resistance force with negative operational sign and the Downgrade force with positive sign are exist when the vehicle is moving up or down on the hill _climbing surface respectively. This force depends on the mass of the vehicle, gravity, and the inclination angle of the vehicle to the horizontal. When the vehicle moves on the flat road, the inclination angle becomes zero. So, the Hill _Climbing force is zero. The speed of the vehicle that used in Equation 3.7 is assumed 51.444Km/hr. The speed of the vehicle and the torque is inversely proportional. So, to maintain the torque of the vehicle, the speed of the vehicle should be reduced. Figure 3.5 shown, the relationship between the power of the vehicle and the inclination angle of the vehicle to horizontal. This force is calculated as:

$$F_{cl} = M \times g \times \sin(\alpha) \tag{3.5}$$

$$F_{cl} = 1500kg \times 9.81\frac{m}{s^2} \times \sin(26^0) = 6450.631425\text{N} \tag{3.6}$$

where M is the mass of the vehicle platform in kg, g is the acceleration due to gravity in m/s^2, α is the road or the hill-climbing angle. The power is required to overcome the hill-climbing force at a speed of 51.44 km/hr. is:

$$P_{gradient} = F_{cl} \times speed(\frac{m}{\sec}) = 6450.631425\text{N}\, N \times \frac{51.444m}{3600\sec} = 92.1795\, kW \tag{3.7}$$

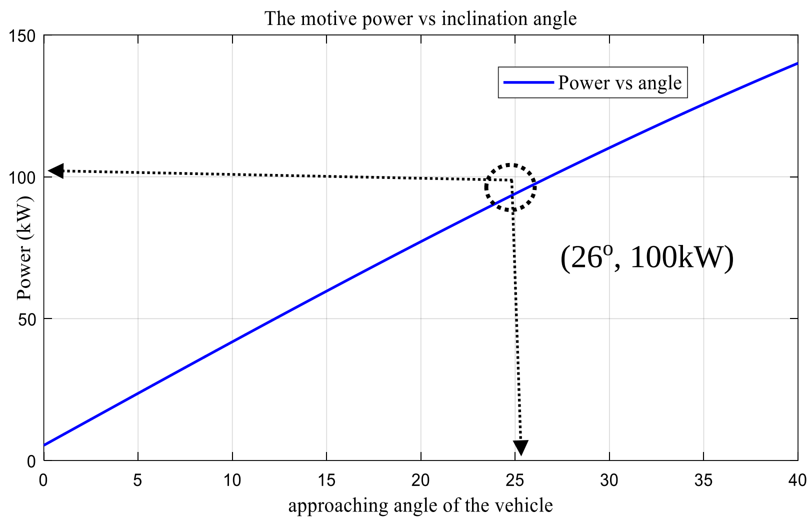

Figure 3.5 The power concerning to inclination angle of the vehicle

3.5.1.3 Aerodynamic Drag Force

Aerodynamic drag force is the resistive force that appears when the vehicle moves in the presence of air. There is friction between the vehicle body and the air. This restive force is known as an aerodynamic drag force which is the opposite direction of the vehicle to horizontal [27]. This force is mainly depending on the frontal area of the vehicle (A_f), the velocity of the vehicle (V), head -wind velocity (V_0) that present when the vehicle in motion and drag coefficient (C_d). Assume the head-wind speed less compared to the velocity of the vehicle, the head-wind speed is zero. So, the equation of the aerodynamic drag coefficient force as shown Equation 3.9.

$$F_{ad} = 1/2 \times \rho_a \times A_f \times C_d \times (v - v_0)^2 \qquad (3.8)$$

$$F_{ad} = \frac{1}{2} \times \rho_a \times A_f \times C_d \times V^2 \qquad (3.9)$$

where A_f is the frontal area of the vehicle (for the case of ECADO-4EV) in m^2, C_d is the aerodynamic drag coefficient. It is can be reduced by good vehicle design. The value of the drag coefficient has between ($0.2 \le C_{ad} \le 0.4$), V is the velocity of the vehicle in m/sec and V_0 is head-wind speed velocity in m/s, r_r is the radius of the wheel and ρ_a is density of the air in $\frac{kg}{m^3}$. Figure 3.6 shows, the graph of the aerodynamic force versus the speed of the vehicle and the aerodynamic force is directly proportional to the velocity of the vehicle respectively.

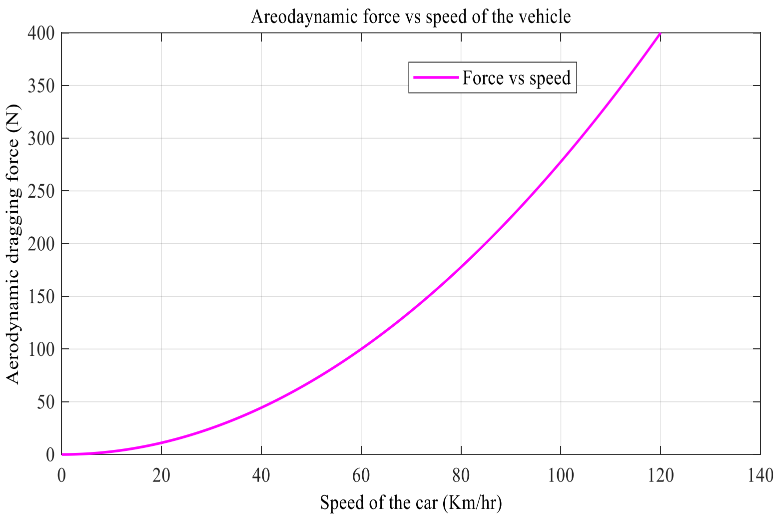

Figure 3.6 The aerodynamic drag force versus speed of the vehicle

Different types of resistive force present when the vehicle is in motion Such as aerodynamic force, hill climbing force (this force is positive when the vehicle moves up on the hill while it is negative when the vehicle moves down on the hill and this force becomes zero when the vehicle moves on a horizontal surface), rolling resistance force, gravitational force (this present due to gravity), the normal force of the vehicle, acceleration force (this force is zero when the vehicle moves at a constant speed. ($\frac{\Delta v}{\Delta t} = 0, F_a = m * a = m * \frac{\Delta v}{\Delta t} = 0$). So, the total tractive force that is given to the vehicle should overcome those resistive forces. Some of the resistive force is calculated as shown above and the rest of the resistive forces are less when compared to other forces, taken as assumptions 1.5kW. The maximum driving power of the vehicle becomes.

$$P_{out\ total(\max)} = 3.673kW + 92.1795kW + 1.5kW = 97.3525kW \tag{3.10}$$

When the power transfer from the tractive motor to the vehicle's wheels through the gearbox and shaft of the motor. Due to that mechanical transmission, there is a power loss present at that process. So, to compensate the loss that is present in a mechanical transmission system, the mechanical driving power should be greater than that of the total maximum power calculated from vehicle dynamics. The mechanical output power considers with the loss of mechanical transmission system can be calculated as:

$$\eta = \frac{Output\ \ power}{Output\ \ power + loss} \tag{3.11}$$

$$P_{total\ driving\ \ power} = \frac{P_{out\ total(\max)}}{\eta_{gear\ transmission\ efficiency}} = \frac{97.3525kW}{0.95} \approx 100kW \tag{3.12}$$

Figure 3.7 shows the relationship between the mechanical output power and the speed of the vehicle. The graph shows, when the speed of the vehicle increases, the optimal power also increases. Even the vehicle reaches at maximum speed (130 Km/hr.), it does not use the total mechanical driving power. So, in this study, 60 kW PMSM is selected to drive the vehicle. If it needs extra speed or torque in the system, it is compensated by mechanical transmission systems [28].

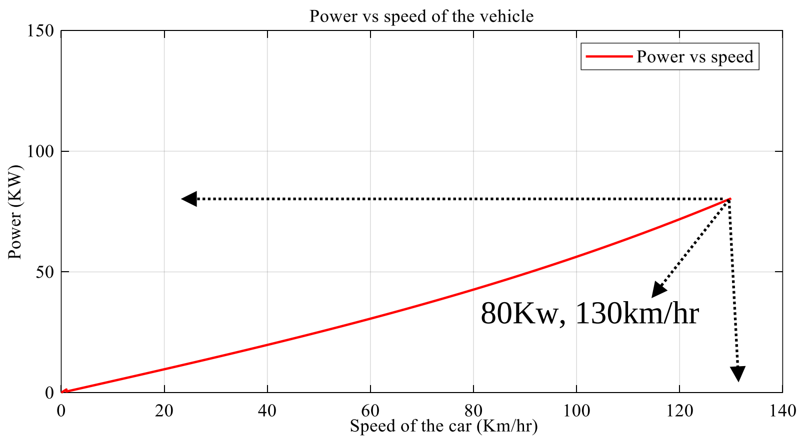

Figure 3.7 Output power versus vehicle speed characteristic graph

3.5.1.4 Relationship Between Torque and Power

Figure 3.8 shows, the speed of the machine increases up to base speed, the torque should be constant. The region is called the torque constant (armature voltage control) region. To maintain the optimal power exited to the system, the developed torque should be reduced above base speed. The terminal voltage is controls using air-gap flux. So, the region is called the constant Power or flux-weakening region [27]. Figure 3.8 shows, the torque-speed characteristics graph of the selected motor at optimal power. To reduce the volume, cost, and weight of the motor, the selected motor for the propulsion system should be below maximum mechanical output power. It can be describing the relationship mathematically:

$$\mathrm{P} = \mathrm{T} \times \omega \tag{3.13}$$

$$T = \kappa_a \Phi I_a h \tag{3.14}$$

$$\mathrm{T} = \frac{\mathrm{K}_e \Phi v_a}{R_a} - \frac{\mathrm{K}_e^2 \Phi^2 \omega_m}{R_a} \tag{3.15}$$

$$= \frac{\kappa_a \kappa_f v_a^2}{(R_a + \kappa_a \kappa_f \omega_m^2)^2}$$

$$\mathrm{E} = \mathrm{K} \times \phi \times \omega_m k \tag{3.16}$$

$$V_a = \mathrm{E} + R_a I_a \tag{3.17}$$

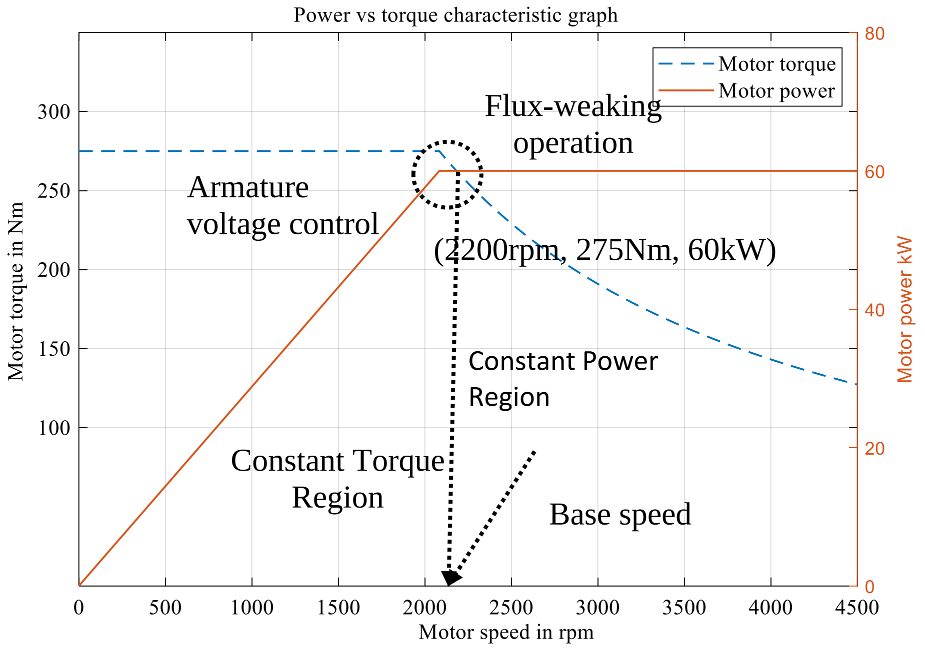

Figure 3.8 Torque versus speed characteristics of the selected PMSM

3.5.1.5 Mechanical Transmission Calculation

The tractive motor shaft connecting with the wheels of the vehicle through a mechanical transmission system. The tractive motor speed and torque should be balanced with the torque and speed at the wheels of the vehicle. The transmission system is used to increase or decrease the torque and speed that are present at the wheels of the vehicle based on the tractive motor speed and torque [27][18]. To calculate torque at the wheels of the vehicle, first to identify the torque, speed, and power of the motor. The motor output power can be calculated as:

$$P = \mathrm{T} \times \omega_m \tag{3.18}$$

where ω_m the rated speed of the selected motor in rad/sec, T is the rated torque in Nm, and P is the rated torque of the selected motor in kW. Using the relation, 2π = 1rev =360^0 the rated speed in rad/sec becomes:

$$\omega_m = \frac{2 \times \pi \times N}{60} = \frac{2 \times \pi \times 2200}{60} = 230.2667 rad / \sec \tag{3.19}$$

Where N is the rated speed of the selected motor in revolution per minute. Based on the equation of 3.18 and 3. 19, the rated torque of the motor can be calculated as:

$$T_{motor} = \frac{P_{rated}}{\omega_{rated}(rad / \sec)} = \frac{60000}{230.2667} = 260.58 Nm \tag{3.20}$$

Based on Equations 3.18, 3.19, and 3.20, the value of the gear transmission system ratio, torque, and speed of the vehicle at each wheel can be identified. The speed at the wheels depends on the velocity of the selected vehicle and the radius of the selected tire of the vehicle [31][27]. The angular speed (ω_{wheels}) at the wheel can be calculated as:

$$\omega_{wheal} = \frac{v}{r} = \frac{36 m / \sec}{0.2532} = 142.18 rad / \sec \tag{3.21}$$

where V is the speed of the selected vehicle in m/sec whereas r is the radius of the tire. From equations 3.20 and 3.21, the gear ratio can be calculated as follows.

$$G_r = \frac{\omega_{motor}}{\omega_{wheel}} = \frac{\mathrm{T}_{wheel}}{\mathrm{T}_{motor}} = \frac{230.2667 rad / \sec}{142.18 rad / \sec} = 1.62 \tag{3.22}$$

Where G_r is the value of the gear system that is located between the motor shaft and the wheel of the vehicle, ω_{motor} and ω_{wheel} are the angular speed of the motor and wheel respectively.

$$T_{wheal} = T_{motor} \times G_r = 260.58Nm \times 1.62 = 422.14Nm \tag{3.23}$$

Where T_{wheel} the tractive torque of the driving wheel. The torque of each wheel becomes:

$$t_{wheel} = \frac{T_{wheel}}{2} = \frac{422.14}{2} = 211.07Nm \tag{3.24}$$

Therefore, to move the selected vehicle that has a mass of 1500kg and 130Km/hr. requires 260.58 Nm, 230.2667 rad/sec rated torque, and speed of the motor respectively, and with gear ration 1.62. so, the selected tractive motor should be delivered 211.07 Nm for each wheel of the vehicle at the tire radius of 0.2532 meters.

3.6 Electric Vehicle Specification

The parameter specification data presented in Table 3.2 is taken from electric vehicle (ECADO_4EV) documentation and Matlab simulation of speed versus torque characteristic graph of the PMSM.

Table 3.2 Data specification of the vehicle (ECADO_4EV) [32]

Parameters	Symbol	Value [Unit]
Maximum power	P_m	100 kW
Vehicle mass	M	1500 kg
Tire radius of the vehicle	r	0.25324
The frontal area of the car	A_f	2.00 m^2
Rated power	P_r	60 kW
Maximum torque	T_m	450Nm
Rated torque	T_r	275 Nm
The maximum speed of the car	V_{mc}	130 km/hr
Rated speed of the car	V_{rc}	100 km/hr
Maximum gradient	degree	26 ^{o}
The capacity of seating	person	4

3.6.2 PMSM Parameter Specification

The specification data of the PMSM shown in Table 3.3 is selected based on the overall analysis of the vehicle dynamics and the maximum power. The maximum power is calculated based on all forces exerted on the vehicle when it is in motion.

Table 3.3 Parameter specification of PMSM used in this thesis [L1] [L2]

Parameters	symbols	Value [Unit]
Number of pole-pairs	P	4
Efficiency at rated	η	95 %
Rated motor power	P_r	60 kW
Maximum motor power	P_m	100 kW
Rated DC battery voltage	V_{dc}	350V
Rated AC voltage of the motor	V_r	540V
Rated current of the motor	I_r	350A
Nominal stator resistance	R_s	0.020 Ω
Nominal d-axis inductance	L_{ds}	0.00147 H
Nominal q-axis inductance	L_{qs}	0.00147H
Rated speed	ω_r	2200 r/m
Maximum speed	ω_r	4500 r/m
Rated torque of the motor	T_r	275 N·m
The maximum torque of the motor	T_m	528 N·m
Current feedback constant	H_c	0.28V/A
Speed feedback constant	H_m	0.4132 V/V
moment of inertia of the motor	J	0.045 kg·m^2
Permanent magnet flux	ψ_r	0.03Wb-turn
Frequency	Ƒ	50Hz
Model number		60kw PMSM motor
Name		PMSM motor driving kit for EV
Application		Electric car vehicle or Boat
Phase		3ϕ

3.6.3 Battery Specifications and Selection

The battery is used as storage of electric energy. In electric vehicles, the battery is the main part used in a propulsion system. There are different types of DC batteries used in an electric vehicle which are lithium-ion, nickel-metal, nickel-cadmium, and lead-acid batteries. The selection of electric energy storage batteries to energize the tractive motor used for EVs is based on energy density, memory effect, voltage stability, longer life, weight, cost, design flexibility, discharging rate, etc. In this thesis work, lithium-ion battery is selected among them because It has fulfilled the required criteria used for EVs [33][34]. Almost all people focused on the physical part of the vehicle. But they should be focused on the entire part of the vehicle such as the battery and tractive motor. The battery state of charge can be calculated as follows:

$$P = P_{\max} \times 0.15 + 0.85 \times P(zero\ grad) \tag{3.25}$$

$$P_m = \frac{P}{\eta_m} \tag{3.26}$$

$$W_{road} = P_m t = \frac{P_m S}{V} \tag{3.27}$$

$$\mathrm{SOC}(\%) = \frac{(\mathrm{W}_{\mathrm{rated}} - \mathrm{W}_{\mathrm{road}}) \times 100\%}{\mathrm{W}_{\mathrm{rated}}} \tag{3.28}$$

where P is the driving power, S is distance, W_{road} is required energy, Pm is the tractive motor input power and η_m is motor efficiency.

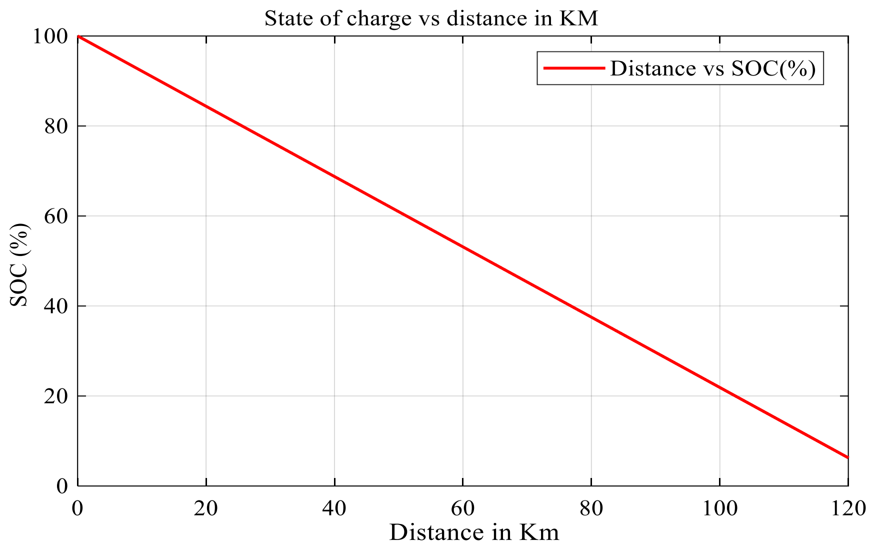

Figure 3.9 The distance of the vehicle versus the state of charge

Figure 3.9 shows, the relationship between the distance of the vehicle and the state of charge of the battery. When the distance of the vehicle goes to increases, discharging of the battery also increases. 80% of stored electric energy is used for driving the vehicle whereas 20% of stored electric charge is should be left in the battery pack to maintain the lifespan of the battery.

Table 3.4 Parameter specifications of DC battery used in [ECADO-4EV]

Parameters	Value [Unit]
Cell type	Lithium-ion
Total battery power pack	32[kWh]
Capacity	90[Ah]
Rated DC voltage	350 [V]
Nominal voltage	4.2[V]
Energy density	154 [W*h*/kg]
Operating temperature	-10 to 50 [^oC]
Mass	4.3kg

3.7 Modeling of PMSM Drive for Electric Vehicle

To improve energy consumption, battery life, life Span of Electric vehicles, and the collision of the vehicle, one of the reasons vehicle collisions occurs is the vehicle's speed. This depends on the speed of the motor, so it requires an accurate and precise model of electric motor derive [28]. To design the control system, an accurate model PMSM is required to drive a four-wheel electric vehicle (ECADO-4EV).

In the permanent synchronous motor, there is no electrical connection between the stator and the rotor part. Therefore, all motors have two main parts: the stator part and the rotor part. PMSM also presents two parts: - The stationary parts of the motor are called Stator, and the rotation part of the motor is called the Rotor. In the stationary part, three-phase Stator windings have a sinusoidal distribution and are displaced by 120^0, but there is no winding in the Rotor part. It’s mounted on a permanent magnet. The magnate that is present in the Rotor part has important to eliminate the brushes, the Rotor losses due to rotor winding, and the weight of the motor [18].

3.7.1 Mathematical Modeling of PMSM

A permanent magnet synchronous motor (PMSM) is one type of AC motor. It is excited by three-phase AC power on the Stator part and a permanent magnet placed on the rotor part. It has distributed winding on the Stator part, and it is excited by a sinusoidal three-phase current source. There is no winding in the rotor part of the motor. Due to this, the motor becomes light in weight, has no additional rotor copper loss, and it is simple in construction. It motor has three-phase voltage and current equations. For simplification purposes and easy implementation, the three-phase voltage and current equation were converted to a two-phase equation based on the following transformation process.

3.7.2 Transformations

"Transforming from a stator reference frame into a rotary reference frame is used to get the time-variant values of the motor parameters. Hence, the measured stator currents have to be transformed from the three-phase time-variant stator reference frame to the two-axis rotating d-q rotor reference frame. This transformation can be done by using two steps Clark and Park transformation".

3.7.2.1 Clark and Park Transformations

The Clarke and Park transformation is a coordinate transformation that are design to convert a multiphase stationary coordinate system into two axes stationary and rotational coordinate systems. This transformation is used to simplify the control technique and lower the system's complexity. The stationary two-phase variables of Clarke's transformation are denoted as α and β [35].

Clark Transformation

The Clarke transformation reduces a complex (abc) system to two components in an orthogonal stationary frame (αβ). To represent any given space vector or phasor, the representation uses two orthogonal axes (90 degrees apart). Three-phase balanced stator voltages of PMSM can be expressed as:

$$V_a = \sqrt{2}V_{rms}\sin(\omega t) \tag{3.29}$$

$$V_b = \sqrt{2}V_{rms}\sin(\omega t - \frac{2\pi}{3}) \tag{3.30}$$

$$V_c = \sqrt{2}V_{rms}\sin(\omega t + \frac{2\pi}{3}) \tag{3.31}$$

$$\begin{bmatrix} V_\alpha \\ V_\beta \end{bmatrix} = \frac{2}{3} \begin{bmatrix} 1 & -\frac{1}{2} & -\frac{1}{2} \\ 0 & \frac{\sqrt{3}}{2} & -\frac{\sqrt{3}}{2} \end{bmatrix} \begin{bmatrix} V_a \\ V_b \\ V_c \end{bmatrix} \tag{3.32}$$

$$\begin{bmatrix} V_a \\ V_b \\ V_c \end{bmatrix} = \begin{bmatrix} 1 & 0 \\ -\frac{1}{2} & -\frac{\sqrt{3}}{2} \\ -\frac{1}{2} & -\frac{\sqrt{3}}{2} \end{bmatrix} \begin{bmatrix} V_\alpha \\ V_\beta \end{bmatrix} \tag{3.33}$$

where V_a, V_b *and* V_c is the three-line voltage. To reduce the complexity of the equation, the three-phase voltage and current equation converted to a two-phase equation by using Clark and park transformation method. Transformation of V_{abc} to $V_{\alpha\beta}$ and inverse Clark transformation of $V_{\alpha\beta}$ to V_{abc} can be defined as shown above Equations 3.32 and 3.33 Figure 3.10 shows, the graph of Clark transformation used to convert the three-phase system two-phase (αβ) system.

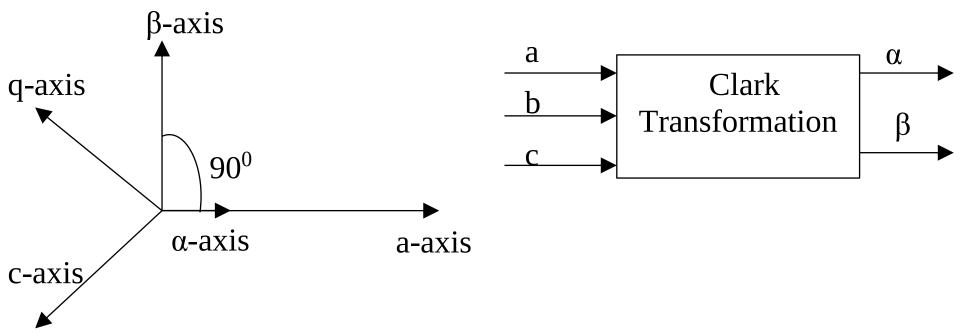

Figure 3.10 Clark transformation [35]

Park Transformation

The Park transform transfers the two components from Clarke transformation in the αβ frame to an orthogonal rotating reference frame (dq). The letters d and q stand for direct and quadrature components, respectively. Figure 3.11 shows, the graph of Park transformation used to convert the αβ frame to an orthogonal rotating reference frame (dq).

$$\begin{bmatrix} V_d \\ V_q \end{bmatrix} = \begin{bmatrix} \cos(\theta) & \sin(\theta) \\ -\sin(\theta) & \cos(\theta) \end{bmatrix} \begin{bmatrix} V_\alpha \\ V_\beta \end{bmatrix} \tag{3.34}$$

The inverse park transformation is as follows:

$$\begin{bmatrix} V_\alpha \\ V_\beta \end{bmatrix} = \begin{bmatrix} \cos(\theta) & -\sin(\theta) \\ \sin(\theta) & \cos(\theta) \end{bmatrix} \begin{bmatrix} V_d \\ V_q \end{bmatrix} \tag{3.35}$$

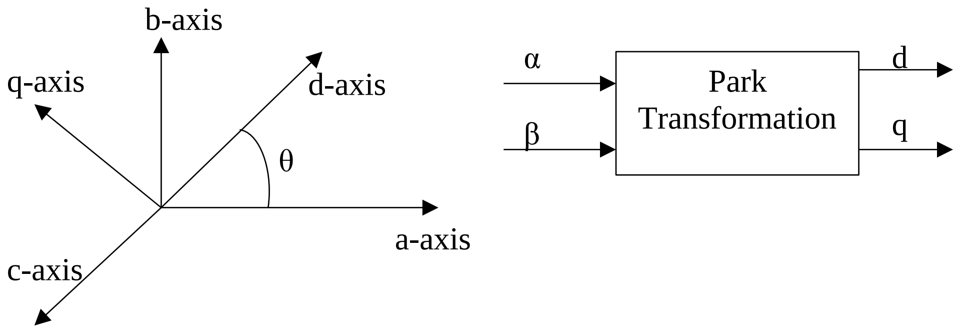

Figure 3.11 Park transformation [35]

The mathematical model of the PMSM is obtained based on the following assumptions:

- The stator coil resistance and inductance assume constant.
- The stator windings are sinusoidally distributed.
- There is no rotor winding.
- Saturation is neglected.
- The invertor switches are ideal.
- the losses eddy current and hysteresis are ignored.

The voltage equation of the PMSM motor in quadrature and direct axis form can be calculated as [36][37].

$$v_{ds} = R_d i_{ds} + \frac{d\varphi_{ds}}{dt} - \omega_r \varphi_{qs} \tag{3.36}$$

$$v_{qs} = R_q i_{qs} + \frac{d\varphi_{qs}}{dt} + \omega_r \varphi_{ds} \tag{3.37}$$

where quadrature axis winding resistance (R_q) and direct axis winding resistance (R_d) are equal to stator resistance (R_s). The equation becomes

$$v_{ds} = R_s i_{ds} + \frac{d\varphi_{ds}}{dt} - \omega_r \varphi_{qs} \tag{3.38}$$

$$v_{qs} = R_s i_{qs} + \frac{d\varphi_{qs}}{dt} + \omega_r \varphi_{ds} \tag{3.39}$$

The flux linkage along with the d-axis and q-axis in the rotor reference frame becomes

$$\varphi_{qs} = L_q i_{qs} + L_m i_{qr} \tag{3.40}$$

$$\varphi_{ds} = L_d i_{ds} + L_m i_{dr} \tag{3.41}$$

where L_m is the mutual inductance between the stator winding and rotor magnet whereas L_d, L_q are the self-inductance of stator d- and q-axis windings respectively. In the rotor reference frame, the winding inductances do not change. So, the q-axis current in the rotor part is zero (i_{qr}=0). The flux equation becomes:

$$\varphi_{qs} = L_q i_{qs} \tag{3.42}$$

$$\varphi_{ds} = L_d i_{ds} + L_m i_{dr} \tag{3.43}$$

Substitute the flux equation into voltage equation, the voltage equation in matrix form given as:

$$\begin{bmatrix} v_{qs} \\ v_{ds} \end{bmatrix} = \begin{bmatrix} R_q + \frac{dL_q}{dt} & \omega_r L_d \\ -\omega_r L_q & R_d + \frac{dL_d}{dt} \end{bmatrix} \begin{bmatrix} i_{qs} \\ i_{ds} \end{bmatrix} + \begin{bmatrix} \omega_r L_m i_{dr} \\ 0 \end{bmatrix} \tag{3.44}$$

Torque equation can be given as:

$$T_e^* = \frac{3}{2}\frac{p}{2}\left(\varphi_{ds} i_{qs} - \varphi_{qs} i_{ds}\right) \tag{3.45}$$

where T_e is electrical torque, φ_{ds} and φ_{qs} are direct and quadrature axis winding respectively. It can be described in terms of self-inductance of d- axis, q-axis winding, and mutual-inductance.

$$T_e^* = \frac{3}{2}\frac{p}{2}\left[L_m i_{dr} i_{qs} + (L_d - L_q) i_{qs} i_{ds}\right] \tag{3.46}$$

In surface-mounted PMSM motor, Stator windings inductance along direct magnet axis (L_d) and Stator windings inductance along quadratic magnet axis (L_q) are equal (L_d = L_q = L_s). The electrical torque becomes [21]:

$$T_e^* = \frac{3}{2}\frac{p}{2}(L_m i_{dr} i_{qs}) \tag{3.47}$$

The quadrature stator current component reference i_q^* and direct axis reference component i_d^* can be given as:

$$i_{qs}^* = (\frac{2}{3})(\frac{2}{P})(\frac{L_r}{L_m})(\frac{T_e^*}{\psi_r}), \qquad i_{ds}^* = \frac{\psi_r^*}{L_m}$$

where T_e^* is the speed controller output is called electromagnetic torque and ψ_r^* is the reference nominal flux linkage. The sinusoidal three-phase current equation exited to the motor given as:

$$I_{as} = i_s \sin(\omega_r t + \delta) \tag{3.48}$$

$$I_{bs} = i_s \sin(\omega_r t + \delta - \frac{2\pi}{3}) \tag{3.49}$$

$$I_{cs} = i_s \sin(\omega_r t + \delta + \frac{2\pi}{3}) \tag{3.50}$$

where ω_r is the rotor speed of the motor, i_s is the stator three-phase current and δ is the angle between stator phase current and rotor field, which is called torque angle. It can be defined as in matrix form:

$$\begin{pmatrix} i_{qs} \\ i_{ds} \end{pmatrix} = \frac{2}{3}\begin{bmatrix} \cos\omega_r t & \cos(\omega_r t - \frac{2\pi}{3} & \cos(\omega_r t + \frac{2\pi}{3} \\ \sin\omega_r t & \sin(\omega_r t - \frac{2\pi}{3} & \sin(\omega_r t + \frac{2\pi}{3} \end{bmatrix}\begin{pmatrix} i_{as} \\ i_{bs} \\ i_{cs} \end{pmatrix} \tag{3.51}$$

3.7.3 Equivalent Circuit of the PMSM

Based on Equations 3.44, The overall and steady-state equivalent circuit of permanent magnet synchronous motor is defined as respectively as shown below. PMSM at steady state, the derivative part becomes zero.

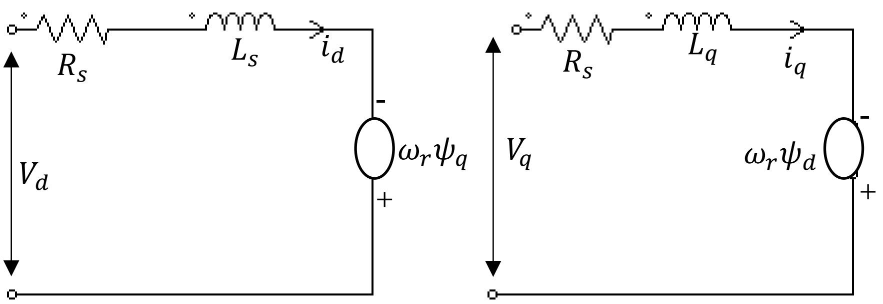

Figure 3.12 The overall equivalent circuit of the PMSM [38]

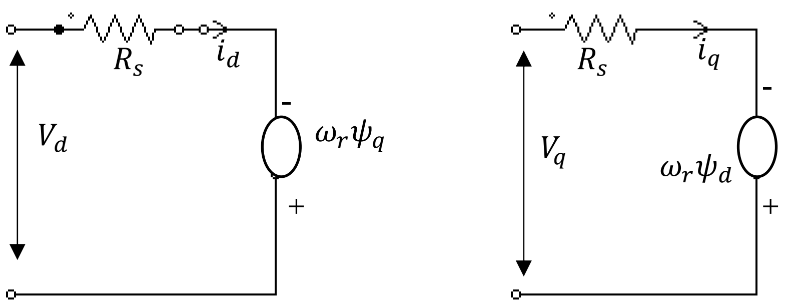

Figure 3.13 The equivalent circuit of the PMSM under steady-state [38]

3.7.4 Transfer Function of the Controlled Object

In a complicated system, it's better to find the transfer function of each component. For the simplicity of implementation, it is better to make i_{ds} becomes zero. In this case, the PMSM is analogous to separately excited DC motor. It can easily obtain the overall transfer function of the drive system. The overall system block diagram becomes:

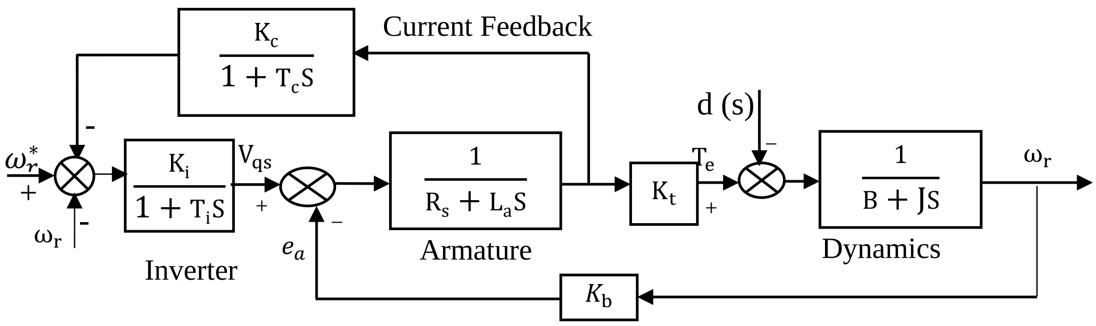

Figure 3.14 The Block diagram of the overall system using transfer function

3.7.4.1 Transfer Function Analysis of the System

The overall system has two inputs which are the reference speed and disturbance. The actual speed is obtained based on disturbance and reference speed. To get the transfer function of output speed over input speed, set d(s)=0, and also to get the transfer function of output speed over disturbance, set $\omega_r^*(s) = 0$. In this research work, a disturbance is considered as load torque due to passenger boarding. The output speed becomes the sum of input speed and disturbance which is the effect of input speed and disturbance. The transfer functions are obtained using the block diagram reduction technique method. It can be given as:

$$\omega_r(s) = \left[\frac{K_t K_{in} K_c}{\left[RJs^2 + L_a Js^2 \left[(BR + L_a B)s) \right] \right] (1 + T_{in} s)} \right] \omega_r^*(s) - \left[\frac{K_t K_c K_t (1 + T_c s) - K_b K_c K_t}{(B + Js)(R_s + L_a s)(1 + T_c s)} \right] d(s)$$

(3.52)

The transfer function analysis of each component is calculated as follows: The inverter can be given as:

$$G_{in} = \frac{K_{in}}{1 + sT_{in}} = \frac{22.75}{1 + 6.25e^{-0.5}} \tag{3.53}$$

$$K_{in} = \frac{0.65V_{dc}}{V_{cm}} = \frac{0.65 * 350V}{10} = 22.75$$

$$T_{in} = \frac{1}{2 \times f_c} = \frac{1}{2 \times 8000} = 6.25 \times 10^{-5} \sec$$

The armature transfer function of the motor becomes:

$$G_a = \frac{1}{R_s + L_s s} = \frac{1}{0.02 + 0.00147s} \tag{3.54}$$

Dynamic transfer function of the motor becomes:

$$G_m = \frac{1}{B_t + Js} = \frac{1}{0.01 + 0.045s} \tag{3.55}$$

Current feedback transfer function becomes:

$$G_c = \frac{1}{1 + 0.0001s} \tag{3.56}$$

Torque constant (K_t) can be calculated as the multiplication of pole pair and rotor flux as shown below:

$$K_t = \frac{3}{2} \times (\frac{p}{2})^2 \times \Psi_r = \frac{3}{2} \times (\frac{8}{2})^2 \times 0.03wb = 0.72N.m / A \tag{3.57}$$

where K_{in} is inverter gain, V_{dc} is DC link volage input to the invertor, V_{cm} is maximum controlled voltage, T_{in} is a time constant, f_c is the switching frequency of the invertor. It is different from the supply frequency of the system, R_s is stator resistance, L_s is stator inductance. Surface-mounted PMSM motor has equal stator inductance in d-axis and inductance in q- axis (L_d = L_q = L_s), B_t is total viscous friction. It is the sum of friction due to motor and friction due to load, J is a moment of inertia of the motor, K_c is the current gain, T_c is a current time constant, K_t is torque time constant, K_b is back EMF, ψ_r is rotor flux, ω_r rotor speed in rad/sec, and $e_a$is induced EMF voltage due to rotor flux linkage [36].

3.8 Voltage Source Inverter Topology

To provide variable speed operation, permanent magnet synchronous motor drives require a changeable voltage or current input at a variable frequency. The utility power source cannot be directly utilized in this equipment because of its constant frequency and voltage. As a result, a power conversion procedure is required to convert a fixed frequency and voltage ac power source into a variable voltage/current, variable frequency power supply.

The importance of power electronic control is growing, and a substantial percentage of motors are equipped with frequency converters to enable motor speed control. The most common setup for supplying three-phase motors is a two-level voltage source converter [27]. The three-phase two-level VSI consists of six active power semiconductor switches. They use a variety of power devices for electric propulsion. Because of its advantages over the others, IGBT is virtually solely employed in current EVs. The inverter's basic setup is shown in Figure 3.15. The converter consists of three legs with semi-conductor switches.

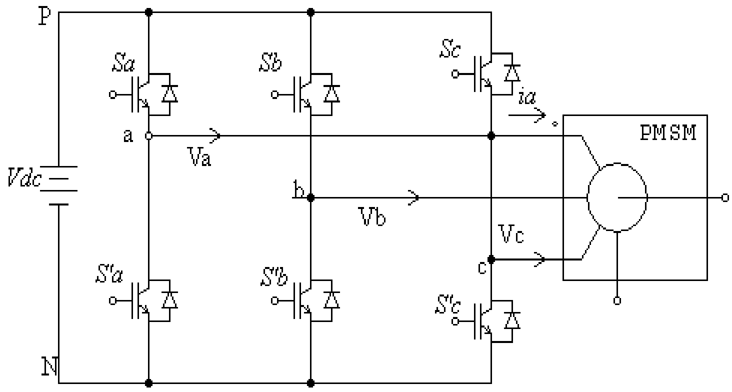

Figure 3.15 The picture of voltage source inverter with PMSM motor [13]

3.9 Space Vector Pulse Width Modulation

The complex reference voltage vector is processed as a whole in the SVPWM technique instead of using a separate modulator for each of the three phases. In contrast to sinusoidal modulation techniques, SVPWM produces less harmonic distortion in output Voltages and wind currents of the engine load and makes more efficient use of the DC supply voltage. As SVPWM offers a continuously changing frequency, it is easy to adjust the switching frequency. Although SVPWM is more complicated than sinusoidal PWM, modern DSP-based control systems can easily be used [39][40].

Calculating the position θ and magnitude of V_{ref}

The three-phase voltages are transformed into two phases with Clarke transformation to calculate the magnitude and position of the reference voltage. From Figure 3.16, it can be seen that the input to the SVPWM is the dq voltage vectors therefore instead of Clarke transformation inverse Park transformation is used.

$$\begin{pmatrix} V_\alpha \\ V_\beta \end{pmatrix} = \begin{pmatrix} \cos\theta & -\sin\theta \\ \sin\theta & \cos\theta \end{pmatrix} \begin{pmatrix} V_d \\ V_q \end{pmatrix} \quad (3.58)$$

Determining sectors

From Figure 3.16, it can be seen that if the V_{ref} is in sector 1 the angle θ is between 0 to 60. Since the reference voltage rotates in space at an angular velocity of $2\pi f_1$ where f_1 is the fundamental frequency of the inverter output voltage, the reference voltage can be located in any one of the six sectors.

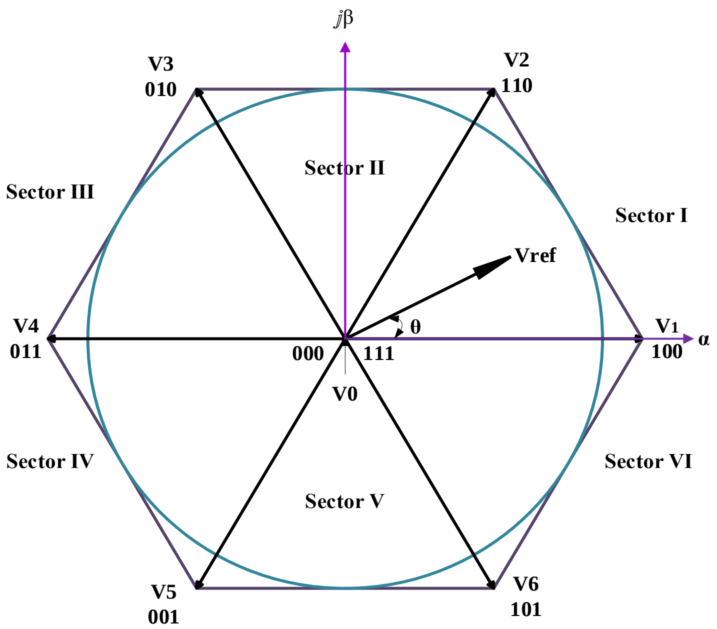

Figure 3.16 Space vector diagram for the two-level inverter [40]

A space vector can be generally expressed in terms of the three-phase voltages in the abc plane.

$$V(t) = \frac{2}{3}\left(V_{an}(t)e^{j0} + V_{bn}(t)e^{j\frac{2\pi}{3}} + V_{cn}(t)e^{j\frac{4\pi}{3}}\right) \quad (3.59)$$

Every six active vectors can be obtained by substituting the corresponding line to neutral voltage from Table 3.5 into Equation (3.60).

$$V_k = \frac{2}{3} V_d e^{j(k-1)\frac{\pi}{3}} \qquad K = 1, 2, ...6 \tag{3.60}$$

Table 3.5 Valid switching states and output line to neutral voltage of three-phase VSI

Voltage Vector	Switching vectors			Line to neutral voltage		
	a	b	c	V_{an}	V_{bn}	V_{cn}
V_0	0	0	0	0	0	0
V_1	1	0	0	$2/3\, V_d$	$-1/3\, V_d$	$-1/3\, V_d$
V_2	1	1	0	1/3	1/3	-2/3
V_3	0	1	0	-1/3	2/3	-1/3
V_4	0	1	1	-2/3	1/3	1/3
V_5	0	0	1	-1/3	-1/3	2/3
V_6	1	0	1	1/3	-2/3	1/3
V_7	1	1	1	0	0	0

Modulation index calculation

The maximum value of M_a is 1 therefore, $V_{\text{ref becomes}}$:

$$V_{ref}, \max = \frac{V_d}{\sqrt{3}} \tag{3.61}$$

The maximum fundamental line to line voltage (rms) produced by the SVPWM scheme can be calculated as:

$$V_{ref,\max} = \sqrt{3}\frac{V_{ref}, \max}{\sqrt{2}} = \frac{\sqrt{3}}{\sqrt{2}}\left(\frac{V_d}{\sqrt{3}}\right) = 0.707 V_d \tag{3.62}$$

Equation (3.62) indicates that for a given dc bus voltage the maximum inverter line to line voltage generated by the SVPWM scheme is 70.7% of the applied DC bus voltage.

Table 3.6 Space vectors and their corresponding switching state

Space vectors	Switching state	On state switches	Off-state switches	Vector definition
V_0	0 0 0	S_1, S_3, S_5	S_4, S_6, S_2	$v_0 = 0$
V_1	1 0 0	S_1, S_6, S_2	S_4, S_3, S_5	$v_1 = \frac{2}{3} v_d e^{j0}$
V_2	1 1 0	S_1, S_3, S_2	S_4, S_6, S_5	$v_2 = \frac{2}{3} v_d e^{j\frac{\pi}{3}}$
V_3	1 1 0	S_4, S_3, S_2	S_1, S_6, S_5	$v_3 = \frac{2}{3} v_d e^{j\frac{2\pi}{3}}$
V_4	0 1 0	S_4, S_3, S_5	S_1, S_6, S_2	$v_4 = \frac{2}{3} v_d e^{j\frac{3\pi}{3}}$
V_5	0 0 1	S_4, S_6, S_5	S_1, S_3, S_2	$v_5 = \frac{2}{3} v_d e^{j\frac{4\pi}{3}}$
V_6	1 0 1	S_1, S_6, S_5	S_4, S_3, S_2	$v_6 = \frac{2}{3} v_d e^{j\frac{5\pi}{3}}$
V_7	1 1 1	S_4, S_6, S_2	S_1, S_3, S_5	$v_0 = 0$

Dwell time calculation:

The dwell time calculation is based on the volt-second balancing principle. V_{ref} can be approximated by two adjacent active vectors and one zero vector. The volt second balancing equation is given by:

$$V_{ref} T_s = V_1 T_a + V_2 T_b + V_0 T_0 \tag{3.63}$$

where T_a, T_b and T_0 are dwell times for the vectors V_1, V_2 and V_0 respectively. Table 3.7 shows the location of V_{ref} and its corresponding dwell time value for one sector.

Table 3.7 V_{ref} location and dwell times

V_{ref} location	$\theta = 0$	$0 < \theta < \frac{\pi}{6}$	$\theta = \frac{\pi}{6}$	$0 < \theta < \frac{\pi}{3}$	$\theta = \frac{\pi}{3}$
Dwell times	$T_a > 0$ $T_a = 0$	$T_a > T_b$	$T_a = T_b$	$T_a < T_b$	$T_a = 0$ $T_b > 0$

CHAPTER FOUR

CASCADE CONTROLLER DESIGN

4.1 General Block Diagram of Cascade Controller

In cascade controller, at least two controllers are present in the system. It is used for more than two controlled variable is present in the system. The controllers that used in the system can be improve using cascade controller. It is not easily exposed to disturbance of the system. This type of controller is mostly used for industrial applications (cascaded system) and electric motors. In cascade controller, if the disturbance occurs in secondary loop, the secondary controller improves the disturbance before affected the primary controller of the system leads to the system has better performance [L5].

Figure 4.1 shows, the overall block diagram of cascade controller of the system. Here, e_1 is the error input to the primary controller. u_{s1} is the primary controller output of the system. The primary controller adjusts the input of the secondary loop. e_2 is the error input to the secondary loop of the system. u_{s2} is the secondary controller output of the system. In this research work, GA tuned FOPID controller as a primary controller whereas GA tuned PI with Anti-Windup technique used as secondary controller of the system.

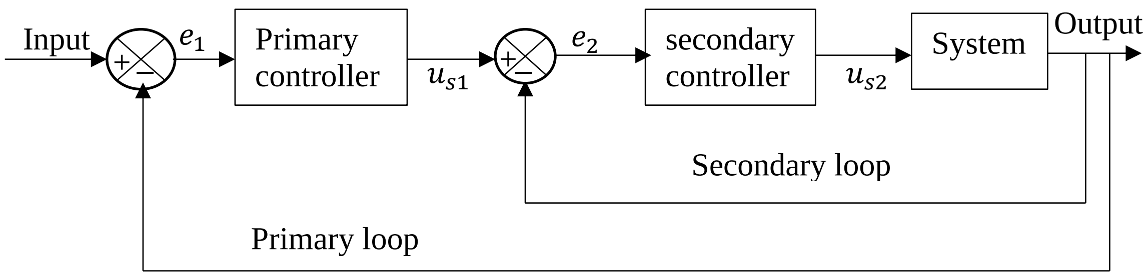

Figure 4.1 General block diagram of cascade controller

4.1.1 Design of a FOPID Controller as a primary controller

A proportional-integral (PID) is an ancient controller used in industrial and other systems. It has three gains K_p, K_i, K_d whereas Fractional Order PID (FOPID) controller has five parameters K_p, K_i, K_d, λ and μ. λ and μ are integral and derivative orders respectively. The integral and derivative order makes the system has better response and robustness.

Fractional-order PID (FOPID) controller is derived from the fractional-order differential equation. It can be defined as [41] [42][43][44].

$$G(s) = \frac{b_0 s^{\gamma} + b_1 s^{\gamma_1} + \ldots + b_m s^{y_m}}{a_0 s^{\beta_0} + a_1 s^{\beta_1} + \ldots + a_n s^{\beta n}} \tag{4.1}$$

$$_a D_t^{q} = \begin{cases} \dfrac{d^q}{dt^q} & q > 0 \\ 1 & q = 0 \\ \displaystyle\int_a^t (d\tau)^{-q} & q < 0 \end{cases} \tag{4.2}$$

where b_i ($i = 0;1...m$); a_i ($i = 0;1...n$) are constants and Υ_i ($i = 0;1...m$); β_i = ($i = 0;1...n$) are arbitrary real or rational. q is the integral order. it is any real number, t and a are the boundaries of the operation.

Riemann-Liouville definition of fractional order derivative

$$aD_t^{\alpha} \; f(t) = \frac{1}{\Gamma(m-\alpha)} \frac{d^m}{dt^m} \int_a^t (t-\tau)^{m-\alpha-1} f(\tau)\, d\tau \tag{4.3}$$

Where $m - 1 < \alpha \le m \in N$ and $\alpha \in R$ is a fractional order of differentiation of function f(t) and Γ(.) Represents gamma function.

Grünwald-Letnikov definition fractional-order derivative

$$aD_t^{\alpha} f(t) = \lim_{h\to 0} \frac{1}{h^{\alpha}} \sum_{j=0}^{[\frac{t-a}{h}]} (-1)^j \binom{\alpha}{j} f(t - jh) \tag{4.4}$$

Where [·] means the integer part, h is the step size

Laplace transform of the Grünwald-Letnikov fractional operator for the causal system is given by

$$\ell[{}_0D_t^{\alpha} f(t)] = s^{\alpha} F(s) \tag{4.5}$$

$$\binom{a}{j} = \frac{\alpha!}{j!(\alpha - j)!} = \frac{\Gamma(\alpha+1)}{\Gamma(j+1)\Gamma(\alpha - j + 1)} \tag{4.6}$$

Rieman-Liouville and Caputo definitions are very close. The only variation is the order of initial conditions and these conditions of integer order which makes them easier to interpret.

4.1.2 PMSM Motor Speed Control using FOPID Controller

Figure 4.2 shows, the general block diagram of FOPID controller which has five parameters K_p, K_i, K_d, λ, and μ. These parameters are tuned using GAs optimization technique. The tuned parameters are obtained after GAs optimization is terminated. Figure 4.2 shows. the overall structure of fractional order PID controller [45][44][46]

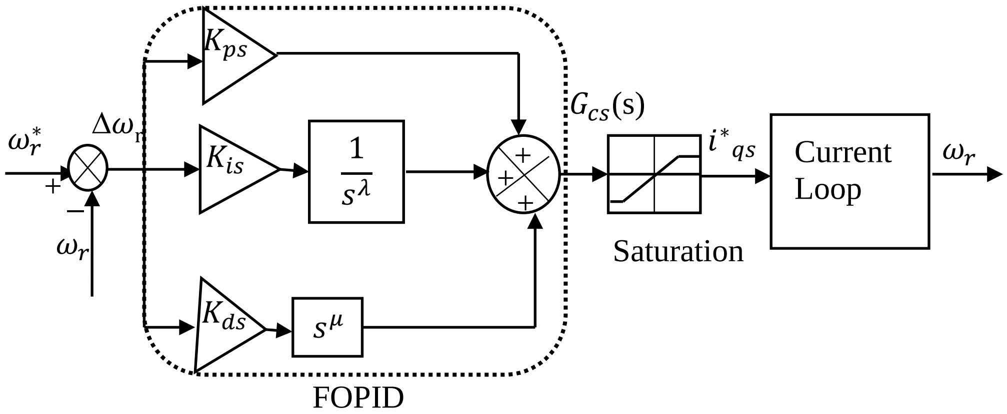

Figure 4.2 Structure of FOPID controller for speed control of PMSM motor

where ω_r^* (s) is the Laplace transform of ω_r^* (t). It is the desired speed set by the user, ω_r (s) is the Laplace transform of ω_r (t) which is the measured speed of the system, E(s) is the Laplace transform of e(t). It is the difference between the desired speed and measured speed. It can be defined as E(s) = ω_r^* (s) - ω_r (s). The speed error is the input of the speed controller. The speed controller is regulating the error that occurs between the two speeds. The error should be zero as much as possible. The time-domain of the controller becomes:

$$G_{cs}(t) = K_p\left[e(t) + \frac{1}{T_i}\int_a^t e(\tau)(d\tau)^{-\lambda} + T_d\frac{d^{\mu}}{dt}e(t)\right] \tag{4.7}$$

where a and t are the interval of the integration part whereas λ and μ are the integral and derivative order of the controller respectively. The FOPID controller has K_{ps}, K_{is} and K_{ds} gain like PID controller and also it has an additional parameter λ and μ. The S-domain or the transfer function of the controller becomes:

$$\begin{aligned} G_{cs}(s) &= K_{ps} + \frac{K_{is}}{S^{\lambda}} + K_{ds}S^{\mu} \\ &= \left[1\ S^{-\lambda}S^{\mu}\right]\left[K_{ps}\ K_{is}\ K_{ds}\right] \end{aligned} \tag{4.8}$$

Where K_{ps}= K_{ps}, K_{is} = $\frac{K_{ps}}{T_i}$ and K_{ds} =K_{ds}*T_d. K_p , T_i and T_d are proportional, integral, and derivative time constants respectively. Whereas K_{ps}, K_{is}, and K_{ds} are the proportional, integral, and derivative gain of the speed controller respectively and G_{cs} is the speed controller of the system.

To simulate the FOPID controller that is present in the system modelling, it needs a software package that adds in the set path of MATLAB/Simulink toolbox. There are different software packages such as LMI (linear matrix inequality) and FMINCON (interior-point algorithm). FMINCON (interior-point algorithm) technique is used in this thesis. It is working based on the FMINCON (interior-point algorithm) optimization method. It is a non-linear constraint optimization algorithm technique [47]. The Fomcon is a toolbox add-on MATLAB using a set path to help the FOPID controller working properly. It is easily downloaded from the website.

4.2 Anti-Windup Techniques for PI Controller

The error signal that is input to the controller is large or remains non-zero for a long time. The integrator part works based on the summation of the present error and reminds the past error. This causes the integrator part of the controller to accumulate the error in one region. The region is known as the windup region. In this case, the control signal to be outside the operating region. This leads to the system goes to unstable, presents large overshoot and high settling time. To improve this, different tracking anti-windup techniques have been proposed such as integrator limiter, conditional integration, and back-calculation (error recalculation) To improve this, different tracking anti-windup techniques have been proposed such as integrator limiter, conditional integration, and back-calculation (error recalculation) [48][49][50][51].

4.2.1 Conditional Integration of Anti-Windup Technique

In this technique, there is no additional tuning parameter. It works manually based on the switch ‘on’ and ‘off’ cascaded in the integral term. But this technique is not consistence between the controller output and the input signal to the system. It is updating the integral term of the controller only if a certain condition is met. Figure 4.3 shows the overall block diagram of the conditional integration Anti-Windup technique.

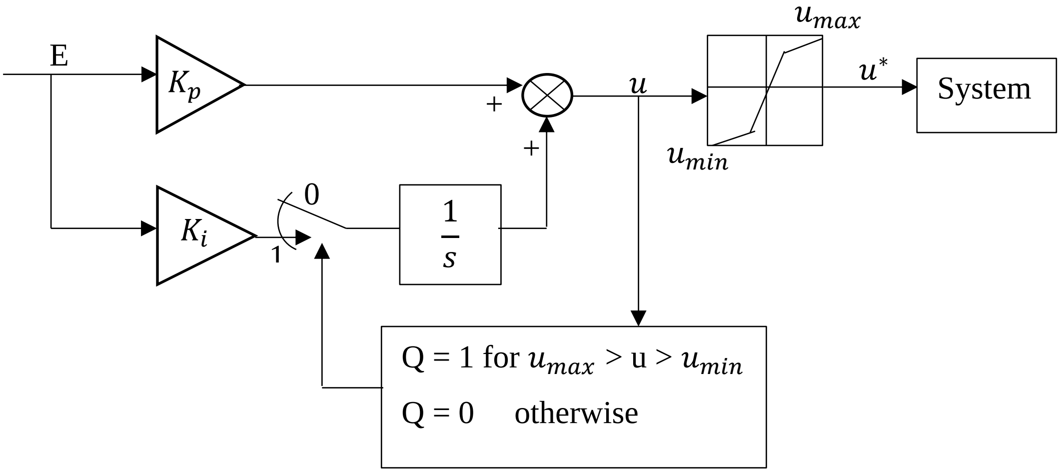

Figure 4.3 Block diagram of conditional integration Anti-Windup technique

When the switch Q is 'on' that is the control signal u is greater than the minimum value of the signal that is input to the system, the integral term is connected to the controller, and the integral term is update and working again. Otherwise, the integral term is 'off''. It can be expressed mathematically as follows:

$$u^* = \begin{cases} u & for\ u_{\max} > u > u_{\min} \\ u_{\max} & for\ u \geq u_{\max} \\ u_{\min} & for\ u \leq u_{\min} \end{cases} \tag{4.9}$$

Where u is the controller output signal, u^* is the actuator signal input to the system, u^{min} and u^{max} are the minimum and maximum value of the actuator signal respectively.

4.2.2 Back-Calculation or Error Recalculation

Here, the overall block diagram of back-calculation or Error Recalculation controller has three tuning parameters K_p, K_i and an additional user parameter α. In this case, there is a consistence between the control output signal and the system input signal. The difference between the controller output and the signal input to the system is the input to the feedback gain of K_{lim} to reduce the error that input to the integrator. When the error is zero, the Anti-Windup technique has no effect.

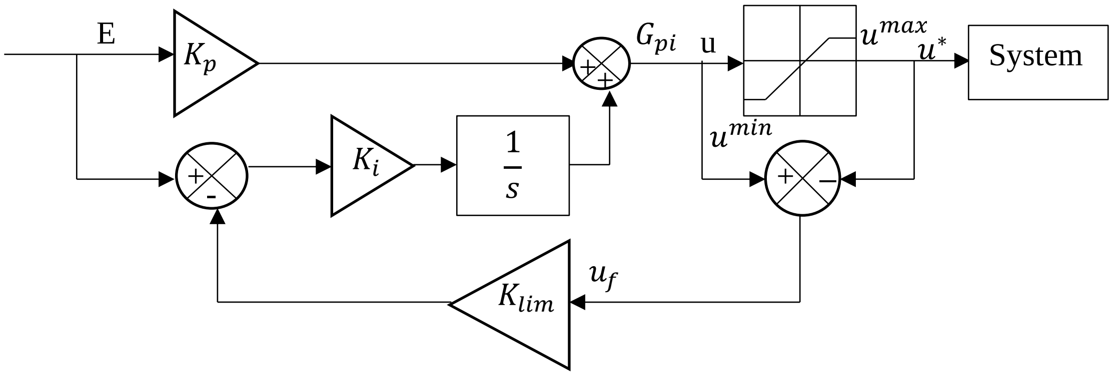

Figure 4.4 Block diagram of error recalculation of Anti-Windup technique

where $K_{lim} = \frac{1}{\alpha * T_t}$, α is the user parameter and T_t is tracking time constant. It determines the time to reset the integrator part of the controller. It depends on the integral time and can be calculated as $T_t = \frac{K_p}{K_i}$.

4.2.2.1 Design of Current Controller with an Anti-Windup Scheme

Naturally, the motors have high starting current. This problem causes overheating of the stator winding and burning of an internal circuit. To improve these problems, the starting current of the motor should be regulated using a current controller. Figure 4.5 shows, PI current controller with error recalculation Anti-Windup technique is proposed in this research work. The speed controller generates the input signal (current command) for current controller. So, the current controller becomes simple and easy to reduces the complexity of the overall cascade controller. This thesis proposes a GA tuned PI current controller incorporating with advanced error recalculation anti-windup schemes. Figure 4.5 shows, the overall block diagram of current controller using for PMSM motor.

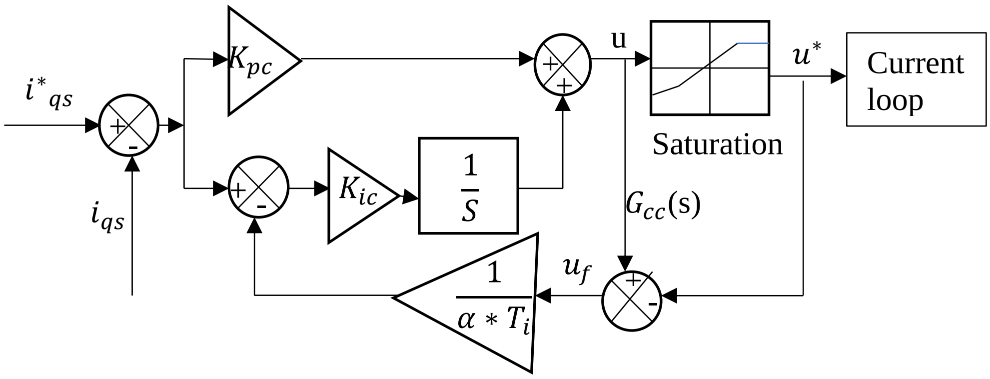

Figure 4.5 Overall Structure of internal current loop controller

The overall current controller has three tuning parameters K_{pc}, K_i and α. The derive part of PID controller becomes zero and Constant $\frac{1}{\alpha * T_i}$ is inserted into the integral feedback circuit. The transfer function of the controller becomes:

$$G_{CC}(s) = (K_p + \frac{K_i}{S}) * E(s) + \frac{1}{\alpha * T_i s} * u_f(s) \tag{4.10}$$

where α is the user parameter, $K_i = \frac{K_p}{T_i}$. so, the constant $T_t = \frac{K_p}{K_i}$, i_{qs} is the measured motor current whereas $i^*{}_{qs}$ is the reference current based on the output speed controller and G_{cc}(s) is the overall current controller of the system. u_f (s) = u(s)-u^*(s).

4.3 GA Optimization Technique

In terms of minimizing some evaluation functions and getting a better system performance, an optimization algorithm is needed to tune the parameters properly. There are various methods of optimization tool that are have been proposed such as Ant Colony Optimization (ACO), Evolution Strategies (ESs), Simulated Annealing (SA), Particle Swarm Optimization (PSO), and Genetic Algorithm (GA) than other empirical methods such: trial and error method, continuous cyclic method (Ziegler Nichols method) and process reaction curve method (Ziegler Nicholas and cohen-coon method). Especially trial and error method is time-consuming and tedious than other empirical methods, but genetic algorithms have been widely used [52][53].

The evolutionary genetic algorithm optimization technique (GAs) works based on cross-over, mutation, natural selection, and genetics. The fitness function is focused on minimizing evaluation functions. To build the next generation from the current population, the genetic algorithm employs three sorts of rules at each phase. This procedure is performed for several generations until it reaches individuals who represent the best solution to the problem.

- Selection rules determine which individuals, referred to as parents, will contribute to the next generation's population.
- Crossover rules combine the children of two parents to create the following generation.
- To generate children, mutation rules apply random modifications to individual parents.

The genetic algorithms technique is used in this research work. It can be described in Pseudocode as follows:

Basic structure of GA

K=0;

Compute an initial population P (0);

Evaluate the fitness;

While <stopping condition not fulfilled> DO

BEGIN

k= k+1;

Select individuals for reproduction;

Create offspring by crossover;

Mutate some individuals;

Evaluate the fitness;

end

Figure 4.6 shows, the GA optimization of FOPID speed controller with cascaded in PI with an anti-windup current controller of PMSM. The GA optimizes the cascade controller based on the upper and lower boundaries of the tuning parameter. The lower boundaries of the tuning parameter are the starting values of the tuning parameter. In contrast, the upper boundaries of the tuning parameter are the ending value of the tuning parameter. For more understanding, the parameters of GAs such as maximum generation, population size, number of parameters, lower boundaries, and upper boundaries of the tuning parameters are given as shown in Table 4.1.

The GA optimization technique is run according to upper and lower boundaries of the parameter that set on GA Matlab code. The GA optimization technique is written on Matlab editor. It has also population size and maximum generation value. GA optimizes the parameter that set on the Simulink model. The name of the Simulink model is assigned on GA Matlab code. The GA tuner tunes the parameter based on the Simulink model name. For more understanding, the Matlab code of GA optimization technique is mentioned in appendix [B]. Figure 4.6 shows, the overall block diagram of GA tuned FOPID speed controller cascaded in PI with Anti-Windup current controller of PMSM.

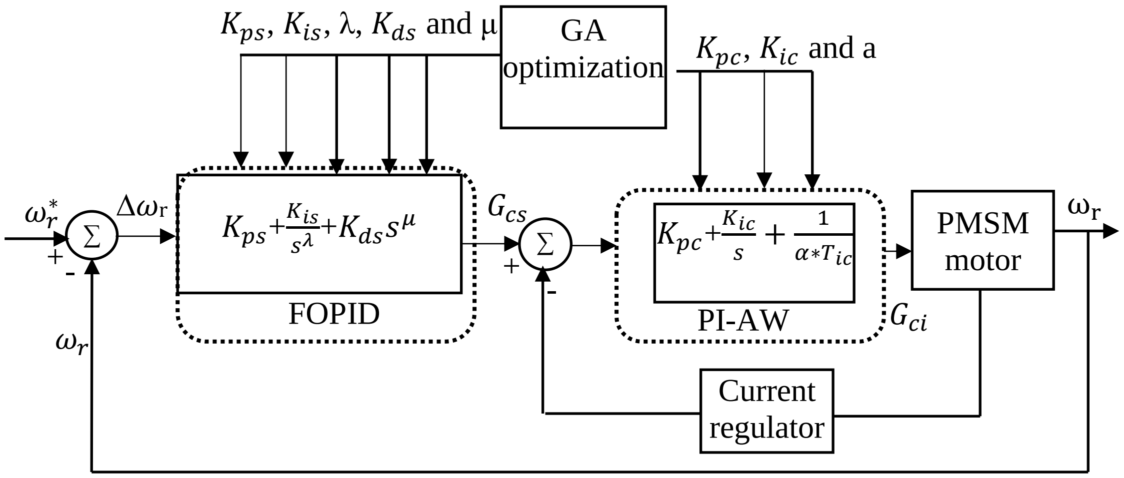

Figure 4.6 Block diagram of GA implementation in cascaded control of PMSM motor

4.3.1 The Tuning Parameter of FOPID Cascade with PI-AW Controller

GA runs based on population size and maximum generation. It terminates when reaches maximum generation. It is repeatedly running until the minimum result of error value is obtained. The GAs runs based on error evaluation methods (ISE, ITAE, IAE, and ITSE). The error that occurs between the two speeds is calculated using the trapezoidal rule ($\frac{h}{2}$ (a+b). where *h* is the height of the area, that is the integrated part. The error can be described mathematically as:

$$ISE = \int_0^\infty (|e_1(t)| + |e_2(t)|)dt \tag{4.11}$$

$$IAE = \int_0^\infty ([e_1(t)]^2 + [e_2(t)^2])dt \tag{4.12}$$

$$ITAE = \int_0^\infty t(|e_1(t)| + |e_1(t)|)dt \tag{4.13}$$

$$ITSE = \int_0^\infty t([e_1(t)]^2 + [e_2(t)^2])dt \tag{4.14}$$

where e_1 is the error input to speed (FOPID) controller whereas e_2 is the error input to the current controller of the PMSM motor. The above error evaluation methods briefly describe in the MATLAB code concerning the GA optimization method mentioned in appendix [B]. Error evaluation methods used in GA and the controller in the velocity form can be given as:[54]:

$$J(K_p, T_i, T_d) = \omega_1(ISE) + \omega_2(IAE) + \omega_3(ITAE) + \omega_4(ITSE) \quad (4.15)$$

$$G_c(k) = K_p[(e(t) - e(k-1) + \frac{T}{T_i}e(k) + T_d(e(k) - 2e(k-2)] + u(k-1) \quad (4.16)$$

FOPID controller cascaded PI with Anti-Windup controller has eight tuning parameters: K_{ps}, K_{is}, λ K_{ds} and μ, for FOPID controller K_{pc}, K_{ic}, and α. K_i and K_d are between 0 and 15 whereas the parameter range of λ, μ, and α are between 0 and 2. Table 4.1 shows, the data specification of GAs used in this research work.

Table 4.1 The data specification of GA used in this research work

Parameter	Type and value
Maximum generation	20
Population size	30
Encoding	Binary
Selection	Uniform
Crossover	Single point crossover
Mutation	Uniform
No of parameters	8
Lower boundary	[0.001 0.001 0.001 0.001 0.001 0.001 0.001 0.001]
Upper boundary	[15 15 2 10 2 5 5 2]

The GA optimization technique runs concerning error evaluation methods (IAE, ISE, ITAE, and ITSE). The error value is obtained based on IAE, ISE, ITAE, and ITSE. Finally, to figure out which one is to reduce the error value approach to zero. In this thesis, the ITAE error evaluation method has less error value among them. The error evaluation methods have different performances from system to system. IAE or others have the best error value in other systems. The simulation result is discussed in chapter four. Table 4.2 shows the value of the controller parameters that present in the system modeling.

Table 4.2 The tuned parameter of FOPID cascaded with PI-Anti-windup.

Controllers	Optimized parameters	Optimized results
FOPID speed controller	K_{ps}	12.9069
	K_{is}	9.2581
	λ	0.0451
	K_{ds}	6.0048
	μ	0.0117
PI-AW current controller	K_{pc}	1.0234
	K_{ic}	1.1433
	α	0.4026

After GAs optimization, the transfer function of the given speed controller (GA tuned FOPID) cascaded in the current controller (GA tune PI-AW) for PMSM becomes:

$$G_{FOPID} = K_{ps} + \frac{K_{is}}{s^{\lambda}} + K_{ds}s^{\mu} = 12.9069 + \frac{9.2581}{s^{0.0451}} + 6.0048s^{0.0117} \quad (4.17)$$

$$G_{PI-AW} = (K_{pc} + \frac{K_{ic}}{s}) * e(s) + \frac{1}{\alpha * T_{is}} * u_f(s) \quad (4.18)$$

$$= (1.0234 + \frac{1.1433}{s}) * e(s) + \frac{1}{0.4026 * 0.89513} * u_f(s)$$

4.3.2 Tuning Parameters of PID Cascaded with PI Current Controller

For comparison purposes with the proposed controller, PID controllers for speed cascade with PI controller for current loop are implemented using GA optimization technique. The cascade controller has five parameters: K_{ps}, K_{is}, K_{ds}, K_{pc} and K_i. When the power of integral and derivative order λ and μ is equaled to zero respectively. The FOPID controller became a conventional PID controller. It can be described mathematically as shown below.

$$G_{fopid}(s) = K_p + \frac{K_i}{s^{\lambda}} + \frac{K_p}{s^{\mu}} = K_p + \frac{K_i}{s^1} + K_d s^1 = K_p + \frac{K_i}{s} + K_d s = G_{pid}(s) \quad (4.19)$$

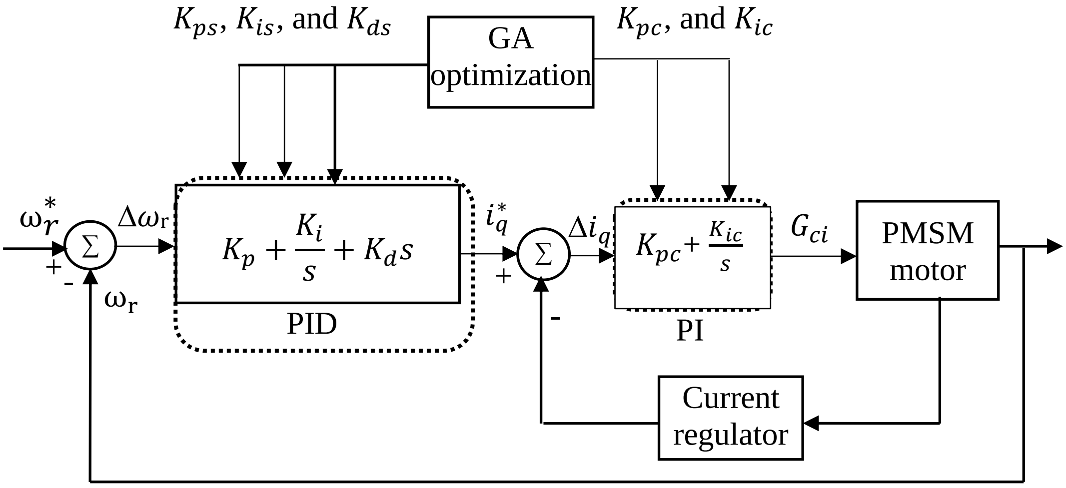

Figure 4.7 The overall block diagram of PID cascaded with PI

In this cascade controller also, GA is optimized based on the objective function. The best fitness value of this cascade controller based on ITAE is 0.113677. The FOPID controller cascaded with PI with Anti-Windup current controller is more reduced than the PID controller cascade with PI current controller. The simulation part is discussed in the next chapter. The parameters of the GA optimization technique used in PID cascaded with PI current controller are given as shown in Table 4.3 below.

Table 4.3 The data specification of GA used in this Research Work

Parameter	Type and value
Maximum generation	30
Population size	40
Encoding	Binary
Selection	Uniform
Crossover	Single point crossover
Mutation	Uniform
No of parameters	5
Lower boundary	[0.001 0.001 0.001 0.001 0.001 0.001]
Upper boundary	[15 15 15 15 15]

After the GA optimization technique is terminated, the value of the tuning parameters is obtained.

The tuned parameter of PID speed controller cascaded with PI current controller are given in Table 4.4 as shown below.

Table 4.4 The tuned parameter of PID cascaded with PI current controller

Controllers	Optimized parameters	Optimized results
PID speed controller	K_{ps}	9.1842
	K_{is}	8.8005
	K_{ds}	0.0501
PI current controller	K_{pc}	6.4105
	K_{ic}	1.3854

After GAs optimization, the transfer function of the given speed controller (GA tuned PID) cascaded in the current controller (GA tuned PI) for PMSM motor becomes:

$$G_{PID} = K_{ps} + \frac{K_{is}}{s} + K_{ds}s = 9.1842 + \frac{8.8005}{s} + 0.0501s \tag{4.20}$$

$$G_{PI} = (K_{pc} + \frac{K_{ic}}{s}) * e(s) = (6.4105 + \frac{1.3854}{s}) * e(s) \tag{4.21}$$

4.4 Review of ANFIS Controller

Electric vehicles are subjected to severe disturbance while driving due to passenger boarding, road condition, and wind. This leads to an error that is varied between the actual speed and input speed set by the users and the error should be trained with continuous intervals of time using an error observer. The disturbance is not recovered easily using a traditional controller like PID. Fractional-order PID controller is more suitable in industrial and other systems due to the presence of integral and derivative order, but during load change, the actual response is going to an unstable condition and changes the transient response parameters like rising time, peak time, settling time and maximum overshoot. In this case, traditional controller combine with artificial intelligence technique has better system performance [55].

Artificial intelligence controllers like Fuzzy logic control using scale factor, Neural Network, and ANFIS have been used for load variation and non-linear systems which is the system has a better transient response. Fuzzy logic controller and ANFIS artificial intelligence techniques have been commonly used for load variation and non-linear systems. In a fuzzy logic controller, fuzzy sets or rules are generating using trial and error which is tedious and time-consuming. This problem is compensated using ANFIS artificial intelligence technique which is easily accessed on MATLAB/Simulink. It is a combination of a Fuzzy inference system and a Neural network that uses a Sugeno-type fuzzy model which is a non-linear model. If the fuzzy inference system has two inputs x, y, and one output. If-then rule of Sugeno's type fuzzy model can be given as [56][55].

Rule 1: If x is A_1 and y is B_1 then $f_1 = p_1x + q_1y + r_1$

Rule 2: If x is A_2 and y is B_2 then $f_2 = p_2x + q_2y + r_2$

Figure 4.8 shows, the overall structure of ANFIS controller which has two inputs x, y, one output *f*, and five layers.

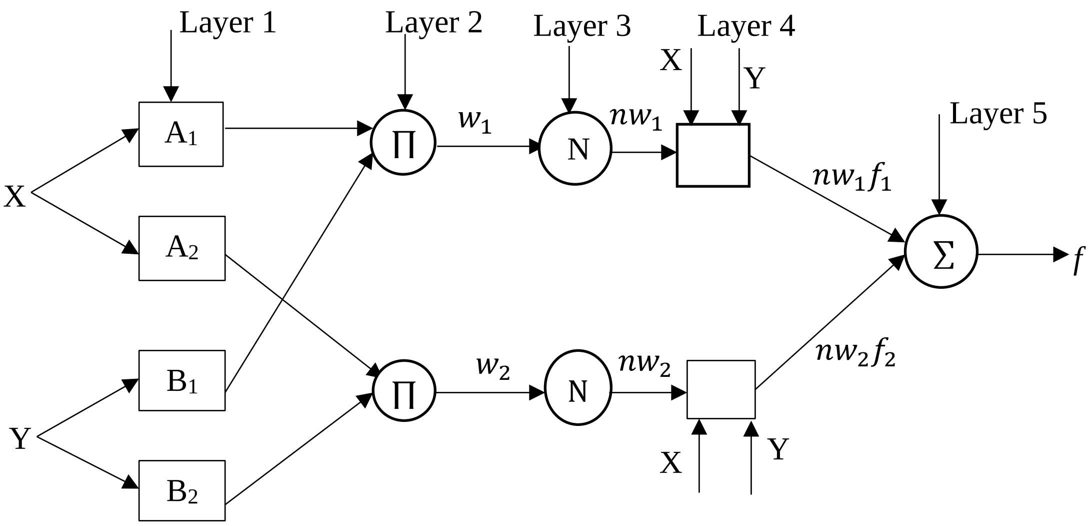

Figure 4.8 The general structure of ANFIS network

4.4.1 Emulate FOPID Speed Controller using ANFIS

In this study, ANFIS controller cascaded in FOPID speed controller during load conditions was implemented. ANFIS controller is the combination of a Neural Network and Fuzzy inference system. The fuzzy (FIS file) rule is generated based on input and output data (data set) that are loaded from MATLAB workspace or file given to ANFIS which needs a suitable data set for training Neural Network to optimize the generated membership function of fuzzy inference system. The Neural Networks train until to obtain minimum root- mean – square error (RMSE) value. Figure 4. shows, the overall block diagram that is used for data training for ANFIS based FOPID controller.

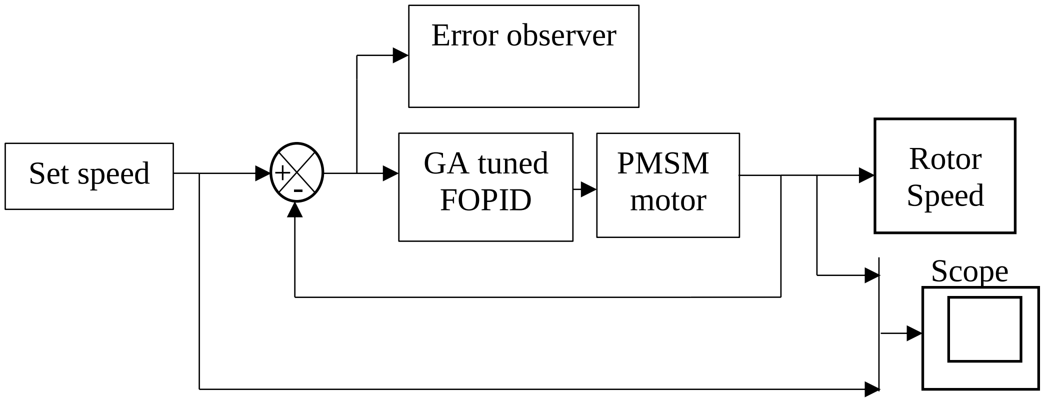

Figure 4.9 The block diagram that used for data training to ANFIS controller

4.4.2 Generate Fuzzy Rule

A fuzzy rule (FIS file) is constructed based on seven assumptions which is the error becomes Negative-Large (NL), Negative-Medium (NM), Negative-Small (NS), Zero (Z), Positive-Small (PS), Positive-Medium (PM), and Positive-Large (PL) as shown Table 4.5. The neural network trains the data that load from workspace or file repeatedly until the minimum root-mean-square error (RMSE) value. Figure 4.10 shows, the training mechanism of the ANFIS controller using input and output data from the MATLAB workspace.

Table 4.5 Rule base for fuzzy rule construction

ce\e	NL	NM	NS	ZE	PS	PM	PL
NL	NL	NL	NML	NM	NMS	NS	ZE
NM	NL	NML	NM	NMS	NS	ZE	PS
NS	NML	NM	NMS	NS	ZE	PS	PMS
ZE	NM	NMS	NS	ZE	PS	PMS	PM
PS	NMS	NS	ZE	PS	PMS	PM	PML
PM	NS	ZE	PS	PMS	PM	PML	PL
PL	ZE	PS	PMS	PM	PML	PL	PL

Write “anfisedit” in the command window. After opening the ANFIS controller, load the data from the workspace or file. Set the epoch value and generate the FIS rule. Train the load data again and again to get the best RMS value. The last step is to save fuzzy rules from files in the ANFIS train table to Matlab workspace or file. Load Fuzzy toolbox from Matlab library and connect to the proposed Simulink diagram, load the fuzzy rule file saved to workspace or file to Matlab toolbox that presents in the proposed Simulink diagram. Run the overall Simulink diagram and get the simulation result. Figure 4.11, shows the neural network structure that generates based on train data of input and output of the system. Table 4.6 shows, the data specification of ANFIS used in this research work.

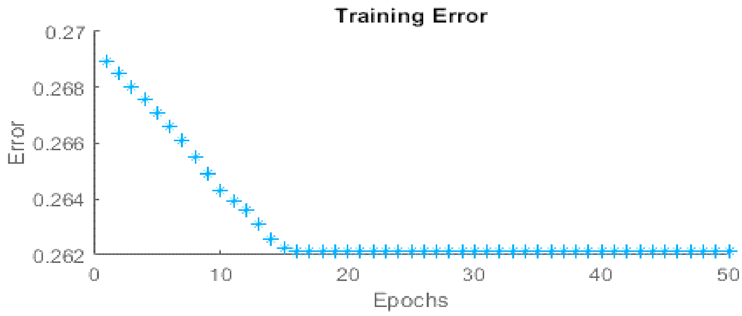

Figure 4.10 Error training mechanism for ANFIS

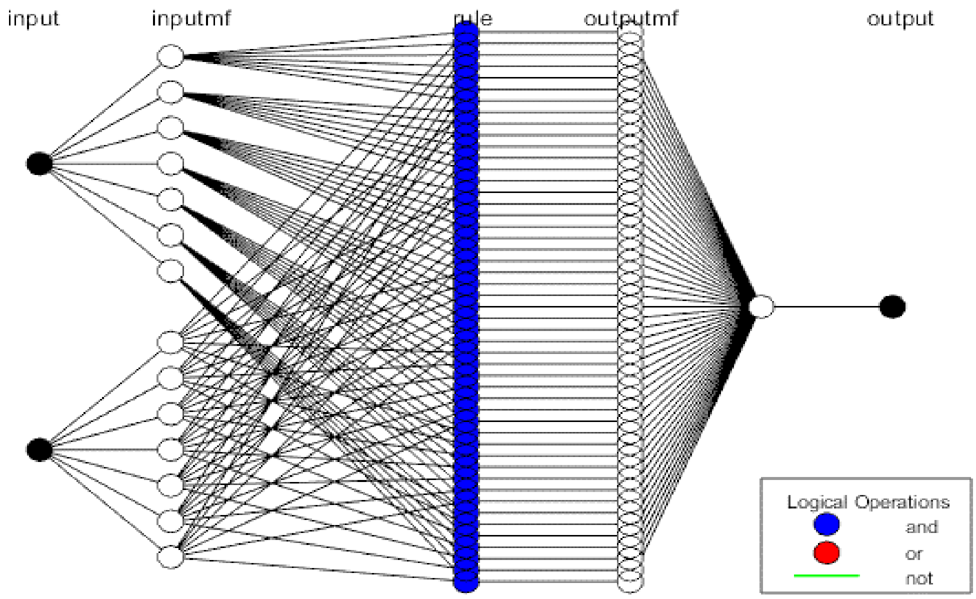

Figure 4.11 Structure of neural network based on input and output data set

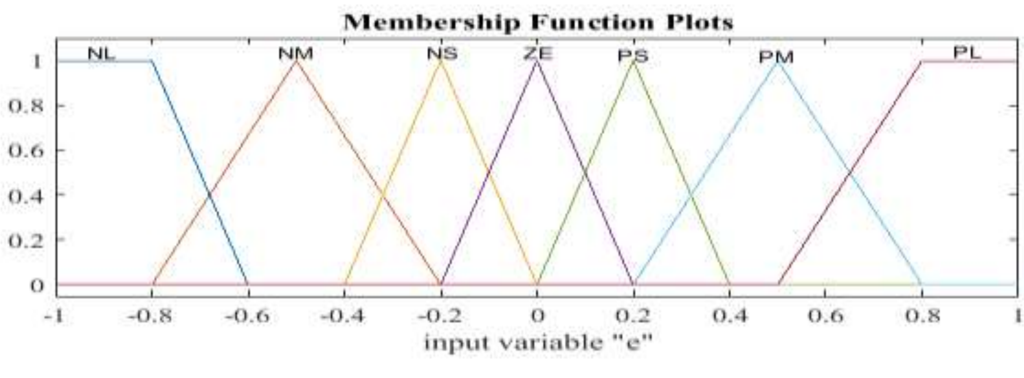

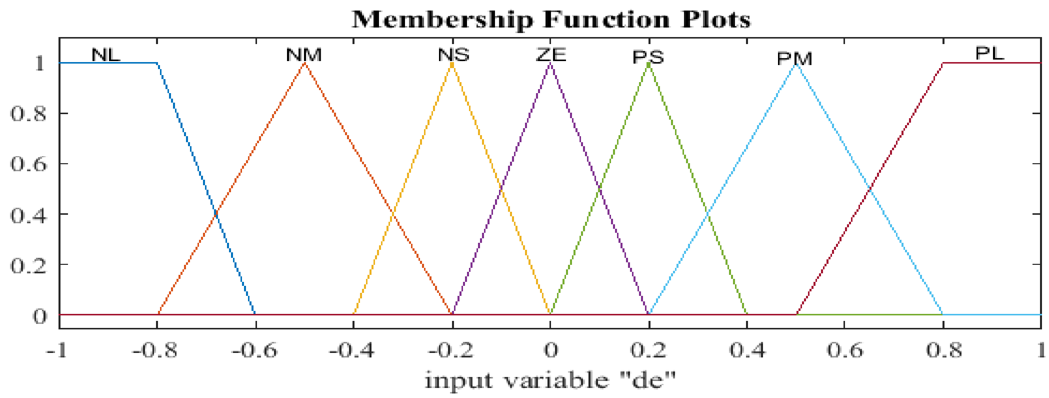

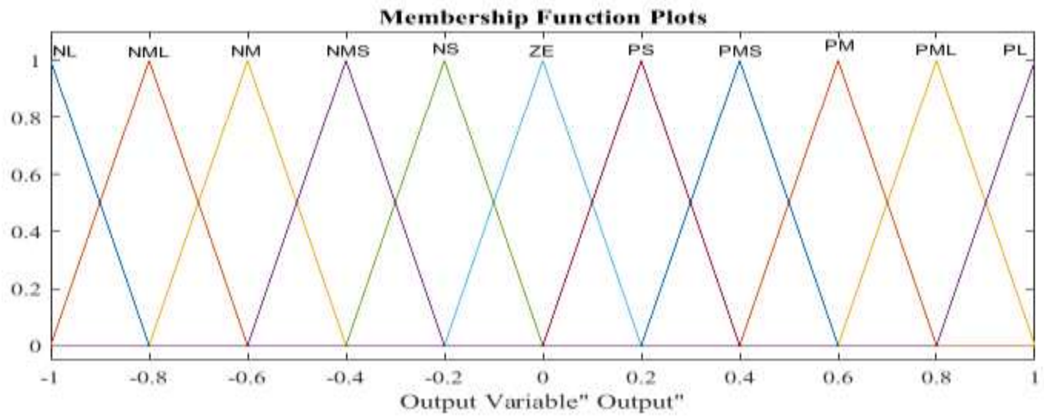

Figure 4.12 Input and Output membership function of fuzzy rule respectively

Table 4.6 Parameter specification of ANFIS used in this research work

Parameters	Value
Number of inputs	2
Number of outputs	1
Training data	1000
Non-linear parameters	43
Linear parameters	243
Fuzzy rule	49
Fuzzy rule type	Takagi-Sugeno type
Optimization method	Hybrid
Types of input MF	Triangular

CHAPTER FIVE

RESULTS AND DISCUSSIONS

The speed control of the PMSM motor using different controllers is mentioned in this chapter. The comparison of speed and current controllers is discussed based on objective functions (IAE, ISE, ITAE, and ITSE) and transient response (rise time, peak time, settling time, and overshoot), and steady-state response using genetic algorithm optimization technique are discussed. At no-load conditions, the starting current is suddenly rising leads to a high overshoot and burn out the internal connection of the motor. To reduce the starting current overshoot, the GA tuned PI with Anti-Windup current control was implemented in cascaded with the speed ANFIS based FOPID controller.

5.1 Three-Phase and Two-Phase Voltages

Based on Clark and Park transformations, the three-phase and two-phase voltage are extracted. Figure 5.1 shows the three-phase stator voltage of the PMSM motor.

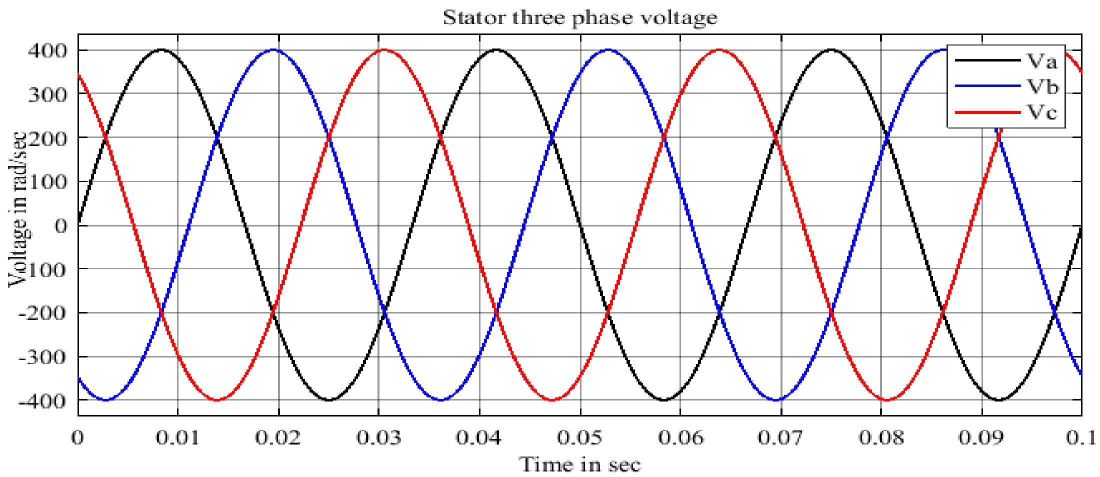

Figure 5.1 Three-phase sinusoidal stator voltage of the PMSM motor

The simulation result of the two-phase sinusoidal stator voltage of the PMSM motor is shown in Figure 5.2. This simulation result is obtained after Park and Clark transformation process was done. Figure 5.3 shows, the signal used in the SVPWM switching technique of the three-phase inverter. Figures 5.4, 5.5, and 5.6 shows, the resulting get signal that is generated sequentially which is used to switch 'on' and 'off' the IGBT to prevent short circuits that present in the inverter and provide a continuous three-phase voltage which is utilized to activate the PMSM motor.

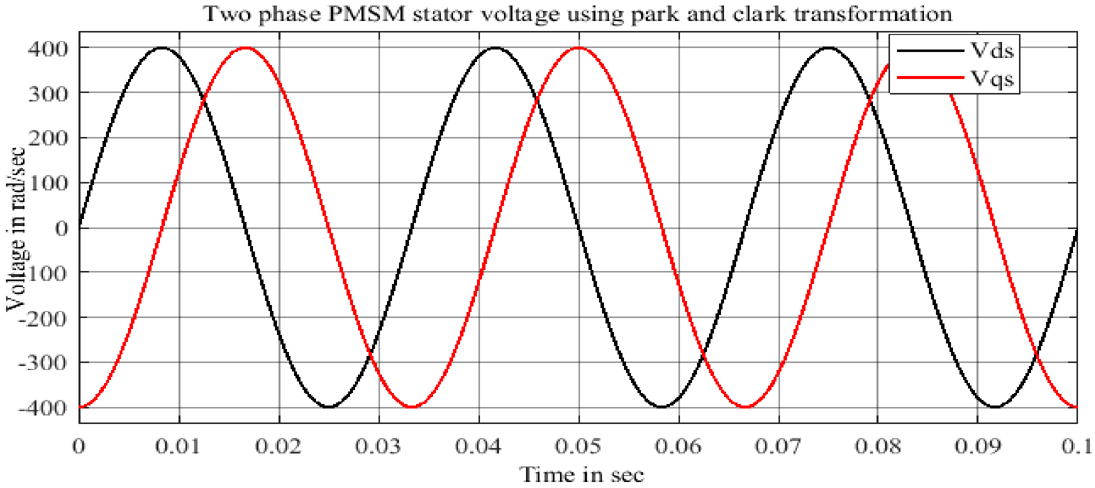

Figure 5.2 Two-phase sinusoidal stator voltage of the PMSM motor

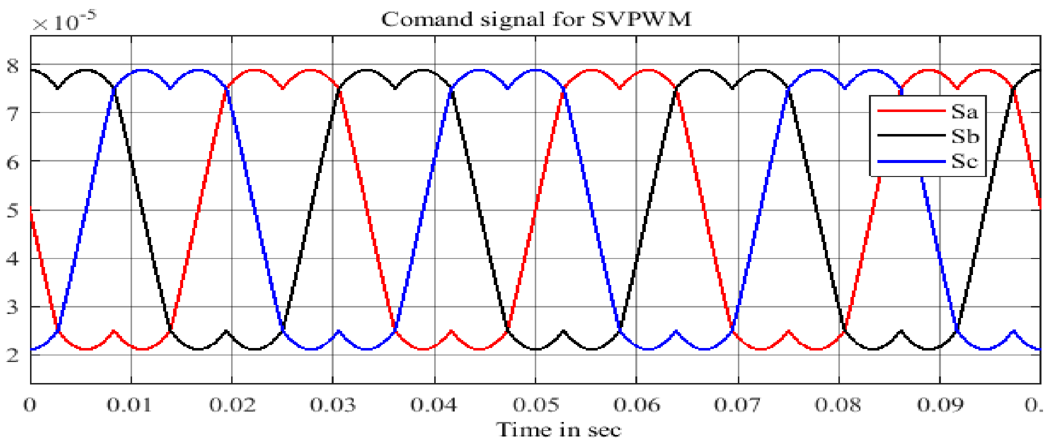

Figure 5.3 Command signal for SVPWM switching technique

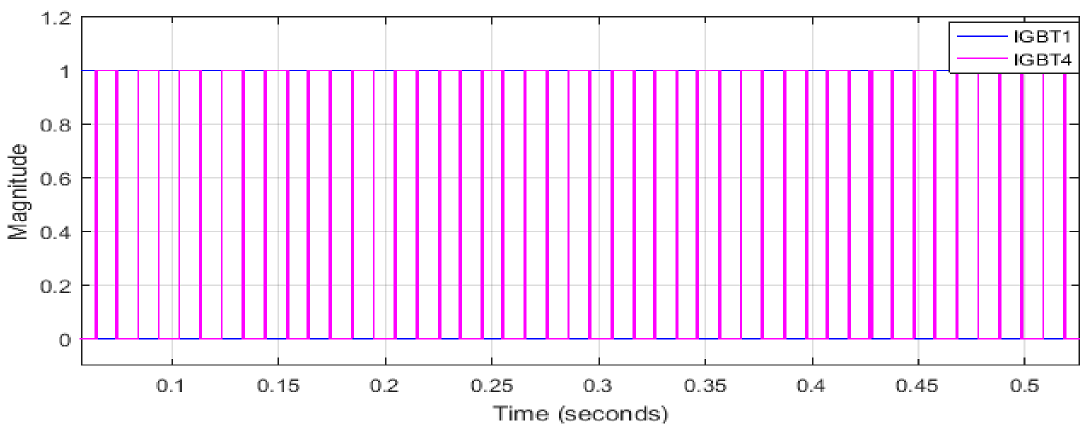

Figure 5.4 The generated gate signal from driver circuit used for $IGBT_1$ and $IGBT_4$

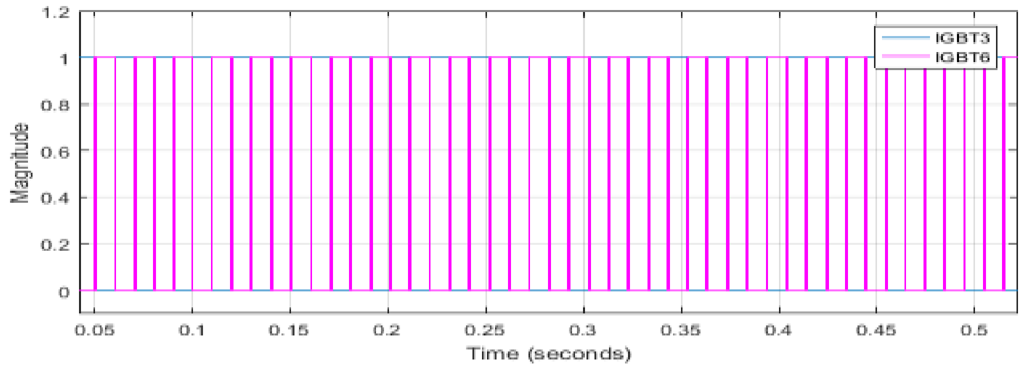

Figure 5.5 The generated gate signal from driver circuit used for $IGBT_3$ and $IGBT_6$

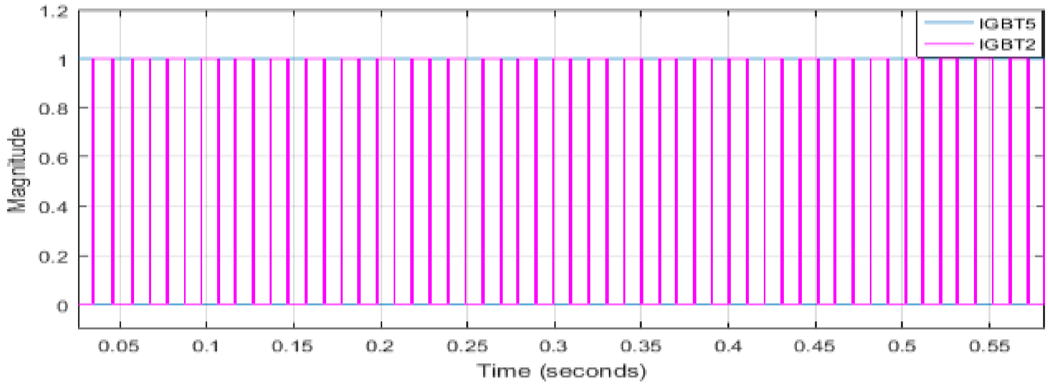

Figure 5.6 The generated gate signal from driver circuit used for $IGBT_5$ and $IGBT_2$

5.2 Speed and Current Controller of PMSM motor

In this research work, ANFIS based FOPID speed controller cascaded with GA tuned PI with an Anti-Windup scheme is developed. For comparison purposes, different controllers are also implemented.

5.2.1 Result of ANFIS based FOPID Speed Control of PMSM Motor

Among the different controllers implemented in this work, ANFIS based FOPID speed controller in cascaded with PI with anti-windup scheme current controller has better transient and steady-state response. Hence depending on the road type and passenger boarding, every time the vehicle has different loads. It leads to the steady-state error in the speed results. To mitigate this effect, the ANFIS controller with FOPID is used on the speed regulator side. Figure 5.4 shows the simulation result of ANFIS based FOPID controller at no-load and setpoint change conditions. The result is almost the same as the FOPID controller at no-load condition. When the load is varied (T_l =40 Nm), ANFIS based FOPID controller has better performance than the GA tuned FOPID and GA tuned PID speed controller of PMSM motor as shown in Figure 5.16.

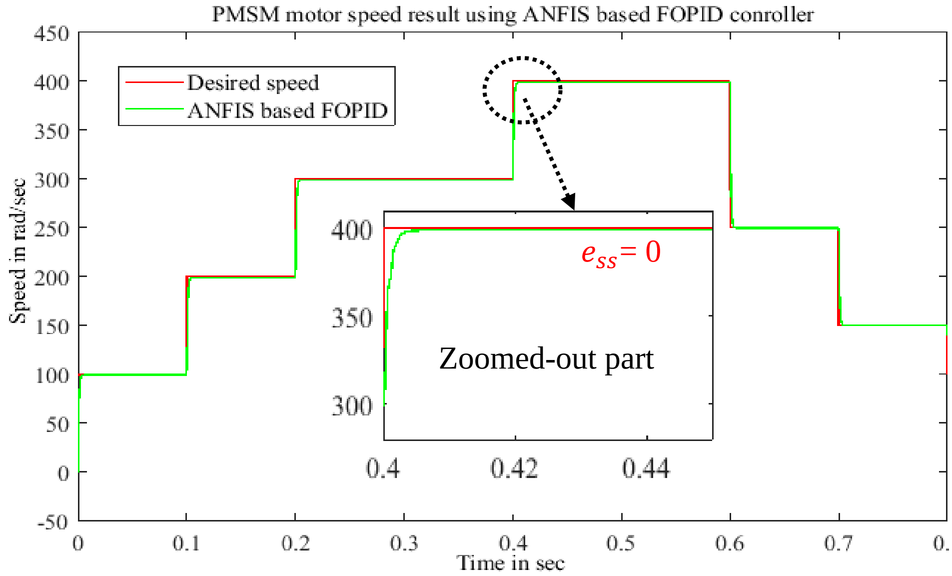

Figure 5.7 The speed result of the PMSM using ANFIS based FOPID controller

5.2.2 PMSM Motor Speed Results Using GA-FOPID Controller

Figure 5.8 shows, the simulation result of the FOPID controller at no-load condition and set-point change. The result shows FOPID has better set-point tracking. It has 0.417sec settling time, 0.004sec rise time, 0.0003% maximum overshoot and 0% steady-state error at no-load.

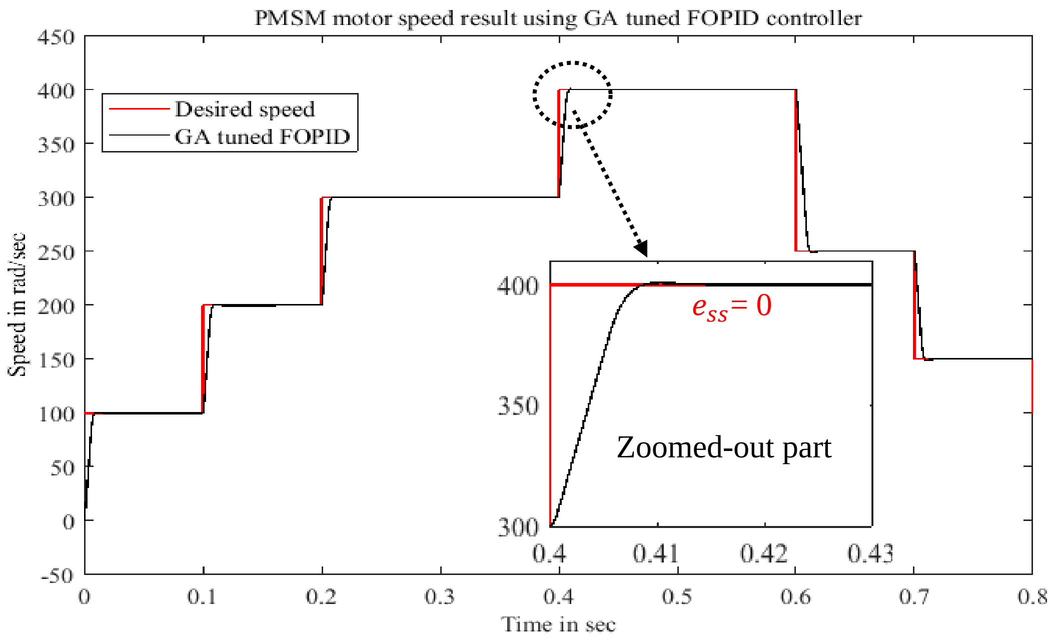

Figure 5.8 The speed result of the PMSM motor using GA tuned FOPID controller

However, due to sudden load change, this controller does not improve the steady-state error. The details of comparative analysis with other controllers are discussed in the discussion part of this chapter. The parameters of the FOPID speed controller in cascaded with PI-AW current controller of PMSM motor tuned with GA optimization technique. The value of the tuning parameters of the speed controller and the current controller is obtained. Figure 5.9 shows, the graphical representation based on ITAE objective function. The best fitness value after optimization is 0.000153354. Figure 5.10 shows, the graphical representation of PID speed controller in cascaded with PI current controller fitness value.

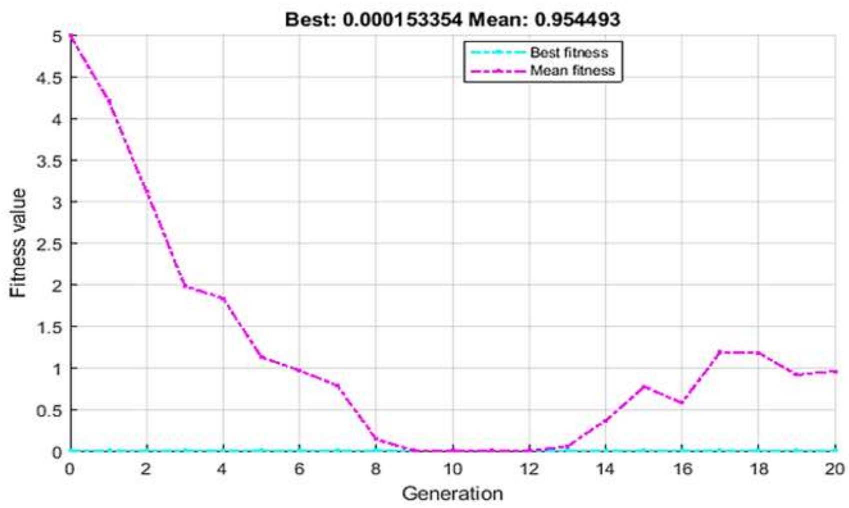

Figure 5.9 GA optimization for FOPID cascade with PI-AW current controller

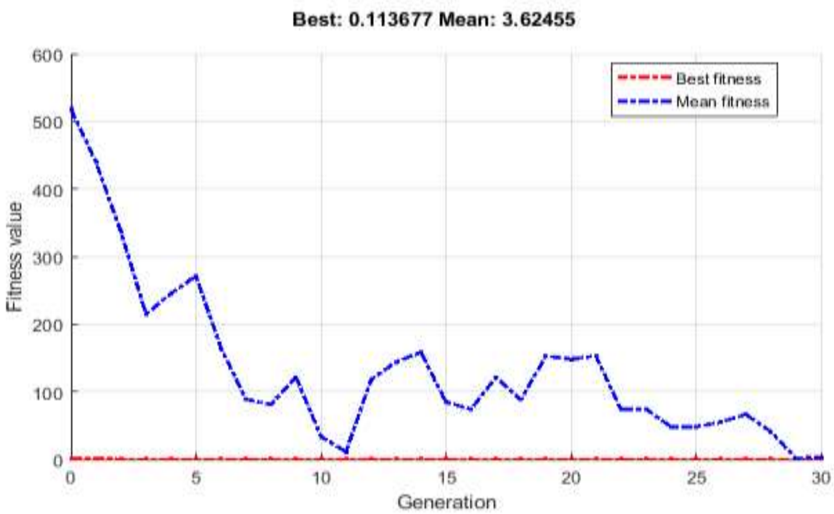

Figure 5.9 GA optimization for PID cascade with PI current controller

5.2.3 PMSM Motor Speed Results Using GA tuned PID Controller

The result of the PID speed controller is as shown in Figure 5.11. This shows that PID speed result has less rise time and peak time. However, it has an overshot, large settling time, and sluggish response compared to the proposed controller. When the load changes, the maximum overshot changes from 0.09% to 0.1%, and also the steady-state error between the input and output speed is changed from 0.016% to 0.1%. This shows that the GA tuned PID controller has poor performance when the load changes.

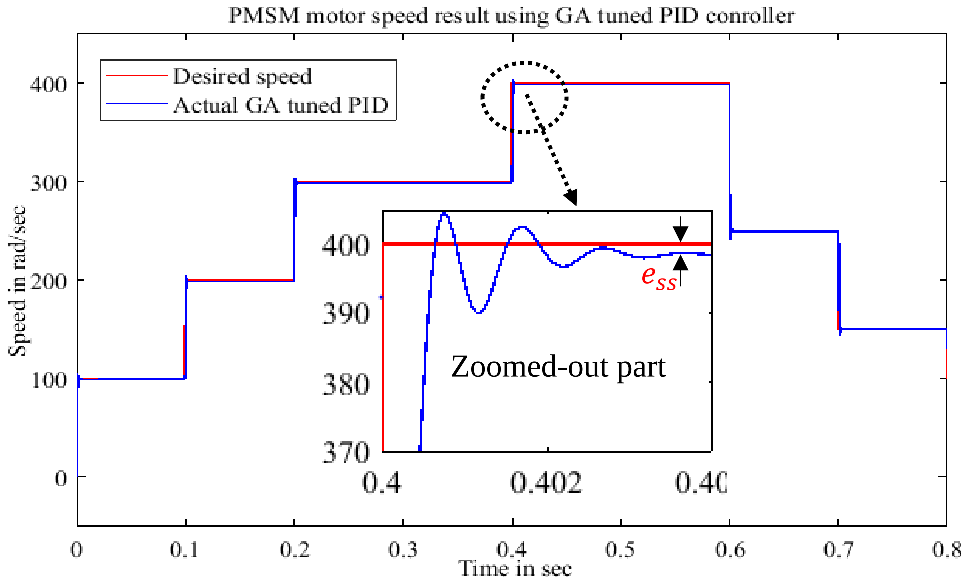

Figure 5.10 The speed result of the PMSM motor using GA-PID controller

5.3 PMSM motor current controller result using GA tuned PI-AW

Figure 5.12 shows, the current result of the PMSM motor using PI with an anti-windup schemes controller. The reference current depends on the speed controller output, and the magnitude of the GA-PIAW current controller is 100A. Figure 5.12 shows, the current result of the PMSM motor using GA tuned PI with error recalculation Anti-Windup technique.

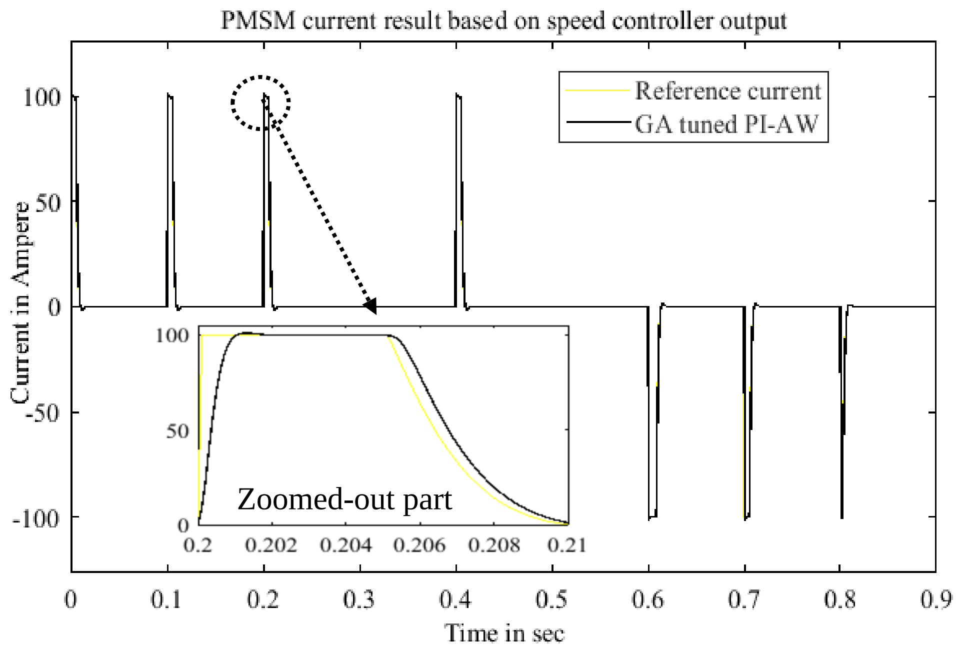

Figure 5.11 The proposed PI-AW current controller simulation result

5.4. PMSM motor current result using GA tuned PI controller

For comparison purposes, the GA tuned PI current controller was also performed As shown in Figure 5.13, the current magnitude of the GA tuned PI current controller is 200A. The GA tuned PI with Anti- Windup current controller is more performed than GA tuned PI current controller. Figure 5.13 shows, the current result of PMSM motor using GA tuned PI current controller. A detailed description of all controllers is present in the discussion part.

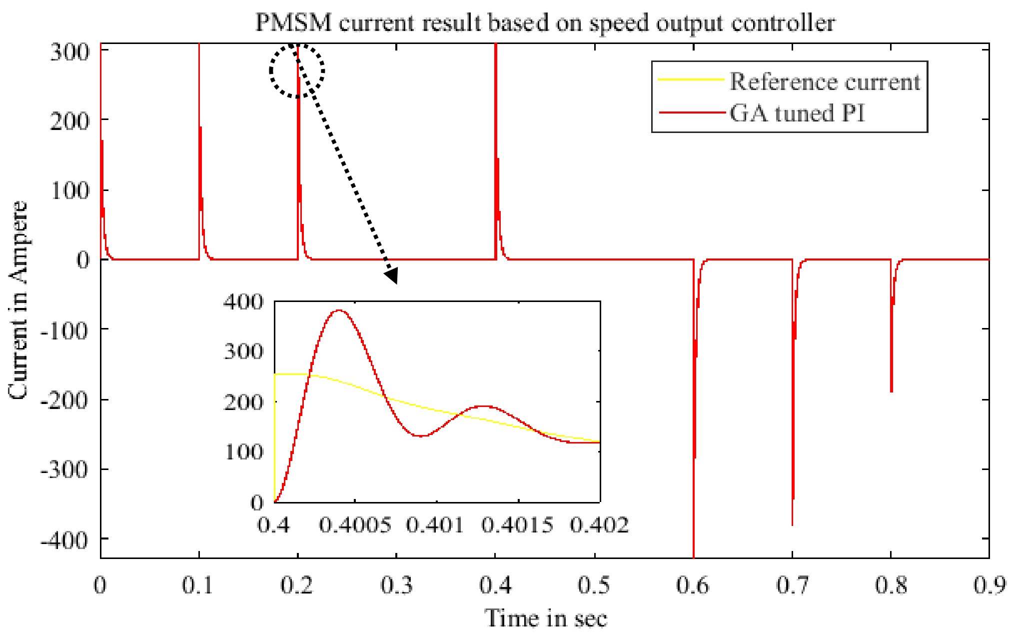

Figure 5.12 The PMSM motor current result using GA-PI current controller

5.5 PMSM Motor Speed and Current Controller Results Discussion

Different speed controllers are discussed to distinguish a controller that has a better performance based on transient and steady-state performance criteria. Also, different current controllers are implemented.

5.5.1 Comparison of Speed Controller at No-load Condition

Figure 5.14 shows, the simulation result PMSM motor speed controller at constant setpoint and no-load conditions. It was performed at no-load using GA tuned PID, GA tuned FOPID, and the proposed ANFIS based FOPID controllers. The proposed controller has a better transient and steady-state response. FOPID controller is almost the same transient and steady-state response with ANFIS based controller at no-load condition.

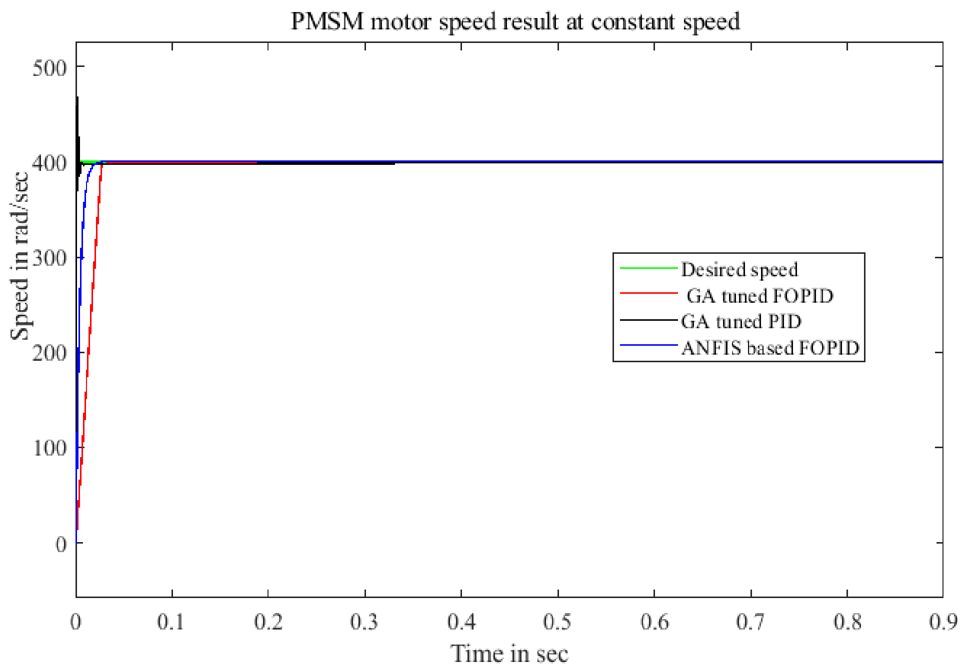

Figure 5.13 Speed controller result of PMSM motor at a constant speed

Figure 5.14 shows, the zoomed-out part of Figure 5.15. The graph is zoomed at the speed of 400 rad/sec and at the time 0.4 up to 0.43 sec. The graph shows, the ANFIS based FOPID controller has better system performance than others. It has 0.413 sec settling time (t_s), 0.003 sec rise time (t_r), 0.4094 peak time (t_p), 0.0002% overshoot (M_p), and 0% steady-state error (e_{ss}). The GA-PID controller has less rise time and peak time. However, it has more oscillation and steady-state error. This leads to instability in the system.

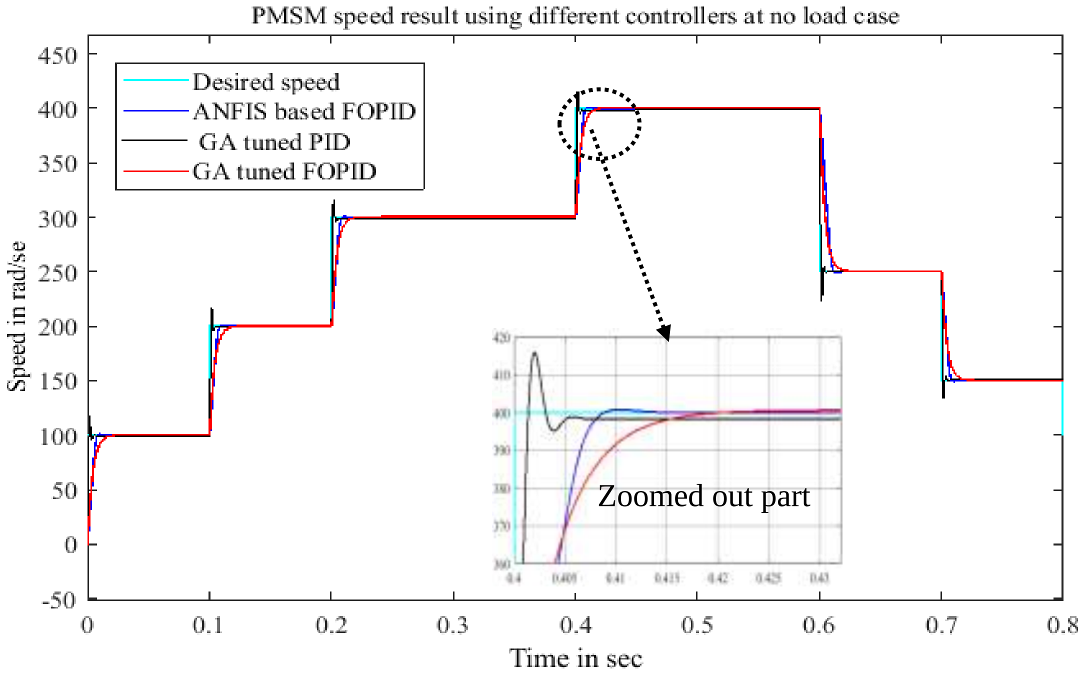

Figure 5.14 PMSM motor speed controller result at no-load with variable speed

Table 5.1 shows the value of set-point tracking performance criteria of the different controllers. The controller that has a shorter rise time, peak time, settling time, minimum steady-state error, and overshoot has better system performance.

Table 5.1 The comparison of speed controllers at no-load

Speed Controllers	Performance parameters result at no-load condition				
	t_s [sec]	t_r [sec]	t_p[sec]	$\%M_p$	$\%e_{ss}$
GA tuned PID	0.406	0.006	0.402	0.159	0.016
GA tuned FOPID	0.417	0.004	0.411	0.0003	0.003
ANFIS-FOPID	0.413	0.003	0.4094	0	0

Figure 5.16 shows that the proposed ANFIS based speed controller is outperformed other controllers. It has 0.0002% overshoot and zero steady-state error. GA-FOPID also has zero steady-state error and 0.0003% overshot. It is almost the same as the proposed controller. Figure 5.17 shows, the setpoint tracking comparison of the controllers in chart form. The data specification was taken from table 5.1.

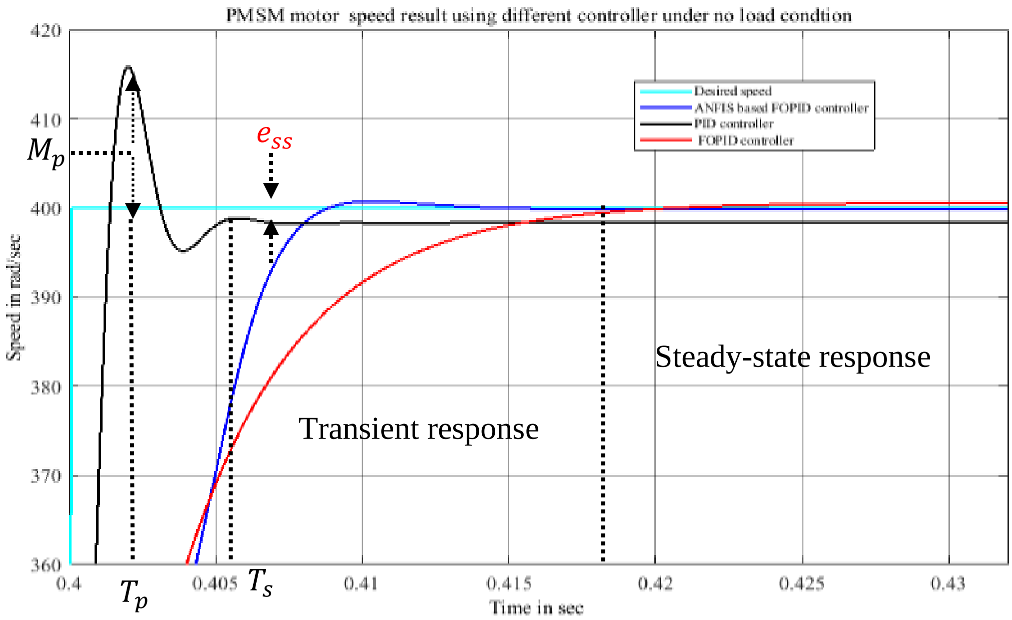

Figure 5.15 PMSM motor speed result of zoomed out part at no load

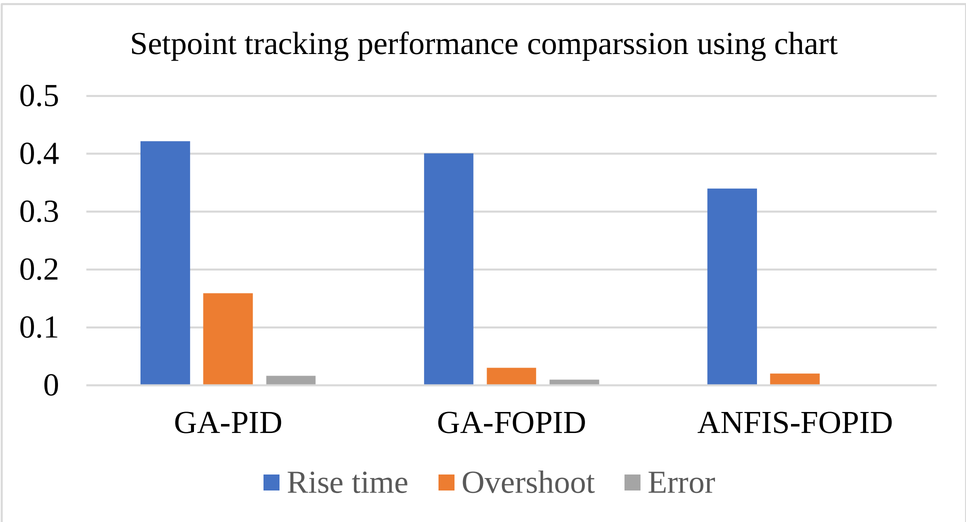

Figure 5.16 System performance of the sped controller in chart form

5.5.2 Effect of Disturbance on The Speed of the Vehicle

Depending on the passenger boarding, road type and resistive force that exerted on the vehicle when its in motion, every time the vehicle has different loads or disturbances. When the disturbance of the system is increased, the desired speed goes to decrease. Figures 5.18 and 5.19 show, the simulation result at the speed of 100 rad/sec corresponding with the disturbance (T_l = 5 Nm) and (T_l = 10 Nm) applies at 1 sec respectively. When the disturbance (T_l = 5 Nm) applies at 1 sec, the set-point is reduced by 12 rad/sec as shown in Figure 5.18 while the disturbance (load = 10Nm) applies at 1 sec, the set-point speed is reduced by 23.15 rad/sec as shown below figure 5.19. When the disturbance increase, the recovery time (t_r) and maximum overshoot (M_p) also increase. Here, the overall system has two responses, set-point response before disturbance applies and set-point response after disturbance is applied.

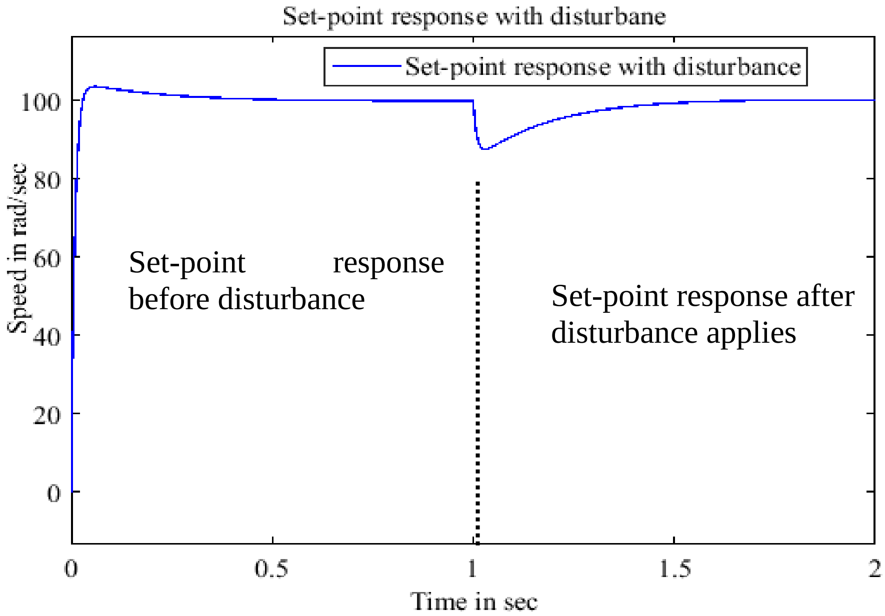

Figure 5.17 Effect of disturbance on the on the speed vehicle at load= 5 Nm

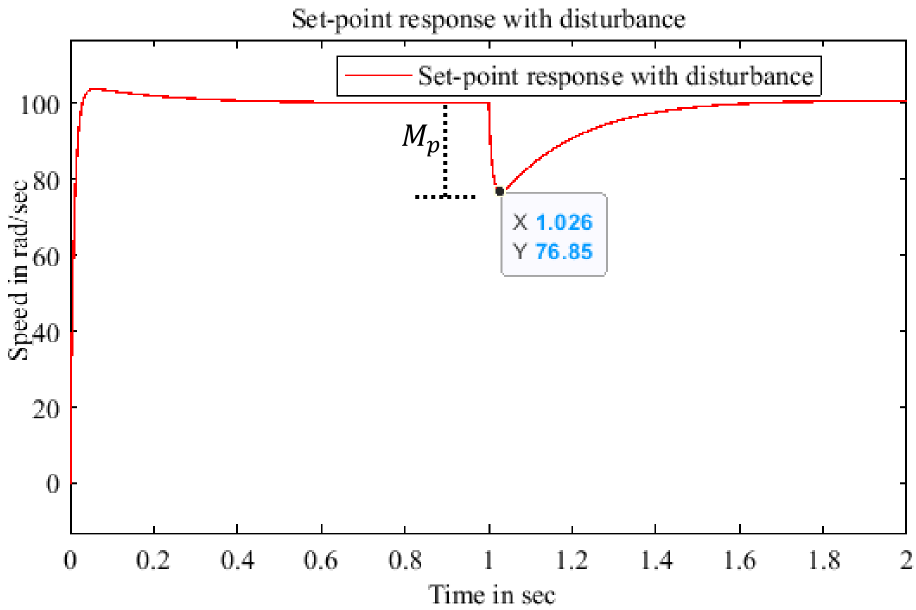

Figure 5.18 **Effect of disturbance on the speed of the vehicle at load= 10 Nm**

5.5.2.1 Set-point Tracking and Disturbance Rejection

Set-point tracking and disturbance rejection are the design objectives in most control systems. These objectives can be met with an adequate feedback control method. The controller should be applied to the system independently during set-point tracking and disturbance rejection to determine the controller's efficiency. Figure 5.19 shows, the system has two responses which are set-point responses before disturbance apply and after disturbance is applied.

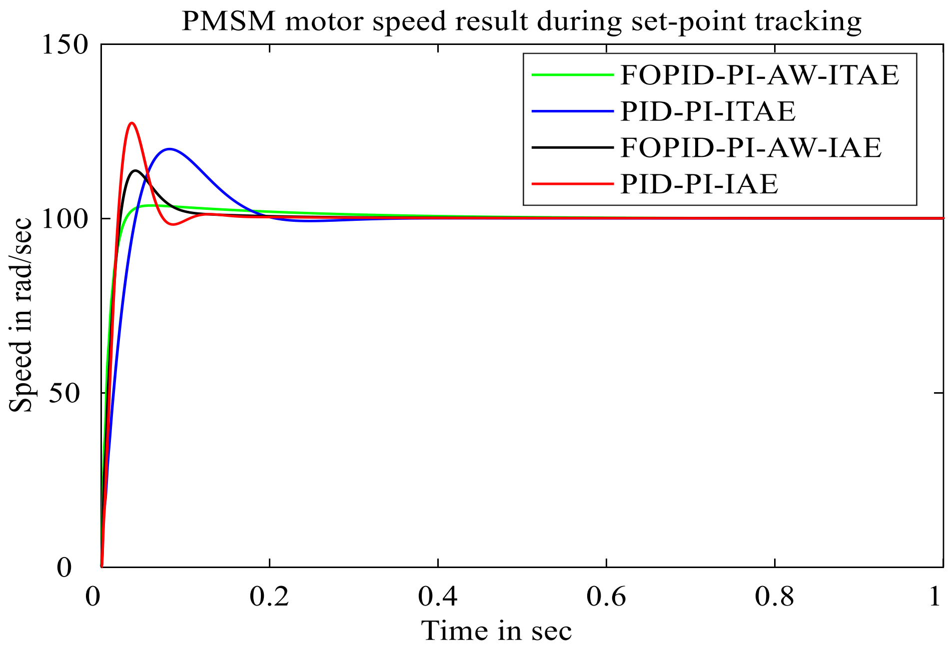

Figure 5.19 Set-point response tracking using different controllers

Figure 5. 20 shows, FOPID-PI-AW-ITAE has a better ability to track the desired speed of the system than other controllers without disturbance applied. However, during disturbance applied the controller has no totally rejected the disturbance as shown in Figure 5.21. In this case, Artificial intelligence controller has a better disturbance compensator. The controller is used to control the speed of the PMSM motor should overcome the disturbance variation.

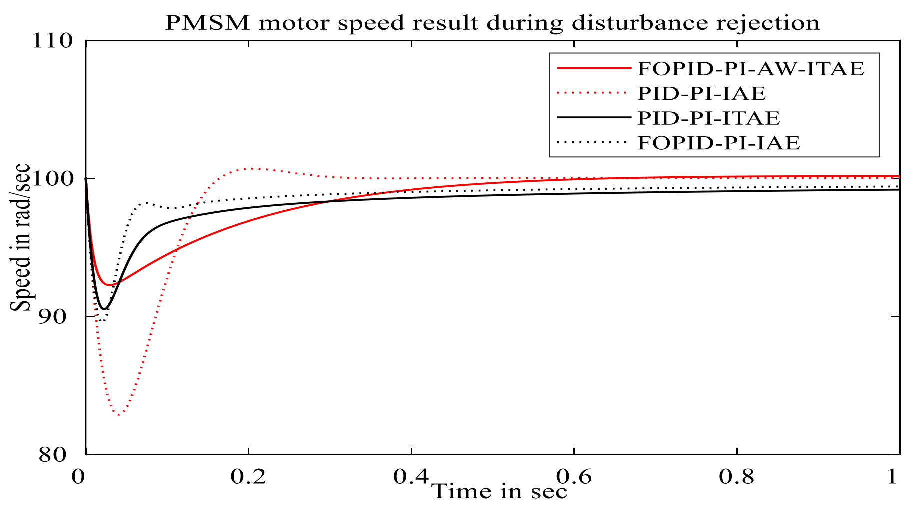

Figure 5.20 Disturbance rejection checking using a different controller

Figures 5.22 and 5.23 show, the speed and current controller output signal used for the PMSM motor respectively.

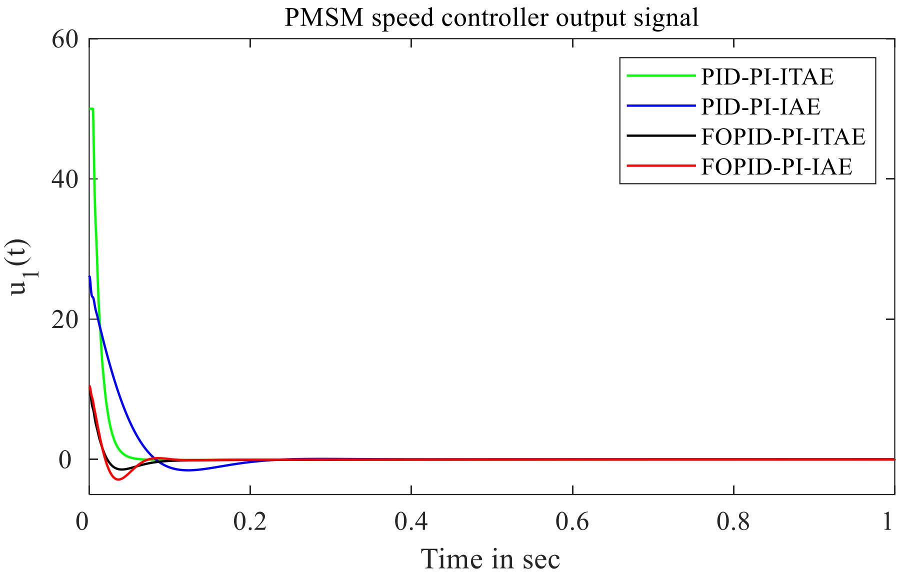

Figure 5.21 Speed controller output signal of PMSM motor

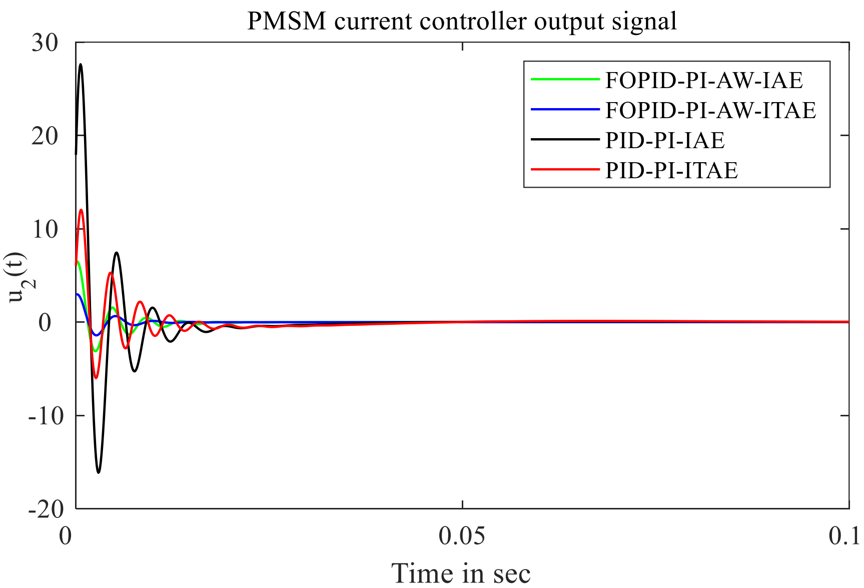

Figure 5.22 Current controller output signal of PMSM motor

5.5.3 Comparison of Speed Controller at Load Change

Figure 5.24 shows the simulation result of the speed controllers of the PMSM motor during load change and variable setpoint. When the load variation occurs, the speed controllers of GA tuned PID and GA tuned FOPID are changing their steady-state error and overshot while ANFIS based FOPID controller as it is.

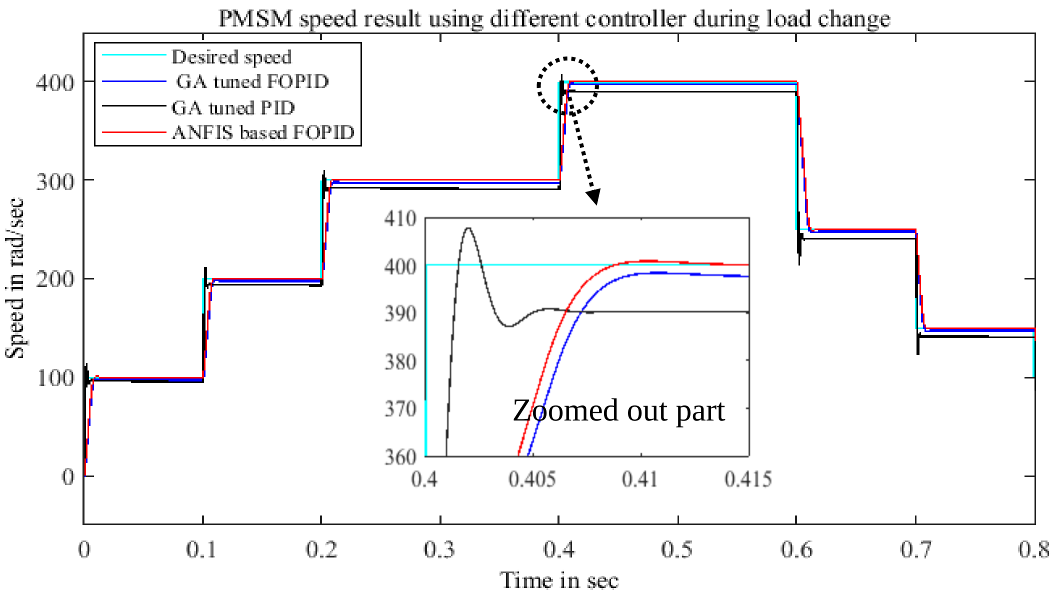

Figure 5.23 PMSM motor speed controller result during load change (T_l = 40)

The simulation shows ANFIS based FOPID controller has the system performance parameters of 0% steady-state error and 0% overshoot whereas GA tuned FOPID controller has 0% overshoot and 0.005% steady-state error and GA tuned PID controller has 0.8% overshoot and 0.1% steady-state error which means During load variation, ANFIS based FOPID controller performed well for both disturbance rejection and set-point tracking of the system. Table 5.2 shows, the value of set-point tracking performance criteria of the different controllers at load (T_l =40) change. At load change condition, ANFIS based FOPID controller has better performance in all aspects of the performance parameter criteria. variation.

Table 5.2 The comparison of speed controllers at load change

Speed Controllers	Performance parameters result at load condition				
	t_s[sec]	t_r [sec]	t_p[sec]	$\%M_p$	$\%e_{ss}$
GA tuned PID	0.4061	0.0027	0.402	0.8	0.1
GA tuned FOPID	0.4121	0.001	0	0	0.005
ANFIS based FOPID	0.4111	0.0021	0.4093	0	0

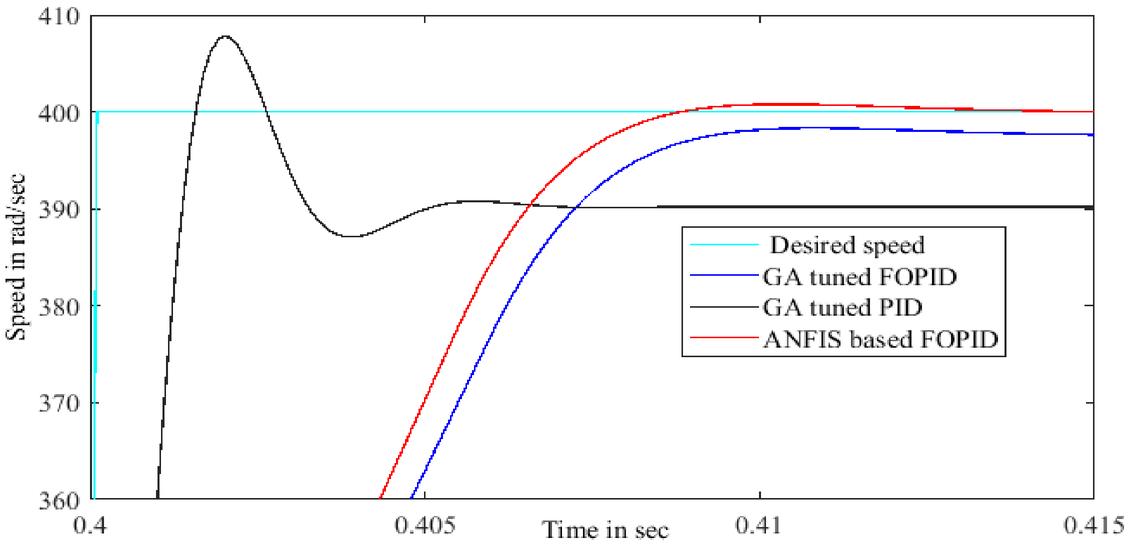

Figure 5.24 PMSM motor speed result of zoomed out part at load condition

Table 5.3 Comparison of speed controllers at no- load and with load

Speed Controllers	No-load	Load change
	Steady-state error	Steady-state error
GA tuned PID	0.016%	0.1%
GA tuned FOPID	0%	0.005%
ANFIS based FOPID	0%	0%

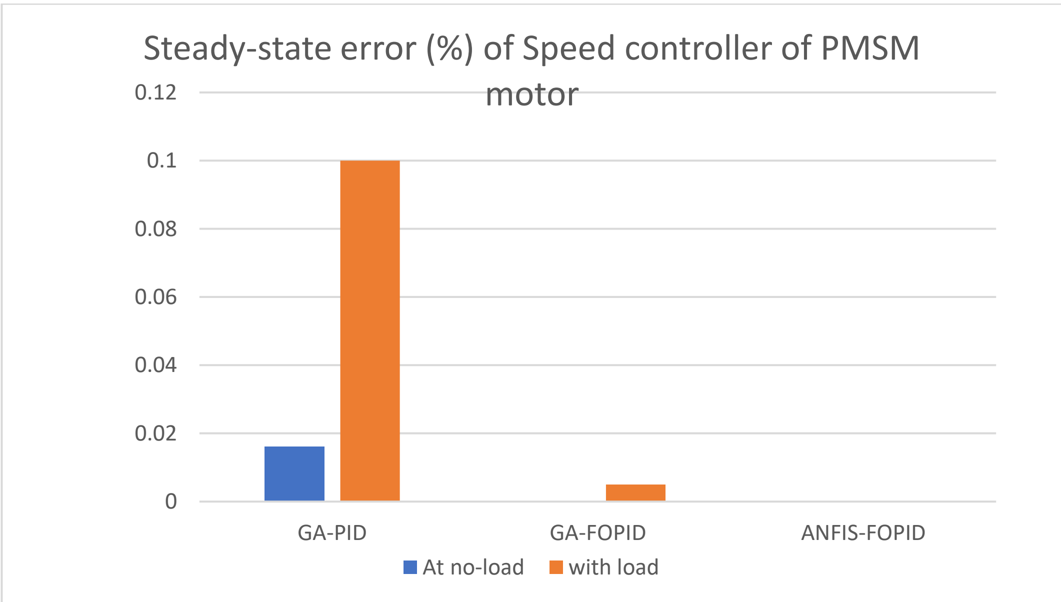

Figure 5.25 The steady-state error speed controller at no-load and with load

5.5.4 PMSM Motor Speed Error Value using FOPID and PID Controller

The value of the objective functions (ISE, IAE, ITSE, and ITAE) are obtained based on GA optimization as shown in Table 5.4. The GA tuned FOPID controller is better to reduce the error than the GA tuned PID controller.

Table 5.4 The fitness values comparison based on GA optimization

Speed Controllers	Performance index (error calculation method)			
	IAE	ISE	ITSE	ITAE
GA-FOPID controller	0.1426	0.1370	0.1570	0.000153354
GA-PID controller	0.362455	0.5425	0.954493	0.113677

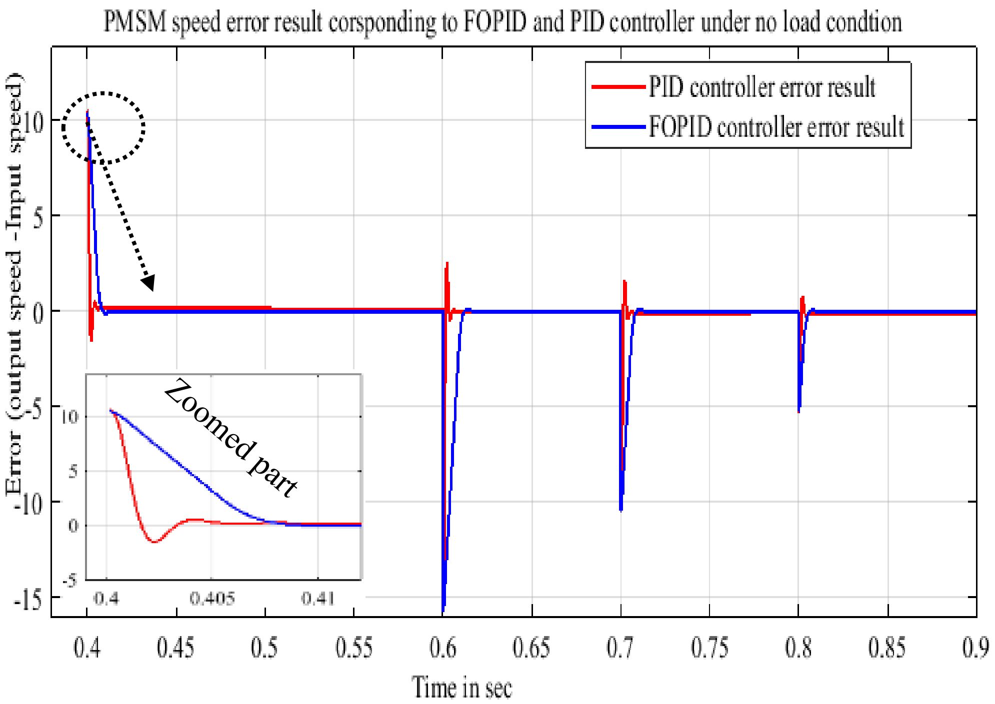

Figure 5.26 PMSM motor speed error value of FOPID and PID controller

Figure 5.27 shows, the error results of the GA tuned PID and GA tuned FOPID speed controllers of the PMSM motor. At the starting, the error is zero. That means the actual speed and desired speed of the motor are equal. The error occurs at a time of 0.4 sec. The positive part of the error result shows that the desired speed is greater than the motor's actual speed. The FOPID speed controller has less oscillation in the error value, whereas the PID controller exhibits an oscillation and overshoot. Figure 5.28 shows, the PMSM motor speed error value in chart form. The data used in this chart were taken from Table 5.4.

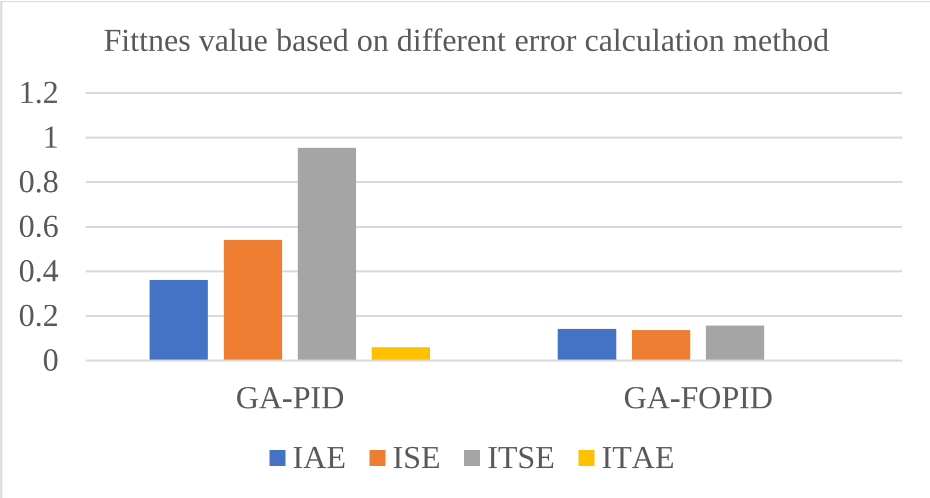

Figure 5.27 The PMSM motor speed error value comparison in chart form

5.5.5 Comparison of PMSM Current Controller Result

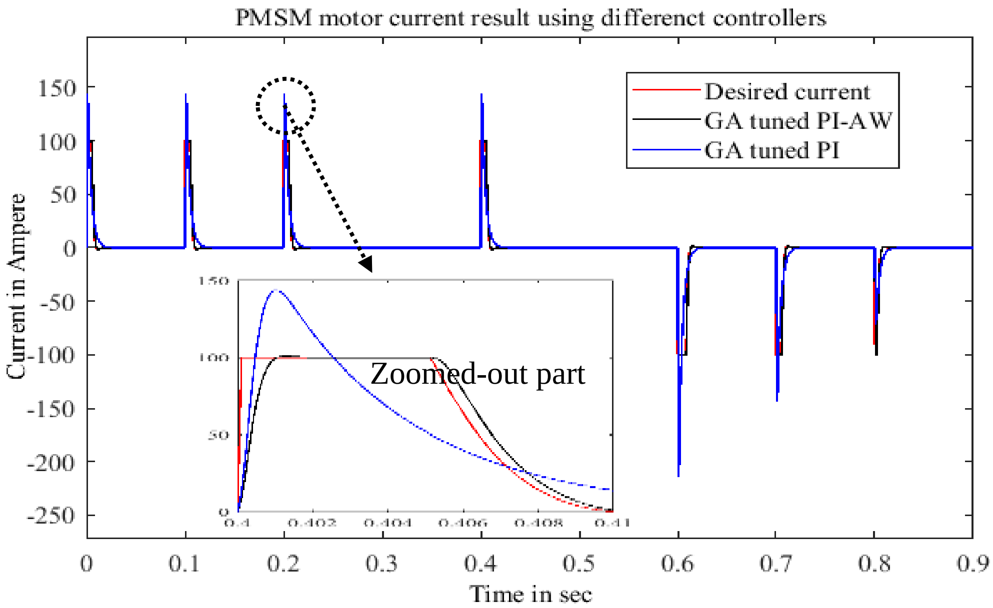

Figure 5.28 PMSM motor current result using different controllers.

Figure 5.29 shows the current control of the PMSM motor. The two current controllers of the PMSM motor. Which is GA tuned PI and GA tuned PI with Anti-Windup schemes were performed. GA tuned PI with an Anti-Windup current controller scheme has better performance than GA tuned PI current controller based on the performance parameters criterion listed in Table 5.5. Figure 5.30 shows, GA tuned PI-AW has 0.4005sec settling time, 0.004 sec rise time, 0.4001 sec peak time, 0.006% overshoot, and 0% Steady-state error whereas GA tuned PI current controller is 0.404sec settling time, 0.005 rise time, 0.4011 sec peak time, 0.44% overshoot, and 0.18% steady-state error. Figure 5.30 shows the

PMSM motor speed error value in chart form. The data used in this chart are taken from Table 5.5.

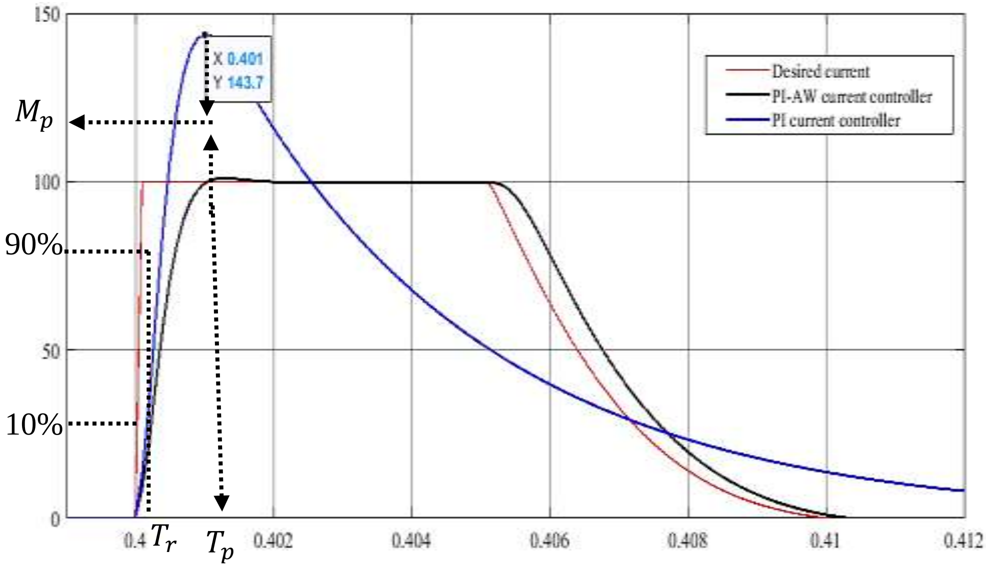

Figure 5.29 PMSM motor current zoomed out part using different controllers

Table 5.5 The comparison of the current controller of PMSM motor

Current controllers	Performance parameters result at no-load condition				
	t_s [sec]	t_r [sec]	t_p[sec]	$\%M_p$	$\%e_{ss}$
GA tuned PI	0.404	0.005	0.4011	0.44	0.18
GA tuned PI-AW	0.4005	0.004	0.4001	0.006	0

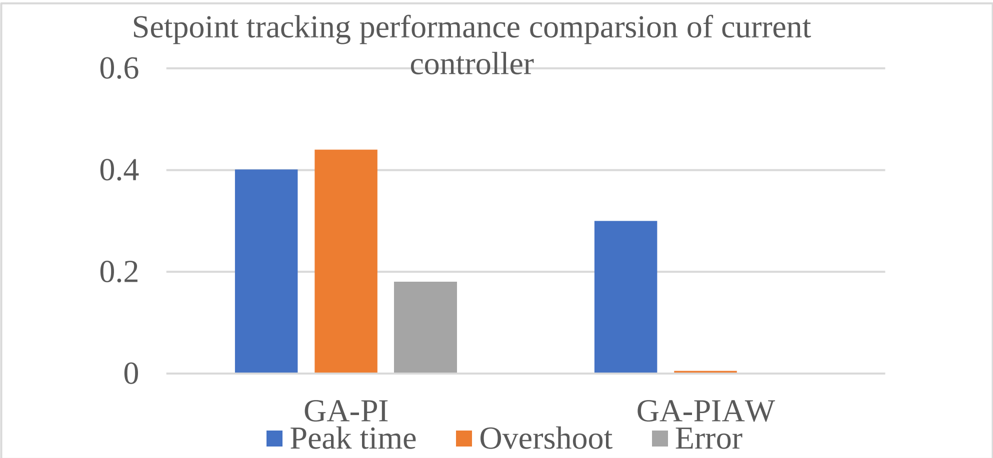

Figure 5.30 Set-point tracking performance comparison of the current controller

CONCLUSIONS AND RECOMMENDATIONS

6.1 Conclusions

Based on the previous chapter discussions, EVs have more benefits than Combustion Engine cars, including reducing air pollution, and unwanted gas emissions. So, Replacing Combustion Engine Vehicles with Electric vehicles is the alternative solution. However, energy utilization and efficiency are the major issues in EVs. Tractive motor is the main part of EVs systems. The speed of EVs varies from time to time due to passengers boarding, resistive force, and road types. So, it needs a tractive motor that has a variable speed. The tractive motors such as PMSM, IMs, BLDCM, and DC motor have been used for EV propulsion systems. They should fulfill the requirements of EVs such as high fault tolerance, less periodic maintenance, high efficiency, high power density, and less torque ripple, and less noisy operation. Among the given electric motors mentioned above, PMSM is recommended for EV drive systems and the rated motor was selected based on the desired parameter specification of the proposed vehicle.

Naturally, PMSM is a non-linear, multi-variable, and time-varying system that leads to unknown disturbance parameter variation. To improve this problem, the controller that is used to controller the PMSM should be efficient and best perform the system. In this study, the comparison of ANFIS based FOPID, GA tuned FOPID and GA tuned PID speed controller of PMSM were implemented in MATLAB/Simulink /Code. The simulation result shows, ANFIS based FOPID controller has 0% steady-state error and 0% overshoot whereas GA tuned FOPID controller has 0% overshoot and 0.005% steady-state error and GA tuned PID controller has 0.8% overshoot and 0.1% steady-state error which means During load variation, ANFIS based FOPID controller performed well for both disturbance rejection and set-point tracking of the system. The performance comparison terms of IAE, ITAE, ISE, and ITSE show the proposed controller performs better than the recently reported method.

Since any electric motor has a high current at starting, this may lead to heating of the motor stator windings and burning the internal circuit of the drive. To mitigate this, GA tuned PI and GA tuned PI with Anti-Windup current controllers were implemented. the simulation shows, GA tuned PI current controller has 0.006% overshoot, 0% steady-state error, whereas GA tuned PI has 0.44% overshoot, 0.18% steady-state error. So, the GA tuned PI with an

Anti-Windup current controller of the PMSM motor has better performance. Generally, among the comparison of speed and current controller, ANFIS based FOPID speed and GA tuned PI with an Anti-Windup current controller of PMSM has better system performance.

6.2 Recommendations

Several research works are discussed and analyzed in the previous chapters. In this section, additional possible research directions to the future are mentioned as follows.

- In this research work, the comparison of speed and current controllers of PMSM implemented in MATLAB Software and also discuss theoretically which means it is not implemented practically. It is recommended ASTU center of transportation and vehicle engineering (CTVE) and firms that are planning to produce Electric Vehicle for Ethiopian Market to evaluate the theoretical part and simulation result in the practical application area.
- In this research work, the controller design is implemented on speed and current control of PMSM the case of electric drive. It is recommended that the academic researchers implement those controllers on other systems.
- In this research work, design and control of PMSM for Electric Vehicle application were evaluated based on a Direct field-oriented control method due to this, it requires a position sensor such as encoder or resolver leads to additional wire and components. It is better to implement a Senseless control mechanism.
- The rotor part of PMSM is mounted on a permanent magnet leads to magnetic saturation and also there is a demagnetization problem. It is recommended that the academic researchers focused on the mechanism that improves the problems mentioned above.

Research fund Acknowledgment

This research project is funded by Adama Since and Technology University under the grant number ASTU/SM-R/161/20, Adama, Ethiopia.

Reference

[1] Y. Chen, G. Wu, R. Sun, A. Dubey, A. Laszka, and P. Pugliese, “A review and outlook of energy consumption estimation models for electric vehicles,” *arXiv*, 2020, doi: 10.4271/13-02-01-0005.

[2] T. Liu, W. Tan, X. Tang, J. Zhang, Y. Xing, and D. Cao, “Driving Conditions-Driven Energy Management for Hybrid Electric Vehicles: A Review,” *arXiv*, pp. 1–42, 2020.

[3] J. Y. Yong, V. K. Ramachandaramurthy, K. M. Tan, and N. Mithulananthan, “A review on the state-of-the-art technologies of electric vehicle, its impacts and prospects,” *Renew. Sustain. Energy Rev.*, vol. 49, pp. 365–385, 2015, doi: 10.1016/j.rser.2015.04.130.

[4] D. Wilken, M. Oswald, P. Draheim, C. Pade, U. Brand, and T. Vogt, “Multidimensional assessment of passenger cars: Comparison of electric vehicles with internal combustion engine vehicles,” *Procedia CIRP*, vol. 90, pp. 291–296, 2020, doi: 10.1016/j.procir.2020.01.101.

[5] W. Cao, A. A. S. Bukhari, and L. Aarniovuori, “Review of Electrical Motor Drives for Electric Vehicle Applications,” *Mehran Univ. Res. J. Eng. Technol.*, vol. 38, no. 3, pp. 525–540, 2019, doi: 10.22581/muet1982.1903.01.

[6] R. T. Sataloff, M. M. Johns, and K. M. Kost, *Electric Vehicle Machines And Drives Design, Analysis And Application*. International Research Centre for Electric Vehicles, 2015.

[7] R. E. Neapolitan, K. Hee Nam, R. E. Neapolitan, and K. Hee Nam, *AC Motor Control and Electrical Vehicle Applications*, Second Edi. 2019.

[8] A. Ranpariya, B. Shah, R. Salecha, V. Shah, and P. Sharma, “Optimization of Required Power for an Electric Vehicle,” pp. 4605–4608, 2019.

[9] D. Eskezia and Advisor:, “Addis Ababa Institute of Technology (AAiT) School of Electrical and Computer Engineering Speed Control of Permanent Magnet Synchronous Motor Using Higher Order Sliding Mode Controller Addis Ababa Institute of Technology (AAiT) School of Electrical and,” 2016.

[10] J. A. A. M. Thomas J. Vyncke, Ren´e K. Boel, “Direct torque control of permanent magnet synchronous motors in MATLAB/SIMULINK,” *Proc. 2016 Int. Conf. Electr. Inf. Technol. ICEIT 2016*, vol. 0, no. 28, pp. 452–457, 2016, doi: 10.1109/EITech.2016.7519641.

[11] S. Chauhan, “Motor Torque Calculations For Electric Vehicle,” *Int. J. Sci. Technol.*

Res., vol. 4, no. 8, pp. 126–127, 2015.

[12] E. A. Grunditz, "Design and Assessment of Battry Electric Vehicle Powertrain, with Respect to Performance, Energy Consumption and Electric Motor Thermal Capability," Chalmers Universty of Technology, 2016.

[13] Q. Guo, C. Zhang, L. Li, D. Gerada, J. Zhang, and M. Wang, "Design and implementation of a loss optimization control for electric vehicle in-wheel permanent-magnet synchronous motor direct drive system," *Appl. Energy*, vol. 204, pp. 1317–1332, 2017, doi: 10.1016/j.apenergy.2017.05.023.

[14] A. Thattil, S. Vachhani, D. Raval, P. Patel, P. Sharma, and U. G. Students, "Comparative Study of using Different Electric Motors for EV," *Int. Res. J. Eng. Technol.*, vol. 9001, pp. 4601–4604, 2008, [Online]. Available: www.irjet.net.

[15] M. Zeraoulia, M. E. H. Benbouzid, and D. Diallo, "Electric motor drive selection issues for HEV propulsion systems: A comparative study," *IEEE Trans. Veh. Technol.*, vol. 55, no. 6, pp. 1756–1764, 2006, doi: 10.1109/TVT.2006.878719.

[16] J. Puranen, *Induction Motor Versus Permanent Magnet Synchronous Motor in Motion Control Applications : A Comparative Study*. 2006.

[17] G. Luthra, "Comparison Of Characteristics Of Various Motor Drives Currently Used In Electric Vehicle Propulsion System," pp. 5–8, 2017.

[18] A. Glumineau and J. de León Morales, *Sensorless AC Electric Motor Control,Robust Advanced Design Techniques and Applications*. 2015.

[19] R. N. Huang, C. Song, and Y. J. Lou, "Observer based Speed Control of PMSM Servo Systems," *Appl. Mech. Mater.*, vol. 121–126, pp. 3376–3380, 2012, doi: 10.4028/www.scientific.net/AMM.121-126.3376.

[20] M. F. Marek ˇStulrajter, Val´eria Hrabovcov´, "Permanent Magnets Synchronous Motor Control Theory," vol. 58, no. 2, pp. 79–84, 2007.

[21] O. M. Arafa, G. A. Abdel Aziz, M. I. Abu El-Sebah, and A. A. Mansour, "Observer-based sensorless speed control of PMSM: A focus on drive's startup," *J. Electr. Syst. Inf. Technol.*, vol. 3, no. 2, pp. 181–209, 2016, doi: 10.1016/j.jesit.2015.05.004.

[22] W. Souhail, H. Khammari, M. F. Mimouni, and N. Jabli, "Field oriented control of permanent magnet synchronous motor: Chaos synchronization," *2015 4th Int. Conf. Syst. Control. ICSC 2015*, vol. 3, no. 3, pp. 224–229, 2015, doi: 10.1109/ICoSC.2015.7152712.

[23] P. V. Chakaravarthi, "Speed Control of PMSM Motor Using Fuzzy and PID Controller," *IJISET-International J. Innov. Sci. Eng. Technol.*, vol. 3, no. 1, pp. 526–

534, 2016, [Online]. Available: www.ijiset.com.

[24] W. A. A. Salem, G. F. Osman, and S. H. Arfa, "Adaptive Neuro-Fuzzy Inference System Based Field Oriented Control of PMSM Speed Estimation," *2018 20th Int. Middle East Power Syst. Conf. MEPCON 2018 - Proc.*, no. 7, pp. 626–631, 2019, doi: 10.1109/MEPCON.2018.8635179.

[25] S. W. Shneen, H. H. Kareem, and H. A. Abdulmajeed, "Available online www.jsaer.com Research Article Fuzzy-PI Control for Speed of PMSM Drive System," vol. 6, no. 4, pp. 31–35, 2019.

[26] S. Z. Moussavi, S. Javadi, M. Alasvandi, and E. Morad, "Speed Control Based on Adaptive Neuro-Fuzzy Inference System for Permanent Magnet Direct Current Motor," *Int. J. Control Autom.*, vol. 7, no. 12, pp. 425–436, 2014, doi: 10.14257/ijca.2014.7.12.39.

[27] L. J. Larminie, James, *James Larminie, John Lowry(auth.)-Electric Vehicle Technology Explained, Second Edition (2012).pdf*. 2012.

[28] B. Tabbache *et al.*, "A Power Presizing Methodology for Electric Vehicle Traction Motors To cite this version : HAL Id : hal-00874371 A Power Presizing Methodology for Electric Vehicle Traction Motors," 2013.

[29] P. R. S. Patil, R. S. Bharambe, V. Y. Pawar, S. Sugandhi, K. S. Thakare, and E. Engineering, "Analysis of Electric Vehicle Drive Train," pp. 3194–3197, 2018.

[30] M. R. T. Reddy, C. S. Virinchy, and T. S. A. Suryakumari, "Investigation of Capacity of Motor and its Simulation for an Electric Vehicle," no. 5, pp. 64–66, 2016.

[31] E. Schaltz, "Electrical Vehicle Design and Modeling," *Electr. Veh. - Model. Simulations*, 2011, doi: 10.5772/20271.

[32] M. G. Geda, "Speed Control of BLDC Motor by using PWM Current Controller Technique for Electric Vehicle Propulsion," Adama Ethiopia, 2018.

[33] R. A. Hanifah, S. F. Toha, and S. Ahmad, "Electric Vehicle Battery Modelling and Performance Comparison in Relation to Range Anxiety," *Procedia Comput. Sci.*, vol. 76, no. Iris, pp. 250–256, 2015, doi: 10.1016/j.procs.2015.12.350.

[34] N. Yang, Z. Song, H. Hofmann, and J. Sun, "Robust State of Health Estimation of Lithium-ion Batteries Using Convolutional Neural Network and Random Forest," 2020, [Online]. Available: http://arxiv.org/abs/2010.10452.

[35] D. Ocen, "Direct Torque Control (DTC) for a Permanent Magnet Synchronous Motor (PMSM)," Politècnica de Catalunya, 2005.

[36] M. H. Rashid, *Power Electronics Devices, Circuits, and Applications*, Fourth Edi.

2014.

[37] A. Mishra, P. Agarwal, and S. P. Srivastava, “A comprehensive analysis and implementation of vector control of permanent magnet synchronous motor,” *Int. J. Power Energy Convers.*, vol. 5, no. 1, pp. 1–23, 2014, doi: 10.1504/IJPEC.2014.059982.

[38] A. A. Mahfouz, “Intelligent Dtc for Pmsm Drive,” no. March 2012, 2016.

[39] E. Prasad, B. Suresh, and K. Raghuveer, “Field Oriented Control of PMSM Using SVPWM Technique,” *Glob. J. Adv. Eng. Technol.*, vol. 1, no. 2, pp. 39–45, 2012.

[40] G. Dong, J. Yang, X. Qiu, X. Liu, and C. Wei, “Space Vector Flux Weakening Control of PMSM Drivers,” *IOP Conf. Ser. Earth Environ. Sci.*, vol. 192, no. 1, 2018, doi: 10.1088/1755-1315/192/1/012010.

[41] R. El-Khazali, “Fractional-order PI λdμ controller design,” *Comput. Math. with Appl.*, vol. 66, no. 5, pp. 639–646, 2013, doi: 10.1016/j.camwa.2013.02.015.

[42] Z. Li, L. Liu, S. Dehghan, Y. Q. Chen, and D. Xue, “A review and evaluation of numerical tools for fractional calculus and fractional order controls,” *Int. J. Control*, vol. 90, no. 6, pp. 1165–1181, 2017, doi: 10.1080/00207179.2015.1124290.

[43] A. Tepljakov, E. Petlenkov, and J. Belikov, “A flexible MATLAB tool for optimal fractional-order PID controller design subject to specifications,” *Chinese Control Conf. CCC*, no. April 2015, pp. 4698–4703, 2012.

[44] N. I. E. Zhuo-yun, Z. Yi-min, W. Qing-guo, L. I. U. Rui-juan, and X. Lei-jun, “Fractional-Order PID Controller Design for Time-Delay Systems Based on Modified Bode ’ s Ideal Transfer Function,” vol. 8, 2020, doi: 10.1109/ACCESS.2020.2996265.

[45] A. M. Lopes, J. A. Tenreiro Machado, C. M. A. Pinto, and A. M. S. F. Galhano, “Fractional dynamics and MDS visualization of earthquake phenomena,” *Comput. Math. with Appl.*, vol. 66, no. 5, pp. 647–658, 2013, doi: 10.1016/j.camwa.2013.02.003.

[46] M. Reza and A. Nemati, “On Fractional-Order PID Design,” *Appl. MATLAB Sci. Eng.*, 2011, doi: 10.5772/22657.

[47] D. G. U. B. B. and M. S. Omar Hanif, “Detailed Study of Fractional Order PID Controllers using different Optimazation Techniques with one Case Study,” vol. 6, no. 10, pp. 1–13, 2017.

[48] D. P. Atherton, “An Analysis Package Comparing PID Anti-Windup Strategies,” *IEEE Control Syst.*, vol. 15, no. 2, pp. 34–40, 1995, doi: 10.1109/37.375281.

[49] A. Ghoshal and V. John, "Anti-windup Schemes for Proportional Integral and Proportional Resonant Controller," no. 2, pp. 1–6, 2010.

[50] O. Hanif, G. U. B. Babu, and M. Siva, "Detailed Study of Fractional Order PID Controllers using different Optimization Techniques with one Case Study," no. 3, pp. 20279–20291, 2017, doi: 10.15680/IJIRSET.2017.0610062.

[51] E. C. El Alaoui, H. Ayad, and S. Doubabi, "Fuzzy Anti-Windup Schemes for PID Controllers," vol. 1, no. 3, pp. 295–306, 2006.

[52] M. Mjahed, "PID Controller Design using Genetic Algorithm Technique," no. April 2013, 2018.

[53] J. F. M. Amaral, R. Tanscheit, and M. A. C. Pacheco, "Tuning PID Controllers through Genetic Algorithms," pp. 2–5.

[54] A. Jayachitra and R. Vinodha, "Genetic Algorithm Based PID Controller Tuning Approach for Continuous Stirred Tank Reactor," vol. 2014, 2014.

[55] Y. Guo and M. E. A. Mohamed, "Speed Control of Direct Current Motor Using ANFIS Based Hybrid P-I-D Configuration Controller," *IEEE Access*, vol. 8, pp. 125638–125647, 2020, doi: 10.1109/ACCESS.2020.3007615.

[56] V. K. Arun Shankar, S. Umashankar, P. Sanjeevikumar, and S. Paramasivam, "Adaptive Neuro-Fuzzy Inference System (ANFIS) based Direct Torque Control of PMSM driven centrifugal pump," *Int. J. Renew. Energy Res.*, vol. 7, no. 3, pp. 1436–1447, 2017.

Reference Links

[L1]. https://www.google.com/search?q=Permanent-Magnet-synchronous+motor+PMSM-Motor60+parametr&tbm=isch&ved=2ahUKEwiUtZ_wivPuAhUNdBoKHUT8B5oQ2-cCegQIABAA&oq=Permanent-Magnet-synchronous+motor+PMSM-Motor-60+parametr&gs_lcp=CgNpbWcQAzoECCMQJ1DmzwRYnYIFYJKFBWgAcAB4AIAByQOIAccakgEHMi0xLjcuMpgBAKABAaoBC2d3cy13aXotaW1nwAEB&sclient=img&ei=kC4uYJStLI3oacT4n9AJ&bih=568&biw=1366&hl=en-GB

(Searched on March 12, 2021).

[L2]. Searched on august 12, 2021

1. https://www.google.com/search?client=firefox-b-ab&biw=1366&bih=596&tbm=isch&sa=1&ei=PWKfW4jQNq2XlwSF4Lm IDA&q=3.4.3.%09Reducer+for+car+figure&oq=3.4.3.%09 Reduce r+ for +ca r+figure&gs_l=img....19302.19302.0.20312.1.1.0.0.0.0.247.247.2-1.1.0....0...1c.1.64.img..0.0.0....0.35W_Pfyib-g

[L3]. The link for table 3. 3 (Searched on august 12, 2021)

1. 60kW PMSM Motor for Electric Vehicle, View PMSM motor for an electric vehicle, Uni Product Details from Foshan Uni Technology Co., Ltd. on Alibaba.com

[L4] The link for figure 4.1 (searched on Jun, 2021)

1. https://forumautomation.com/t/what-is-cascade-control-loop-advantages-of-the-cascade-control-loop/2423
2. https://www.sciencedirect.com/topics/engineering/cascade-control

Appendixes

Appendix A: Electric vehicle dynamic analysis (The case of ECADO-4EV)

A.1 The simulation code of power versus pitch angle (Figure 3.5) for electric vehicle (the case of ECADO-4EV)

```
m=1500; fric=0.01; g=9.81; a=0; r=0.25324; % Radius of the wheel in meter
c_ofriction=0.01; %Coefficient of friction by considering the asphalt road
d=0.25324; v=14.29; % speed of the rotor in m/se=51.444km/h
Tot_effcen.M=0.95; Adnsty=1.2; %Kd/m3
Af=2; %area in m2; vo=0; %air velocity in m/s
Cw=0.5;%Initial condition
angleR=0; angleR1=0;
d_angleR=1e-6; %unit step increment
angleR_final=40; %final value in degree
x=1; n=1;
while(angleR<angleR_final),
Fadyna=0.5*Adnsty*Cw*Af*(v+vo)^2;
theta=angleR*2*pi/360; %Degree to radian conversion
F_tot=m*g*(sin(theta)+c_ofriction*cos(theta))+Fadyna+m*a; % Total force(Nm)
Power=F_tot*v; %W
Torque=(Power*r/v)/0.95;% Nm
angleR=angleR+d_angleR;
angleR1=angleR1+d_angleR;
if x>16,
F_totn(n)=F_tot;
Torquen(n)=Torque;
Powern(n)=Power/1000+1.5; %Power in KW
thetan(n)=angleR;
n=n+1; x=1;
end
x=x+1;
end
plot(thetan,Powern,'b','LineWidth',2); axis([0 40 0 150]);
```

```
grid
xlabel('approaching angle of the vehicle'); ylabel('Power (kW)'
```

The simulation code of aerodynamic force versus speed of the car (Figure 3.6) for electric vehicle (the case of ECADO-4EV)

```
clear all
m=1500; % mass of the Vehicle
g=9.81;
a=1; % acceleratin in m/s^2
r=0.2532; % Radius of the wheel in meter 1142/70-R12
K_friction=0.01; %Coefficient of friction for asphalt road
F_tot=0; v=14.29; %speed of the car in m/s
Tot_effcen.M=0.95; Adnsty=1.2; %air density Kg/m^3
Af=2; %area in m^2
vo=0; %air velocity in m/s
Cd=0.3; % drag coefficient 4
%Initial condition
Vkph=0; Vkph1=0;
d_Vkph=1e-2; %unit step increment
Vkph_final=130; %final value in km/hr.
x=1;
n=1;
while(Vkph<Vkph_final),
   Vmps=Vkph*(1000/3600);
Fadyna=0.5*Adnsty*Cd*Af*(Vmps+vo)^2;
if Vkph<=100*d_Vkph;
   statfric=0.2;
else statfric=0;
end
F_tot=m*g*(K_friction+statfric)+Fadyna+m*a; % Total force(Nm)
Power=F_tot*Vmps/0.95; % Required input power (Watt)
Torque=(Power*r/Vmps);% Nm
Vkph=Vkph+d_Vkph; Vkph1=Vkph1+d_Vkph;
if x>0, F_totn(n)=F_tot;
```

```
Torquen(n)=Torque;
Powern(n)=Power/1000; %Power in KW
Fadynan(n)=Fadyna;
Vkphn(n)=Vkph;
n=n+1; x=1;
end
x=x+1;
end
figure(1); plot(Vkphn,Fadynan,'r','linewidth',1.5);
set(gca,'FontSize',12)
axis ([0 140 0 400]);
xlabel('Speed of the of the car(Km/hr)')
ylabel('Aerodynamic dragging force (N)')
grid xlabel('Speed of the of the car(Km/hr)') ylabel('Aerodynamic dragging force (N)')
```

The simulation code of output power versus the speed of the car (Figure 3.7) for electric vehicle (the case of ECADO-4EV)

```
clear all;
close all;
m=1500; % mass of the Vehicle
fric=0.01; g=9.81; a=1; % acceleratin in m/s^2
r=0.25324; % Radius of the wheel in meter 1142/70-R12
K_friction=0.01; %Coefficient of friction by considering asphalt road
F_tot=0; v=14.29; %speed of the car in m/s
Tot_effcen.M=0.95; Adnsty=1.2; %air density Kg/m^3
Af=2; %area in m^2 vo=0; %air velocity in m/s
Cd=0.3; % drag coefficient
%Initial condition
Vkph=0;
Vkph1=0;
d_Vkph=1e-2; %unit step increment
Vkph_final=130; %final value in km/hr.
x=1;
n=1;
```

```
while (Vkph<Vkph_final),
   Vmps=Vkph*(1000/3600);
Fadyna=0.5*Adnsty*Cd*Af*(Vmps+vo)^2;
if Vkph<=100*d_Vkph;
statfric=0.2;
else
   statfric=0;
end
F_tot=m*g*(K_friction+statfric)+Fadyna+m*a; % Total force(Nm)
Power=F_tot*Vmps/0.95; % Required input power (Watt)
Torque=(Power*r/Vmps);% Nm
Vkph=Vkph+d_Vkph;
Vkph1=Vkph1+d_Vkph;
if x>0,
   F_totn(n)=F_tot;
Torquen(n)=Torque;
Powern(n)=Power/1000; %Power in KW
Fadynan(n)=Fadyna;
Vkphn(n)=Vkph;
n=n+1;
x=1;
end
x=x+1;
end
plot(Vkphn,Powern,'r','LineWidth',2); set(gca,'FontSize',12)
axis([0 140 0 150]); grid xlabel('Speed of the of the car(Km/hr)')
ylabel('Power (KW)')
```

The simulation code of power versus torque (Figure 3.8) for electric vehicle (the case of ECADO-4EV)

```
clear all
Ratedpower=60000; %Rated power in Watt
wrpm=0; %initial condition
wb= 230.266666667; %base speed in rad/sec
```

```
d_wrpm=1e-2; %unit step increment
wrpm_final=4500; %final value in RPM
x=1;
n=1;
while(wrpm<wrpm_final),
wm=wrpm*(2*pi)/60;
Torque= Ratedpower/wm;
if Torque>= 275,
Torque= 275;
end
if Torque<275,
Torque= Torque;
end
Power=Torque*wm;
wrpm=wrpm+d_wrpm;
if x>16,
wrpmn(n)=wrpm;
Torquen(n)=Torque;
Powern(n)=Power/1000;
n=n+1;
x=1;
end
x=x+1;
end
figure(1);[AX,Torque,Power]=plotyy(wrpmn,Torquen, wrpmn,Powern);
axis([0 4500 0 350]);
set(get(AX(1),'ylabel'), 'string','Motor torque in Nm')
set(get(AX(2),'ylabel'), 'string','Motor power kW')
set(Torque,'LineStyle','--')
set(Power,'LineStyle','-')
set(gca, 'FontName','TimesNewRoman')
set(gca, 'FontSize',12)
set([Torque,Power],'LineWidth',1)
xlabel('Motor speed in rpm')
```

```
grid on
legend('Motor torque','Motor power')
```

Appendix B: Controller performance checking using sample system

B.1 The simulation code for checking the Comparison of FOPID controller with PIDs

Sample code for FOPID controller

function aa

```
Kp=1; Ki=1; lam=1; Kd=1; m=1;
s=tf('s');
Gc= fracpid(Kp,Ki,lam,Kd,m);
Gp=exp(-0.5*s)/(s+2);
G=Gc*Gp/(1+Gc*Gp);
t=0:0.1:10;
y=step(G,t);
plot(t,y,'linewidth',3)
buf= [t' y];
save 'FOPID_data' 'buf'
```

Sample code for Practical PID controller

```
function PPID
Kp= 2.1594;Ki=3.2336;Kd= 0.3734;N=10;Td=Kd/Kp;
s=tf('s');
Gc=ppid(Kp,Ki,Kd,Td/N);
Gp=exp(-0.5*s)/(s+2);
G=Gc*Gp/(1+Gc*Gp);
t=0:0.1:10;
y=step(G,t);
plot(t,y,'linewidth',3)
buf= [t' y];
save 'PPID_data' 'buf'
```

Sample code for Ideal PID controller

```
Function PID
```

```
Kp= 2.3512 ;Ki= 3.7888 ;Kd= 0.5270;
s=tf('s');
Gc=pid(Kp,Ki,Kd);
Gp=exp(-0.5*s)/(s+2);
G=Gc*Gp/(1+Gc*Gp);
t=0:0.1:10;
y=step(G,t);
plot(t,y,'linewidth',3)
% size(t)
% size(y)
buf= [t' y];
save 'PID_data' 'buf'
```

The simulation code to draw the graph of the above three mentioned controller in one t,y plane

```
load PID_data;
t= buf(:,1); y1= buf(:,2)
load PPID_data;
t= buf(:,1); y2= buf(:,2)
load FOPID_data;
t= buf(:,1); y3= buf(:,2)
g3= plot(t,y1,'b',t,y2,'r',t,y3,'g');
set(g3(1),'LineWidth',2)
set(gca,'XLim',[0 10],'YLim',[0 1.4]);
xlabel('t'),ylabel('y(t)');
legend ('PID','Practical PID','fractional order PID')
```

Appendix C: Controller Tuning in the System Modeling

C.1 Matlab code to Simulate the cascade speed (FOPID) and current (PI-AW) controller of PMSM

```
 % Tunes a FOPID+PI-AW controller for a step change
function Tune_FOPID_PI_Model
clear all
rng default
```

```
options= optimoptions('ga','PlotFcn',@gaplotbestf);
options.PopulationSize= 30;
options.MaxGenerations= 30;  % Increase value if needed
nvar= 8; % Number of parameters
LB= 0.0001*ones(1,8); % Lower bound of tuning parameters
UB= [10 60 5 2 2 3 3 3]; % Upper bound of tuning parameters
% Kp1 Ki1 Kd1 lam mu Kp2 Ki2 a
[x,fval]= ga(@EvalObj,nvar,[],[],[],[],LB,UB,[],options)
%% Measures a performance index from the simulink model
% Updates the parameter values in Simulink model workspace
function obj= EvalObj(x)
simulink_model= 'FOPID_PI-AW_Model';
load_system(simulink_model);
gains= get_param(simulink_model,'modelworkspace');
gains.assignin('Kp1', x(1));
gains.assignin('Ki1', x(2));
gains.assignin('Kd1', x(3));
gains.assignin('lam', x(4));
gains.assignin('mu', x(5));
gains.assignin('Kp2', x(6));
gains.assignin('Ki2', x(7));
gains.assignin('a', x(8));
% Simulates the simulink model to get the outputs
simOut= sim(simulink_model,'SaveOutput','on');
% Retrieves time t and error e
t= simOut.find('t');
e1= simOut.find('e1'); %the error inupt to speed controller
e2= simOut.find('e2');%error inupt to speed controller
% Calculate a performance index using the trapezoidal integration rule
n= length(e1); q= 1;
%ae= abs(e1)+q*abs(e2); % IAE= Int(|e1|+q*|e2|)
ae= e1.^2+q*e2.^2; % ISE= Int(e1^2+q*e2^2)
obj= 0;
for i= 2:n
```

```
    stepsize= t(i)-t(i-1);
    obj= obj+0.5*stepsize*(ae(i-1)+ae(i));
end
```

C.2 Steps to Optimaze the Simulink Model

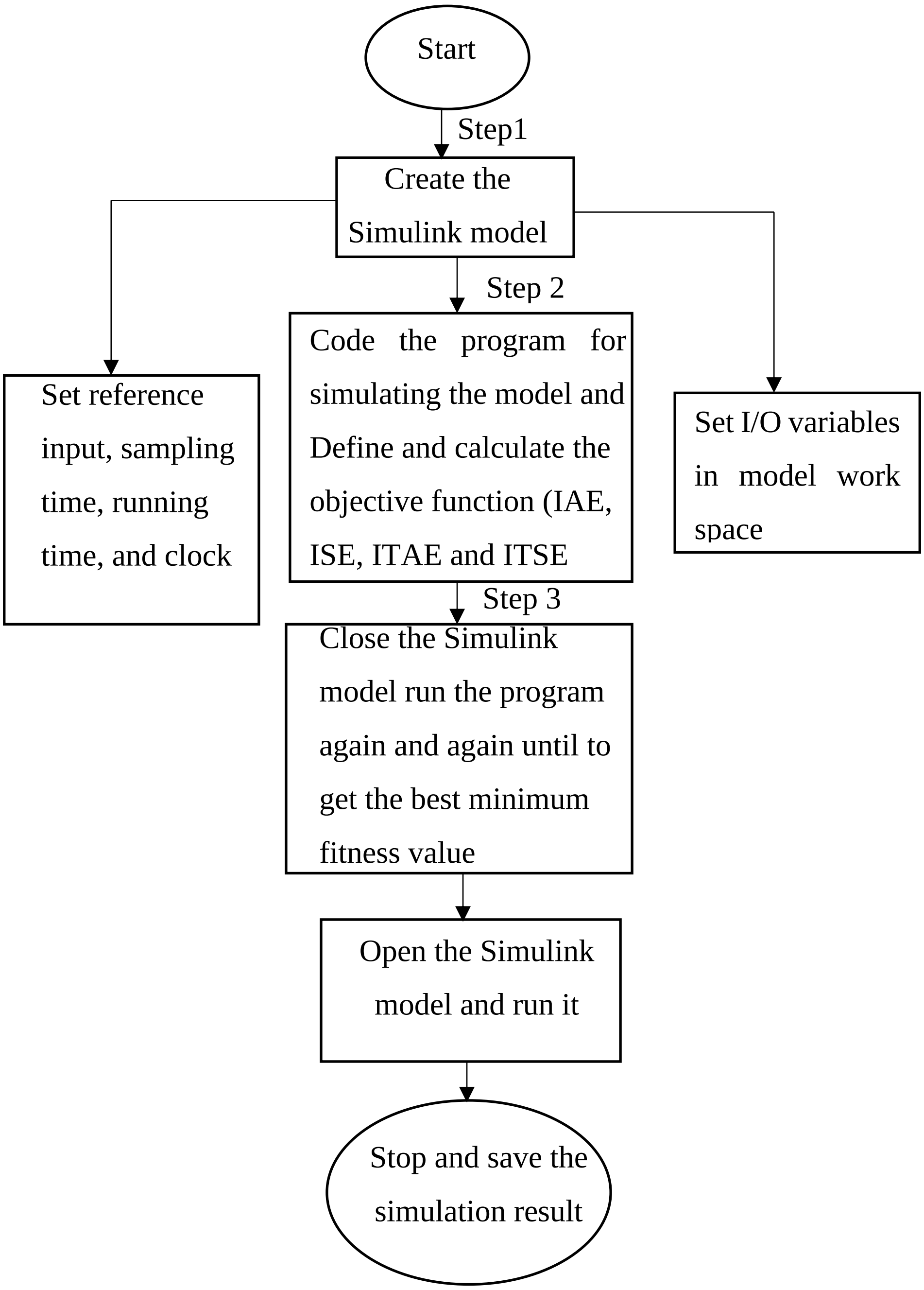

C.3 Matlab code to Simulate the cascade speed (PID) and current (PI) controller of PMSM

```
% Tunes a PID+PI controller for variable change
function Tune_PID_PI_Model
```

```
clear all
rng default
options= optimoptions('ga','PlotFcn',@gaplotbestf);
options.PopulationSize= 30;
options.MaxGenerations= 40;  % Increase value if needed
nvar= 5; % Number of parameters
LB= 0.001*ones(1,5); % Lower bound of tuning parameters
UB= [10 5 3 5 3]; % Upper bound of tuning parameters
[x,fval]= ga(@EvalObj,nvar,[],[],[],[],LB,UB,[],options)
%%
% Measures a performance index from the simulink model
function obj= EvalObj(x)
% Updates the parameter values in Simulink model workspace
simulink_model= 'PID_PI_Model';
load_system(simulink_model);
gains= get_param(simulink_model,'modelworkspace');
gains.assignin('Kp1', x(1));
gains.assignin('Ki1', x(2));
gains.assignin('Kd1', x(3));
gains.assignin('Kp2', x(4));
gains.assignin('Ki2', x(5));
% Simulates the simulink model to get the variables
simOut= sim(simulink_model,'SaveOutput','on');
% Retrieves time t and error e
t= simOut.find('t');
e1= simOut.find('e1'); %the error inupt to speed controller
e2= simOut.find('e2'); % error inupt to speed controller
% Calculate a performance index using the trapezoidal integration rule
 n= length(e1); q= 1; % q is the weight function, it can assign any number start from 1
%ae= abs(e1)+q*abs(e2); % IAE= Int(|e1|+q*|e2|)
ae= e1.^2+q*e2.^2; % ISE= Int(e1^2+q*e2^2)
obj= 0;
for i= 2:n
   stepsize= t(i)-t(i-1);
```

```
   obj= obj+0.5*stepsize*(ae(i-1)+ae(i));
end
```

Appendix D: Error Traing Mechanism using ANFIS

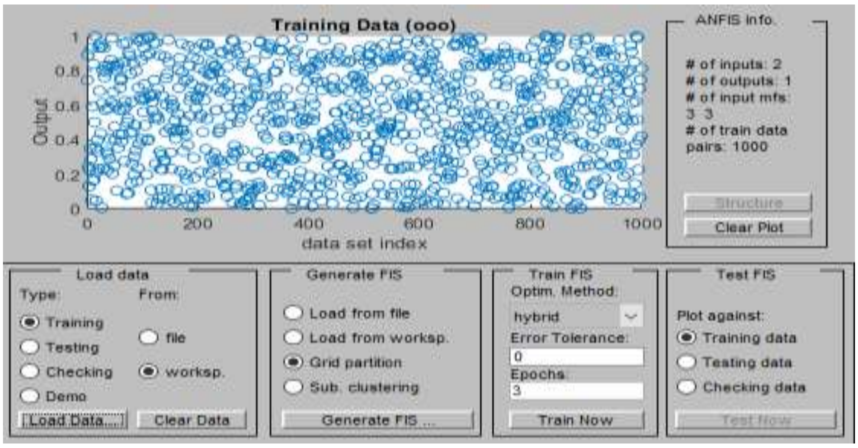

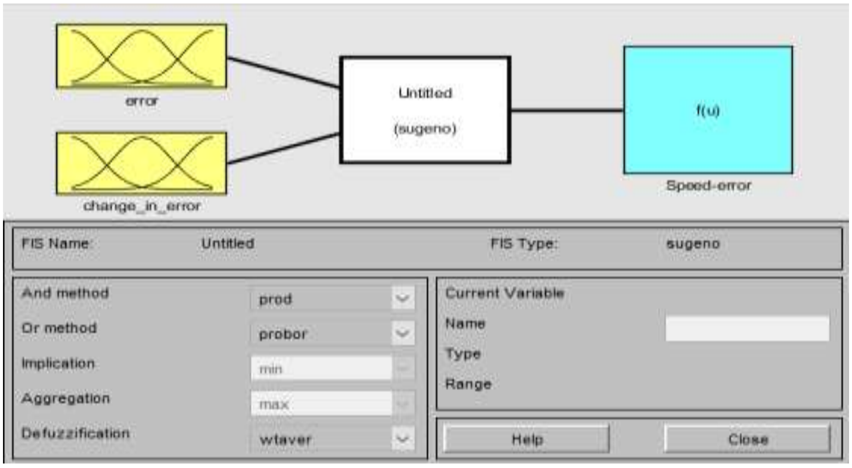

Apply ANFIS to Data

```
Outputs=evalfis(Inputs,fis);TrainOutputs=Outputs(TrainInd,:);
TestOutputs=Outputs(TestInd,:);
%% Error Calculation
TrainErrors=TrainTargets-TrainOutputs;TrainMSE=mean(TrainErrors.^2);
TrainRMSE=sqrt(TrainMSE);TrainErrorMean=mean(TrainErrors);
TrainErrorSTD=std(TrainErrors);TestErrors=TestTargets-TestOutputs;
TestMSE=mean(TestErrors.^2);TestRMSE=sqrt(TestMSE);
TestErrorMean=mean(TestErrors);TestErrorSTD=std(TestErrors);
```